

Spring 1-1-2011

Parallel Computational Modeling and Experimental Studies on Durability of Cementitious Materials and Structures

Okpin Na

University of Colorado at Boulder, nao@colorado.edu

Follow this and additional works at: https://scholar.colorado.edu/cven_gradetds



Part of the [Civil Engineering Commons](#)

Recommended Citation

Na, Okpin, "Parallel Computational Modeling and Experimental Studies on Durability of Cementitious Materials and Structures" (2011). *Civil Engineering Graduate Theses & Dissertations*. 218.

https://scholar.colorado.edu/cven_gradetds/218

This Dissertation is brought to you for free and open access by Civil, Environmental, and Architectural Engineering at CU Scholar. It has been accepted for inclusion in Civil Engineering Graduate Theses & Dissertations by an authorized administrator of CU Scholar. For more information, please contact cuscholaradmin@colorado.edu.

**PARALLEL COMPUTATIONAL MODELING AND EXPERIMENTAL STUDIES
ON DURABILITY OF CEMENTITIOUS MATERIALS AND STRUCTURES**

By

OKPIN NA

B.S, Chonnam National University, 2000

M.S, Hanyang University, 2002

A thesis submitted to the
Faculty of the Graduate school of the
University of Colorado in partial fulfillment
of the requirement for the degree of
Doctor of Philosophy
Department of Civil, Environmental, and Architectural Engineering

2011

This thesis entitled:
**PARALLEL COMPUTATIONAL MODELING AND EXPERIMENTAL STUDIES
ON DURABILITY OF CEMENTITIOUS MATERIALS AND STRUCTURES**

written by OKPIN NA

has been approved for the Department of
Civil, Environmental, and Architecture Engineering

Yunping Xi

Xiao Chuan Cai

Franck Vernerey

Richard A. Regueiro

Date _____

The final copy of this thesis has been examined by the signatories, and we find that Both the content and the form meet acceptable presentation standards of scholarly Work in the above mentioned discipline.

OKPIN NA (Ph.D., Civil, Environmental, and Architectural Engineering)

Parallel Computational Modeling and Experimental Studies on Durability of Cementitious Material and Structures

Thesis directed by Professor Yunping Xi

In order to predict long-term performance of reinforced concrete structures, a clear understanding of deterioration mechanism in portland cement concrete is a crucial issue. There are several deterioration mechanisms, and chloride-induced corrosion of reinforcement is an important one. The transport rates of chloride and other ions from deicing salts determine the time at which the corrosion of reinforcement starts, which is an important parameter for evaluating the durability of the structure. The main objective of this thesis is to develop a generalized framework based on parallel computing technique to analyze the durability performance of reinforced concrete structures with an emphasis on the coupled transport processes of chloride and other species from deicing salts in non-saturated concrete under ambient temperature.

The generalized framework for the coupled transport processes is based on a modified Nernst-Planck equation, which includes the coupling effects of both moisture transfer and thermal conduction in concrete. For the parallel implementation, an overlapping additive Schwarz method as preconditioner is used. In order to predict numerically the transport processes in a large-scale structure with a realistic boundary condition, various chloride concentrations and environmental humidity models. The prediction by the theoretical models and parallel algorithm agree quite well with available experimental data. In addition to the theoretical and numerical studies, experimental studies are conducted to investigate and improve various properties of sustainable cementitious materials made of rubber particles from waste tires, including compressive strength, bond strength, chloride permeability resistance, drying shrinkage, and freeze-thaw resistance.

DEDICATION

To my lovely wife and sons

Kyonghwa Jung,

Yumin Na and Daniel Yuchan Na

And to all of my family

ACKNOWLEDGEMENTS

I would like to express my sincere gratitude to my advisor, Professor Yunping Xi, for his constructive suggestions, guidance, support, criticism and encouragement during my study in the University of Colorado at Boulder. I am also grateful to Professor Xiao-Chuan Cai, M. V. Sivaselvan, Franck Vernerey, and Richard A. Regueiro for taking the time to serve on my thesis committee and for their expert guidance and invaluable discussions. Special thanks are offered to Professor Xiao-Chuan Cai and Yunping Xi for their guidance and financial support (NSF CNS0722023; CDPHE 08-00168), without which my work would not have been possible.

I would like to extend my gratitude to my friends and colleagues, who have offered fruitful suggestions during this work: Dr. Keunkwang Lee, Dr. Jaesung Lee, Dr. Byunghun Kim, Dr. Daehung Kang, Siyoung Park, Dr. Nattapong Damrongwiriyanupap, Dr. Pania Meshgin, Yu-Chang Liang for their encouragement and friendship.

Additionally, I would like to give my sincere thanks to Professor Dongho Choi, who gave me the motivation to study in the U.S. and have offered constant encouragement during my academic life.

Finally, I would like to give my profound appreciation to my parents and parents-in-law for their love, unconditional support, and endless encouragement. Their constant love and sacrifices over the years have made it possible to complete my studies in the U. S. I cannot forget my wife, Kyonghwa Jung, who is the most important person of the last five years. She has been with and encouraged me with her endless love, consistent support and patience that has sustained me throughout this long journey. I would also like to thanks to my lovely sons, Yumin and Yuchan. And I believe that God has been with and led me here.

CONTENTS

CHAPTER	PAGE
1. INTRODUCTION	1
1.1.Motivations	1
1.2.Research Objectives.....	2
1.3.Thesis Organization.....	3
2. BACKGROUND ON CHLORIDE-INDUCED STEEL CORROSION IN CONCRETE AND PARALLEL COMPUTING TECHNIQUES.....	5
2.1.Durability of Concrete structure	5
2.1.1.Mechanism of deterioration in reinforced concrete structure	5
2.1.2.Transport processes in reinforced concrete structures	7
2.1.3.Chloride – induced corrosion in reinforced concrete	8
2.1.4.Chloride threshold values of the steel corrosion	11
2.2.Parallel Numerical Computation	12
3. PARALLEL COMPUTATION ANALYSIS OF COUPLED CHLORIDE AND MOISTURE DIFFUSION IN CONCRETE	14
3.1.Introduction.....	14
3.2.Basic Formulation and Governing Partial Differential Equation	15
3.3.Material Parameters.....	18

3.3.1. Moisture capacity and chloride binding capacity	18
3.3.2. Moisture diffusion coefficient and chloride diffusion coefficient.....	20
3.4. Finite element Formulation	22
3.5. Implementation of Parallel Finite Element Method	25
3.5.1. Various adapted programs in parallel finite element program.....	25
3.5.2. Overlapping domain decomposition with additive Schwarz preconditioner.....	26
3.6. Numerical Example.....	29
3.6.1. Validation of parallel finite element program.....	29
3.6.2. Speed up and Efficiency.....	33
3.7. Conclusions.....	35
4. APPLICATION OF PARALLEL FINITE ELEMENT METHOD OF COUPLED DIFFUSION PROCESSES IN LARGE SCALE CONCRETE STRUCTURES.....	37
4.1. Introduction.....	37
4.2. Applied Bridge Overview	38
4.3. Parallel Finite Method of Large-Scale Concrete Structure	40
4.3.1. Modeling of Castle wood canyon bridge with large meshes.....	40
4.3.2. Environmental humidity model	42
4.4. Numerical Results and Discussion	45
4.4.1. Speed up.....	45
4.4.2. Effect of Boundary Condition.....	46

4.5. Conclusions	51
5. MULTI SPECIES TRANSPORT PROCESS IN NON-SATURATED CONCRETE STRUCTURES	52
5.1. Introduction	52
5.2. Basic Formulation of Governing Equations	54
5.3. Material Model	57
5.3.1. Capacity and diffusivity coefficients of multi species in non- saturated concrete	57
5.3.2. Coupling parameters	59
5.4. Numerical Model	60
5.5. Numerical Results and Discussion	63
5.5.1. Validation of numerical model in saturated concrete	63
5.5.2. Multi-species diffusion in non saturated concrete	66
5.6. Conclusions	72
6. COUPLED CHEMO-HYGRO-THERMAL TRANSPORT PROCESSES IN NON-SATURATED CONCRETE STRUCTURES	73
6.1. Introduction	73
6.2. Basic Formulation of Governing Equations	75
6.3. Material Model	77
6.3.1. Capacity and diffusivity coefficients	77
6.3.2. Coupling parameters	79

6.4. Numerical Model	81
6.5. Numerical Results and Discussion	84
6.5.1.Validation of numerical model in saturated concrete.....	84
6.5.2.Multi-species diffusion in non-saturated concrete considering temperature effect.....	90
6.6. Conclusions	92
7. DURABILITY OF INSULATION MORTAR WITH FINE RUBBER POWDER	93
7.1. Introduction	93
7.2. Experimental Details	94
7.2.1.Materials and mixture portion.....	94
7.2.2.Specimen preparation.....	97
7.2.3.Test methods.....	98
7.3. Test Results and Discussions	101
7.3.1.Compressive and flexural strengths.....	101
7.3.2.Bonding strength.....	106
7.3.3.Dry shrinkage.....	107
7.3.4.Permeability.....	109
7.3.5.Microstructure observed by Scanning Electron Microscope (SEM).....	111
7.4. Conclusions	112
8. DURABILITY OF SURFUR RUBBER CONCRETE	114
8.1. Introduction	114

8.2. Experimental Details	115
8.2.1. Optimum mix design	115
8.2.2. Materials and mixture portion.....	115
8.2.3. Specimen preparation.....	117
8.2.4. Mixing process.....	117
8.3. Test Results and Discussion	118
8.3.1. Compression test.....	118
8.3.2. Suggestion of mix process.....	121
8.3.3. Permeability.....	123
8.3.4. Freezing –thaw resistance.....	124
8.4. Conclusions	130
9. CONCLUSIONS AND FUTURE RESEARCH RECOMMENDATIONS	131
9.1. Conclusions	131
9.2. Future Research Recommendations	137
BIBLIOGRAPHY	138
APPENDIX A. DERIVATION OF DIFFUSIVITY MATRIX	138

TABLE OF TABLES

TABLE.2.1 CHLORIDE THRESHOLD VALUES OBTAINED FROM DIFFERENT RESEARCHERS	11
TABLE.3.1 MATERIAL PARAMETERS USED IN THE ANALYSIS.....	30
TABLE.5.1 MATERIAL PARAMETERS AND INPUT DATA FOR NUMERICAL ANALYSIS.....	61
TABLE.5.2 TOTAL CHLORIDE PROFILE ASSOCIATED WITH TWO DIFFERENT WATER-CEMENT RATIO AND TIME PERIOD ON DEPTH.	63
TABLE.6.1 MATERIAL PARAMETERS AND INPUT DATA FOR NUMERICAL ANALYSIS.....	82
TABLE.6.2 TOTAL CHLORIDE PROFILE ASSOCIATED WITH TWO DIFFERENT WATER-CEMENT RATIO, TEMPERATURE, AND TIME PERIOD ON DEPTH.....	84
TABLE.7.1 MIX DESIGN FOR INSULATION MORTAR	95
TABLE.7.2 PREPARATION OF SPECIMEN	97
TABLE.7.3 COMPRESSIVE STRENGTH ACCORDING TO DIFFERENT RUBBER DOSAGE	103
TABLE.7.4 COMPRESSION STRENGTH OF EACH SPECIMEN ACCORDING TO CONTENTS OF RPP	103
TABLE.7.5 RESULTS OF COMPRESSION TEST WITH DIFFERENT SIZE OF RUBBER POWDERS.....	105
TABLE.7.6 MODULUS OF RUPTURE	106
TABLE.7.7 BOND STRENGTH OF RUBBER MORTAR	106
TABLE.7.8 RESULTS OF CHLORIDE ION PERMEABILITY TEST	109
TABLE.7.9 MIX DESIGNS FOR ADDITIONAL TESTS	110
TABLE.7.10 TEST DATA OF ADDITIONAL RAPID CHLORIDE PERMEABILITY TESTS	111
TABLE.8.1. MIX DESIGN.....	116
TABLE.8.2 PREPARATION AND SIZE OF SPECIMENS.....	117

TABLE OF FIGURES

FIG.2.1 CAUSES OF DETERIORATION OF REINFORCED CONCRETE	6
FIG.2.2 PRINCIPAL FACTORS INVOLVED IN THE TRANSPORT PROCESSES IN CONCRETE	7
FIG.2.3 STAGES IN CORROSION-INDUCED DAMAGE.....	10
FIG.2.4 CORROSION PROCESSES ON THE SURFACE OF STEEL.....	11
FIG.3.1 FLOW CHART FOR PARALLEL PROCESS	28
FIG.3.2 PROCEDURE OF FE SOLVER	28
FIG.3.3 THE PHYSICAL MODEL FOR CHLORIDE ION PENETRATION	30
FIG.3.4 AN EXAMPLE OF MESH PARTITIONING (PARTITIONED INTO 4 SUB-DOMAINS).....	31
FIG.3.5 AN EXAMPLE OF MESH PARTITIONING (PARTITIONED INTO 8 SUB-DOMAINS).....	31
FIG.3.6 CHLORIDE CONCENTRATIONS PROFILE IN 5CM DEPTH ACCORDING TO NO. OF PROCESSORS	32
FIG.3.7 RELATIVE HUMIDITY PROFILE IN 5CM DEPTH ACCORDING TO NO. OF PROCESSORS	32
FIG.3.8 FREE CHLORIDE CONCENTRATION PROFILE IN 5CM DEPTH ACCORDING TO NO. OF PROCESSORS	33
FIG.3.9 SPEED UP OVER A NUMBER OF PROCESSORS USED IN THE ANALYSIS	34
FIG.3.10 EFFICIENCY OVER A NUMBER OF PROCESSORS USED IN THE ANALYSIS	35
FIG.4.1 CASTLEWOOD CANYON BRIDGE, FRANKTOWN, COLORADO	39
FIG.4.2 GEOMETRY OF CASTLEWOOD CANYON BRIDGE	39
FIG.4.3 MODELLING OF CASTLEWOOD CANYON BRIDGE.....	41
FIG.4.4 PARTITIONING OF CASTLEWOOD CANYON BRIDGE WITH 16 PROCESSORS	41
FIG.4.5 ENVIRONMENTAL HUMIDITY RECORD, MIDWAY STATION, CHICAGO (BAZANT ET AL,1993).....	42
FIG.4.6 ENVIRONMENTAL HUMIDITY MODEL WITH RANDOM NOISE	43
FIG.4.7 COMPARISON OF SINGLE AND VARIOUS BOUNDARY CONDITION.....	44
FIG.4.8 COMPARISON OF SINGLE AND VARIOUS BOUNDARY CONDITION.....	45
FIG.4.9 CONTOUR OF CHLORIDE DISTRIBUTION.....	47
FIG.4.10 CONTOUR OF HUMIDITY DISTRIBUTION	47
FIG.4.11 CHLORIDE CONCENTRATION OVER TIME AT 50MM DEPTH	48

FIG.4.12 HUMIDITY OVER TIME AT 50MM DEPTH	48
FIG.4.13 CHLORIDE CONCENTRATION OVER TIME AT 50MM DEPTH	50
FIG.4.14 HUMIDITY OVER TIME ACCORDING TO DEPTH	50
FIG.5.1 NUMERICAL SIMULATION MODEL	62
FIG.5.2 CHLORIDE PROFILES OF CONCRETE SPECIMEN WITH 0.55 WATER-CEMENT RATIO.....	64
FIG.5.3 CHLORIDE PROFILES OF CONCRETE SPECIMEN WITH 0.65 WATER-CEMENT RATIO.....	65
FIG.5.4 CATIONS PROFILES OF CONCRETE SPECIMEN WITH 0.55 WATER-CEMENT RATIO	65
FIG.5.5 A COMPARISON OF TEST AND NUMERICAL RESULT OF SPECIMEN	66
FIG.5.6 PROFILE OF RELATIVE HUMIDITY AT DIFFERENT DEPTH OVER TIME	67
FIG.5.7 PROFILE OF CHLORIDE CONCENTRATION AT DIFFERENT DEPTH OVER TIME.....	68
FIG.5.8 PROFILE OF SODIUM CONCENTRATION AT DIFFERENT DEPTH OVER TIME.....	70
FIG.5.9 PROFILE OF CALCIUM CONCENTRATION AT DIFFERENT DEPTH OVER TIME.....	70
FIG.5.10 PROFILE OF POTASSIUM CONCENTRATION AT DIFFERENT DEPTH OVER TIME.....	71
FIG.5.11 PROFILE OF HYDROXYL CONCENTRATION AT DIFFERENT DEPTH OVER TIME.....	71
FIG.6.1 NUMERICAL SIMULATION MODEL	83
FIG.6.2 CHLORIDE PROFILE IN CONCRETE SAMPLE (0.55 W/C, 3 DAYS)	86
FIG.6.3 CHLORIDE PROFILE IN CONCRETE SAMPLE (0.65 W/C, 3 DAYS)	86
FIG.6.4 CHLORIDE PROFILE IN CONCRETE SAMPLE (0.55 W/C, 6 DAYS)	87
FIG.6.5 CHLORIDE PROFILE IN CONCRETE SAMPLE (0.65 W/C, 6 DAYS)	87
FIG.6.6 CHLORIDE PROFILE IN CONCRETE SAMPLE (0.55 W/C, 12 DAYS)	88
FIG.6.7 CHLORIDE PROFILE IN CONCRETE SAMPLE (0.65 W/C, 12 DAYS).....	88
FIG.6.8 CHLORIDE PROFILE IN CONCRETE SAMPLE (0.55 W/C, 24 DAYS).....	89
FIG.6.9 CHLORIDE PROFILE IN CONCRETE SAMPLE (0.65 W/C, 24 DAYS).....	89
FIG.6.10 CHLORIDE PROFILE ACCORDING TO DIFFERENT WATER-CEMENT RATIO	91
FIG.6.11 CHLORIDE PROFILE ACCORDING TO DIFFERENT INITIAL TEMPERATURE GRADIENT.....	91
FIG.7.1 SIZE DISTRIBUTION OF TWO TYPES OF RUBBER PARTICLES	96
FIG.7.2 EXPERIMENTAL SET-UPS FOR COMPRESSION AND FLEXURAL TESTS	98

FIG.7.3 PROCEDURE OF PULL-OFF DEBONDING TEST	99
FIG.7.4 PROCEDURE OF CHLORIDE ION PERMEABILITY TEST	100
FIG.7.5 RUBBER MORTAR CUBE SPECIMEN.....	102
FIG.7.6 COMPRESSIVE TEST SET-UP	102
FIG.7.7 STRENGTH OF RUBBER MORTAR ACCORDING TO DIFFERENT RUBBER DOSAGE	103
FIG.7.8 STRENGTH OF RUBBER MORTAR ACCORDING TO DIFFERENT RPP CONTENT	104
FIG.7.9 AVERAGE COMPRESSIVE STRENGTH OF DIFFERENT SIZE OF RUBBER POWDERS	105
FIG.7.10 PULL-OUT DEBONDING TEST SPECIMEN	107
FIG.7.11 DRY SHRINKAGE OF INSULATION MORTAR WITH RUBBER POWDER FOR 90DAYS	108
FIG.7.12 RELATIONSHIP BETWEEN VARIOUS MEASURED AND DERIVED STRAIN VALUES	109
FIG.7.13 IMAGES OF SEM ON THE MORTAR SPECIMENS.	112
FIG.8.1 SET-UP AND PROCEDURE OF COMPRESSION TEST	118
FIG.8.2 STRESS-STRAIN CURVE IN DRY AND WET PROCESS.....	119
FIG.8.3 STRENGTH IN DRY AND WET PROCESS ACCORDING TO RUBBER DOSAGE	120
FIG.8.4 NORMALIZED STRESS-STRAIN CURVE AT 30% OF RUBBER DOSAGE	120
FIG.8.5 COMBINED MIXING PROCESS.....	121
FIG.8.6 STRENGTH COMPARISON WITH VARIOUS PROCESS.....	122
FIG.8.7 STRAIN-STRESS CURVE OF SRC SPECIMEN MADE BY COMBINED PROCESSOR.....	123
FIG.8.8 CHARGE ACCORDING TO RUBBER DOSAGE.....	124
FIG.8.9 TEMPERATURE SENSORS IN THE CENTER OF SPECIMEN AND CHAMBER.....	125
FIG.8.10 TEMPERATURE CYCLES IN CHAMBER AND CENTER OF SPECIMEN.....	126
FIG.8.11 SPECIMEN SET-UP IN FREEZE-THAW CHAMBER.....	126
FIG.8.12 EQUIPMENT OF ULTRASONIC PULSE VELOCITY (UPV)	127
FIG.8.13 TRANSMISSION TIME AFTER 300 CYCLES	128
FIG.8.14 EQUIPMENT OF ULTRASONIC PULSE VELOCITY (UPV)	128
FIG.8.15 DIFFERENCE OF STRENGTH AFTER 300 FREEZE-THAW CYCLES	129
FIG.8.16 COMPARISON OF STIFFNESS OF SRC AFTER 300 FREEZE-THAW CYCLES	129

CHAPTER 1

INTRODUCTION

1.1. MOTIVATIONS

Approximately 15% of the bridges in the U.S. are structurally deficient because of corroded steel reinforcement. In 1998, annual direct repair cost for concrete bridges estimates about \$4 billion (FHWA, 1998). The situation is getting worse in recent years because of aging and overuse of the bridge structures.

On the other hand, approximately 15.4 million tons of de-icing salts each year are used on highways and runways in the U.S. (Basu, et al., 1999). The most commonly used de-icing salts are sodium chloride (NaCl), calcium chloride (CaCl₂), and magnesium chloride (MgCl₂). The use of de-icing salts causes rust of bodies and parts of automobile and the corrosion of reinforcing steel in concrete structures of highway roads and bridges.

Therefore, the corrosion of reinforcing steel in reinforced concrete structures has become one of the severe problems affecting safe and efficient operation of the nation's concrete infrastructure system. The corrosion of steel reinforcement reduces the service life of concrete structures, especially in the chloride-rich environments such as marine structures, and roadways and bridge deck subjected to de-icing salts (Basheer et al, 1996). The deterioration process of reinforced concrete structures can be divided into three stages; transport of aggressive chemicals into concrete, corrosion of steel bars, and cracking of concrete cover (Ababneh, 2002). Among the three stages, the first one is the longest one. The entire corrosion process will be briefly discussed and reviewed later in Chapter 2. The focus of the thesis is on

the theoretical and numerical characterization of the first stage.

The research areas of this study are modeling of the transport process and transport mechanism of moisture, chloride, and other ions in non-saturated concrete structures; development of a parallel finite element method that can handle the transport analysis of large-scale reinforced concrete structures; and investigation of long-term durability of sustainable cementitious materials like cement mortar and concrete containing rubber particles from waste tires.

1.2. RESEARCH OBJECTIVES

The overall goal of this study is to evaluate the durability of cementitious material and structures using theoretical, numerical, and experimental methods. In the process of the study, a generalized framework was established which contains systematic prediction models for the transport of multi-species chemicals in non-saturated concrete structures. The coupling effects among moisture, multiple ions, and temperature in concrete materials were taken into account. The system of the coupled equations was solved by a scalable finite element method. The following are the specific objectives of the study.

The numerical analysis of transport of chemicals in concrete was performed by a parallel finite element program with overlapping domain decomposition method. For the parallel implementation of the finite element code, various programs and high level libraries were employed, such as Triangle (Shewchuk, 2005), ParMetis (Karypis, 1996-2005), PETSc (Balay et al., 2008), and MPI (MPICH Team, 2004). The number of processors used in the computation is up to about 2048 and an actual concrete bridge was modeled with approximately 3 million finite elements. The performance of the parallel computational code was evaluated by speed-up.

The theoretical and numerical models developed in this study forms a general framework which can be further extended to consider coupled action of various species and influential factors in a porous media, although the specific physical problem solved in the study was the transport of deicing salts in non-saturated concrete under ambient temperature variation. In order to apply the parallel computing code in a large-scale structure with a realistic boundary condition, various chloride concentrations and

environmental humidity models associated with random stochastic processes were used. Furthermore, material models were developed in order to consider the temperature effect on multi-ionic and moisture transport into non-saturated concrete.

Mechanical and transport properties of sustainable cementitious materials containing rubber particles from waste tires were studied experimentally for their long-term durability. Small rubber particles were used in Portland cement mortar to replace partially natural sand, and the new mortar is called rubberized insulation mortar, which can be used in the construction of exterior walls of residential and commercial buildings to reduce heat transfer and thus increase energy efficiency of the wall. The compression test, pull-out debonding test, dry shrinkage test, and rapid chloride penetration test (RCPT) for mechanical and durability characteristics of the mortar were conducted. In addition, properties of a sustainable concrete made of sulfur and waste rubber particles were studied for their mechanical property and durability performance in terms of chloride ion penetration and freeze-thaw resistance.

1.3. THESIS ORGANIZATION

This thesis has nine chapters. This chapter is an introduction describing background information and objectives of the study. The remaining chapters are organized as follows:

Chapter 2 presents detailed background information of transport mechanisms of chloride ions and deterioration mechanism of chloride-induced corrosion in reinforced concrete structures. Then, parallel computing technique and software used in the study are introduced.

Chapter 3 describes a numerical method for predicting the transport of chloride ions in non-saturated concrete structures. Parallel finite element method is developed to solve the coupled governing equations. For the parallel implementation, an overlapping additive Schwarz method as preconditioner is used. In order to evaluate the performance of the parallel algorithm, the speed-up and efficiency are used as performance indicators.

Chapter 4 introduces a numerical example for large-scale application of the parallel finite element code on an actual reinforced concrete bridge structure. In order to predict numerically the transport process in a

large-scale structure with a realistic boundary condition, various chloride concentrations and environmental humidity models are used. In the parallel computations, the maximum number of processors used in this study is 2048.

Chapter 5 describes the transport mechanisms of multiple components of aggressive chemicals (including but not limited to the chloride) in non-saturated concrete structures. The extension from chloride transport to multi-ionic transport is necessary because different types of deicing salts have been used on highway pavements and bridges for snow and ice controls. Not only is multiple ionic transport mechanism considered but ionic interaction is also taken into account in the governing equations. To this end, the Nernst-Planck equation is used for describing multi-ionic transport processes and it is modified to take into account the moisture effect on the transport of chemicals. The numerical simulations are performed by using finite element method together with the parallel computing technique.

Chapter 6 develops a model to take into account the temperature effect on multi-species transport in non-saturated concrete structures. The Nernst-Planck equation is further modified by incorporating a coupling term related to the temperature effect on ionic transport in concrete. Then, the governing equations are solved numerically by using the parallel finite element method.

Chapter 7 reports the results of an experimental study on the various properties of rubberized insulation mortar. The important experimental parameters are the rubber replacement rate of fine aggregate filler, the content of an additive, and the size of rubber particles. The properties of the insulation mortar are studied by the aid of compression test, rapid chloride permeability test, drying shrinkage test, and pull-out debonding test.

Chapter 8 describes an experimental study on mechanical property and durability performance of Sulfur Rubber Concrete (SRC). The mix design of SRC is optimized in terms of its compressive strength. The durability performance of SRC is studied with the aid of the chloride permeability test and the freeze-thaw test.

Chapter 9 contains conclusions of this study and recommendations for future research.

CHAPTER 2

BACKGROUND ON CHLORIDE-INDUCED STEEL CORROSION IN CONCRETE AND PARALLEL COMPUTING TECHNIQUES

2.1. DURABILITY OF CONCRETE STRUCTURE

2.1.1. *Mechanism of deterioration in reinforced concrete structure*

The durability of a material can be considered as its ability to withstand environmental deterioration. Reinforced concrete is one of the most popularly used materials in construction field. There are several durability problems with concrete. Initial design errors result in built-in problems such as alkali silica reaction (ASR) in which the aggregate in concrete reacts with alkali in the cement paste and produces an expansive gel to cause extensive cracking in the material. Construction defects such as poor workmanship and site practice can cause other types of durability problems. Environmental deteriorations are shown in Fig.2.1.

The onset of a deterioration and its rate may be influenced by the existing defects occurred at the time of construction, or in the very early stage of the life of the structure. At the time of placing a fresh concrete into the mould, the concrete is a fluid mixture consisting of water, cementitious material, fine and coarse aggregates. The top surface of concrete is subject to evaporation and consequent loss of the mixing water. The water lost by the evaporation is usually replaced by water rising to the surface of the concrete. The movement of the solid frame of concrete in response to the reduction of water is resisted by lower (deeper) portion of the concrete. The resistant lead to stress concentration which may cause

cracking. The movement also results in plastic shrinkage cracking because of very low strength at the early age.

As shown in Fig.2.1, concrete in service is exposed to a wide variety of environments for a long time and may degrade as the result of the long-term exposure environment. The internal structure of the matrix of cement paste contains pores of different sizes which form many interconnected passageways. The moisture and aggressive chemicals from the environment can penetrate into concrete along these passageways. The penetration process is quite complicated and will be described briefly in the following section.

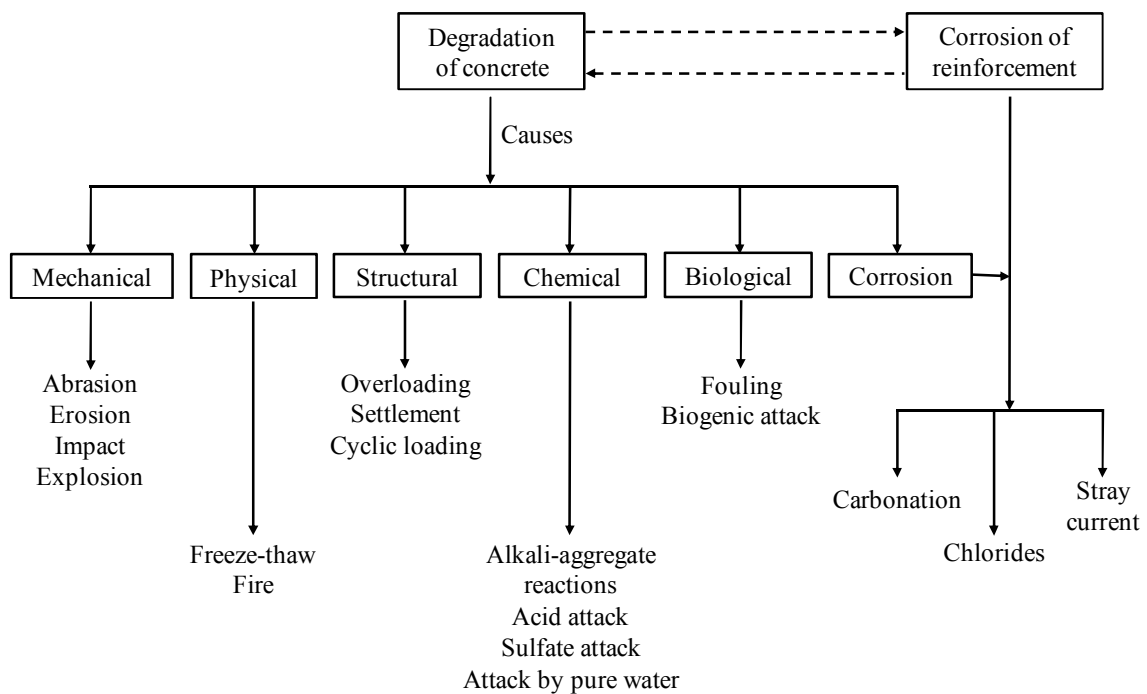


Fig.2.1 Causes of deterioration of reinforced concrete

2.1.2. *Transport processes in reinforced concrete structures*

The transport of fluids and some deleterious chemicals from deicing salts and seawater have a significantly effect on the durability of reinforced concrete as shown in Fig.2.2. Those fluids include gases such as carbon (CO₂) and oxygen (O₂), liquids such as pure water, and dissolved aggressive ions such as sulfates and chlorides. Transport of fluid and ions can be driven by various mechanisms such as pressure gradient, concentration gradient, capillary suction and electrostatic potential gradient. The rate of transport depends on transport properties of concrete properties such as permeability, diffusivity, and sorptivity.

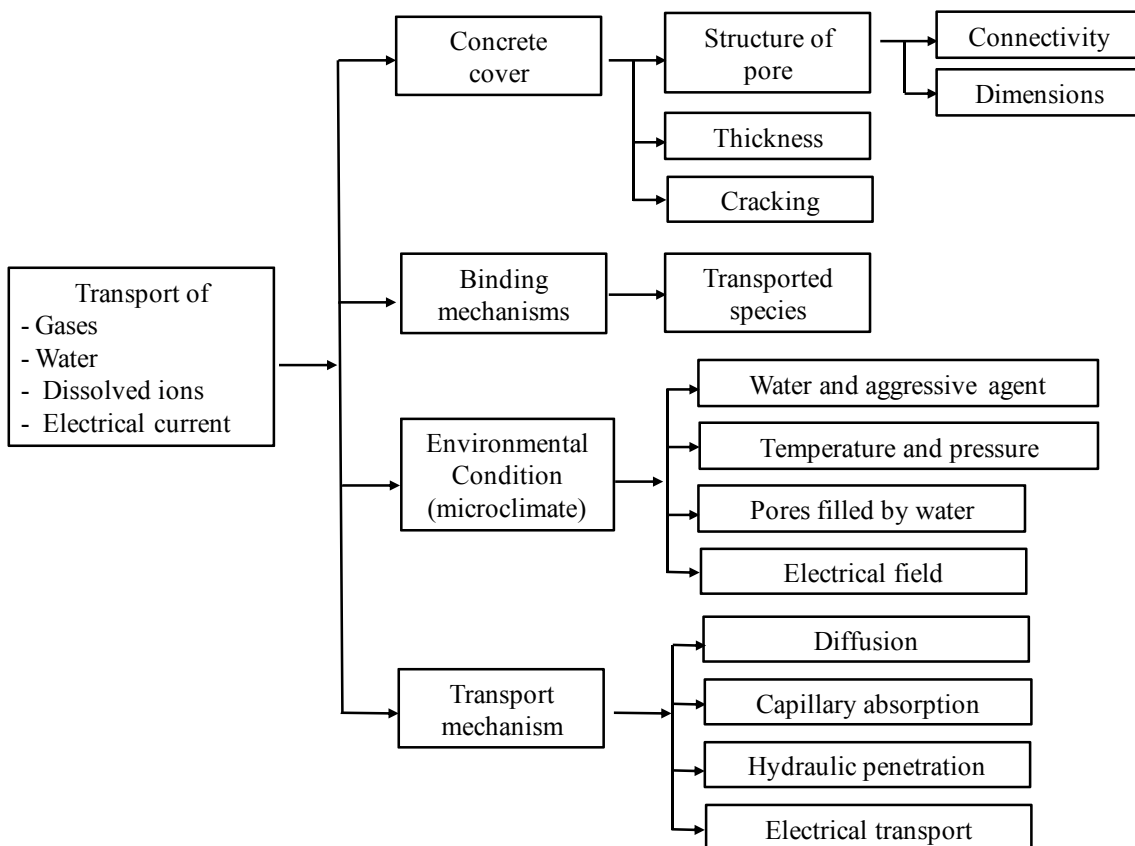


Fig.2.2 Principal factors involved in the transport processes in concrete

The transport properties of concrete are properties of concrete relating to its resistance to the ingress of fluidic and ionic substances and they are decisive factors in terms of the durability of reinforced concrete. Transport properties of concrete rely mainly on its pore structure characterized by porosity, pore size distribution, morphology of pore structure such as shape, connectivity, and tortuosity. Aggregate and cement paste have different pore structures. The pore structure in aggregate is discontinuous, so its contribution to the overall transport processes in concrete is not significant. Therefore, the transport properties of cement paste are very important for the overall transport properties of concrete. The cement paste is composed of calcium silicate hydrate (C-S-H) gel, unhydrated cement particles, calcium hydroxide (CH) crystals, ettringite crystals and pores. The pores in cement paste consists of air voids of 100 μm -10mm, capillary pores of 0.05-100 μm , and gel pores of smaller than 0.05 μm (50nm). The air voids are large and not connected. So, the capillary pores and gel pores have major influence on transport properties of concrete (Ababneh, 2002). These are important factors to consider in the development of theoretical models for transport properties of concrete.

2.1.3. Chloride – induced corrosion in reinforced concrete

Embedded steel in concrete is normally well protected against corrosion, mainly due to the electrochemical passivation of the steel in the highly alkaline pore solution of the concrete. With aging of the concrete structure, the passivity of the steel partly or completely breaks down due to carbonation reaction or chloride ingress, the corrosion of steel starts.

Chlorides stay in concrete in three forms; chemically bound chloride found in the hydration products of cement paste, bound chloride absorbed on the surface of capillary and gel pores, and free chloride diffusing freely through concrete pore networks. The amount of free chloride ions in concrete materials are approximately 20% - 50% of the total chloride ions (Neville, 2002). Many studies have shown that the free chloride (not the total chloride) is the driving force for chloride transport in concrete and it also affect the corrosion mechanism of reinforcement.

As mentioned earlier in Chapter 1, the deterioration process of reinforced concrete structures due

to steel corrosion can be divided in three stages (Ababneh, 2002). The first stage is the period during which chloride ions ingress into concrete and reaches the critical value. As a result, the corrosion of steel bar starts. The second stage is the period during which the rust expansion dominates: the volume of the rust is larger than the volume of the steel when it turns into the rust. The accumulation of rust can lead to a large volume expansion. The third stage is associated with concrete cracking. The propagation of cracks causes the spalling and delamination of the surrounding concrete, as shown in Fig. 2.3. The damage of steel corrosion can affect the serviceability and load-bearing capacity of concrete structures by a reduction of cross-sectional area of steel bar and a weakness of bond strength between rebar and concrete.

Generally, the first stage takes place in the longest time, 15 to 20 years. The period of the second stage is dependent on the porosity of the interfacial transition zone around steel bars and it is generally shorter than the first one. The third process is the shortest one among the three stages because cracks forming around the interface between rebar and concrete develop through the concrete cover in a much faster rate (Ababneh, 2002, Victor et al. 2004).

The corrosion process starts when chloride ions reach the threshold value and then destroy the protective passivity layer. This layer forms on the surface of reinforcing steel bars during the hydration process of cement paste which is a thin protective layer of oxide. In addition, it can protect the steel bar from reacting with oxygen and water thereby preventing steel bars from formation of rust or corrosion (Neville, 2002). As the passivity of the protective layer is destroyed the electrochemical reaction of steel bars starts resulting in the damage process of the corrosion mechanism. The ferrous ions dissolved in the concrete pore water solutions usually react with hydroxide (OH⁻) ions and dissolved oxygen (O₂) molecules to form one of several varieties of rust. There are two electrochemical reactions known as anodic and cathodic reactions as indicated in Fig.2.4.

Anodic reaction : metallic atoms at the steel surface



Cathodic reaction : dissolved oxygen molecules



The hydroxyl ions can combine with ferrous ions as shown in Eq.(2-3).



A further oxidation process of ferrous hydroxide turn into the ferric hydroxide or rust as shown in Eq.(2-4).

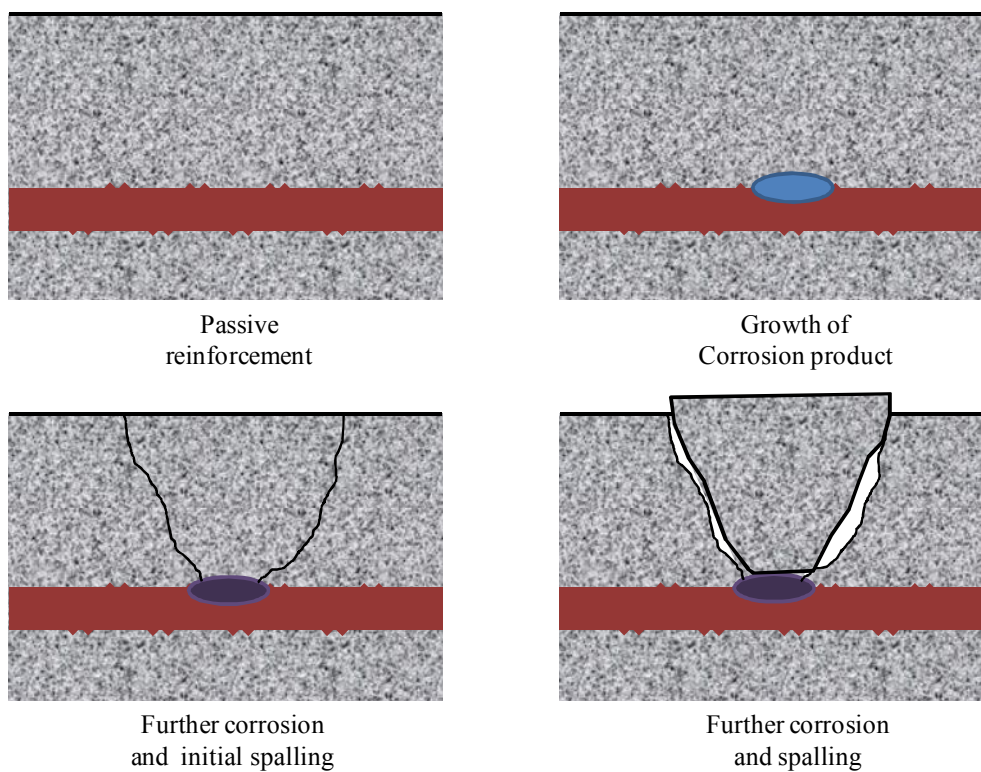


Fig.2.3 Stages in corrosion-induced damage

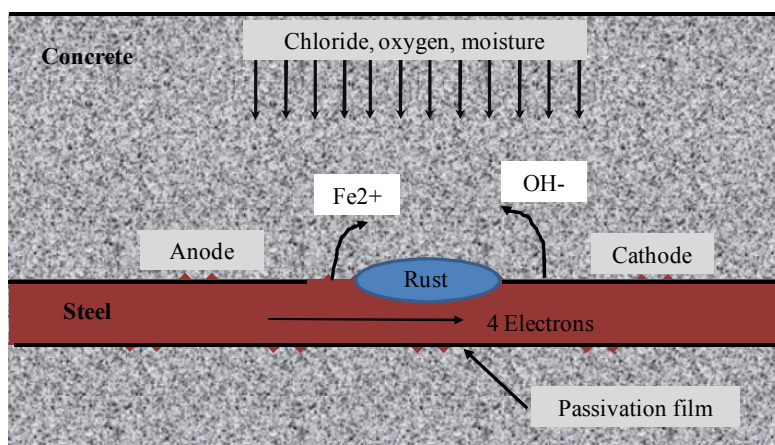


Fig.2.4 Corrosion processes on the surface of steel

2.1.4. Chloride threshold values of the steel corrosion

The chloride threshold value can be defined as the minimum value of chloride concentration that can destroy the passivity layer of embedded steel bars. On the other hand, it can be simply described as the chloride concentration initiates the corrosion mechanism. This value can be considered in two different ways, i.e. in terms of total chloride and free chloride. Many researchers have proposed different chloride threshold values as summarized in Table 2.1. The values are given in different units so there is a need to convert them to an unified unit. Based on AASHTO T 259 and AASHTO T 260, the unit of chloride content is expressed as gram of chloride per gram of concrete (g/g). Therefore, in the present study, we use this unit (g/g) for numerical simulations.

Table.2.1 Chloride threshold values proposed by different researchers

Researchers	Threshold values (gm of chloride / gm of cement)	Type of measured chloride ion	Threshold values (gm of chloride / gm of concrete)
Alonson et al. (2000)	1.24% - 3.08%	Total chloride	0.155% - 0.385%
Alonson et al. (2000)	0.39% - 1.16%	Free chloride	0.049% - 0.145%
Hussain et al. (1995)	0.14% - 0.22%	Free chloride	0.0175% - 0.0275%
Thomas et al. (1990)	0.50%	Total chloride	0.06%
Hansson (1988)	0.6% - 1.4%	Total chloride	0.075% - 0.175%
Hope and IP (1987)	0.097% - 0.19%	Total chloride	0.012% - 0.024%
Gouda (1970)	0.60%	Total chloride	0.08%

The following examples are some unit calculation of chloride content in concrete. Hansson (1988) found the critical chloride content of 0.6% - 1.4% by weight of cement used in concrete. By assuming a cubic meter of concrete contains cement 300 kg; 0.6% - 1.4% of 300 kg cement is 1.8 – 4.2 kg; and then using 2,400 kg/m³ as the density of conventional concrete, thus the critical value is 0.075% - 0.175%. Berke (1986) obtained the critical value of 0.9 – 1.0 kg of chloride per a cubic meter of concrete. As the density of concrete is 2,400 kg/m³, then the critical chloride content in gram of chloride per gram of concrete (g/g) is 0.039% - 0.043%. The chloride threshold values in unit of gram of chloride per gram of concrete proposed by different researchers are given in the fourth column of Table 2.1.

2.2. PARALLEL NUMERICAL COMPUTATION

In the early 1960's, computational analysis technique with finite element method was developed. Finite element method is to obtain the approximate solutions of science or engineering problems with complicated partial differential governing equations. Civil engineers simulate the structural characteristics of large buildings, dams, and highways. Meteorologists use large amounts of computer time to predict the weather changes as well as to make long range predictions of the earth's climate.

To obtain the numerical predictions accurately, a detailed physical and mathematical model is needed. To solve the complicated model problems, fast computational technique is necessary and a parallel computing system becomes favorable.

As will be shown later, in the analysis of transport processes of moisture and aggressive chemicals in concrete, the concentration profiles of the species vary in very shallow portion of the structure, usually in the first a few inches from the surface of the structure. To capture the variation of the species, very small finite element must be used in the structural model, leading to a very large finite element model when a large-scale structure is to be analyzed. In order to handle the large structural model, parallel computing techniques have been used.

A parallel computing system consists of thousands of interconnected microprocessors. There are two memory architectures; shared memory system and distributed memory system. In the study, Blue

Gene/L supercomputer called Frost is used in National Center for Atmospheric Research (NCAR). Frost is a single-rack Blue Gene/L system with 1024 dual-processor compute nodes, and 32 I/O nodes (1 I/O node is allocated for every 32 compute nodes).

The development of parallel finite element program used to be a time consuming and complicated process. However, higher level libraries for parallel implementation such as PETSc (Portable, Extensible Toolkit for Scientific Computation; Balay et al., 2008) can make parallel finite element program relatively easy to develop. PETSc is a suite of data structures and routines for the scalable (parallel) solution of scientific applications modeled by partial differential equations. PETSc uses MPI (Message Passing Interface) standard for communication between processors.

In order to implement the parallel finite element method, a domain decomposition method is employed in this study. There are two types of domain decomposition; overlapping and non-overlapping. These are differentiated by the decomposition into territories on which the elemental sub-problems are defined. The history of domain decomposition was started by H.A. Schwarz in 1869 with the classical paper about the existence of harmonic functions in domains with complicated boundaries. In overlapping domain decomposition methods, the subdomains overlap by more than the interface. This method include the additive and multiplicative Schwarz methods (Cai et al., 1996; Cai et al., 1999). In this study, overlapping additive Schwarz preconditioner will be employed.

CHAPTER 3

PARALLEL COMPUTATION ANALYSIS OF COUPLED CHLORIDE AND MOISTURE DIFFUSION IN CONCRETE

3.1. INTRODUCTION

Most of reinforced concrete structures are affected by chloride attack due to de-icing salt and seawater, which results in penetration of chloride ions into concrete (Han, 2007; Song et al., 2008; Tamimi et al., 2007) and subsequent corrosion of reinforcing steel. The chloride ions penetrate into the concrete and eventually reach the embedded reinforcement bars (rebar). When the concentration of the chloride ion at the location of steel bars exceeds a threshold value, the corrosion of the steel takes place (Basheer et al., 1996; Martin-Perez et al., 2001; Swito et al., 2006; Zhang et al., 2006).

Many researchers have studied chloride diffusion in concrete structures with experimental and numerical methods. Han (2007) investigated the chloride diffusion process with a finite element method for various concrete cover depth, and external and internal conditions. The result of the numerical analysis indicated that the most effective way to reduce the rate of chloride ion penetration is to improve transport properties of concrete by lowering the water-cement ratio. Zhang et al. (1998), Nielsen et al. (2003), Tamimi et al. (2007), and Oh et al. (2007) developed the prediction model of chloride penetration based on the transport mechanism of chloride ion and verified the model with some experiments and numerical simulations. Oh et al. (2007) mentioned that the effective variables are the chloride binding capacity, relative humidity, temperature, exposure condition, and age-dependency. Song et al. (2008) also

studied the influential factors of chloride transport in terms of the diffusion coefficient (D) and surface chloride content (C_s) in marine environment. These two parameters are affected by the proportion of concrete mix, the air void content, the curing method, and the degree of the exposure to the aggressive environment. Martin-Perez et al. (2001) predicted the service life of reinforced concrete structures with chloride diffusion model and finite element formulation.

In all of the researches, the chloride transport in concrete was not related to the moisture diffusion in concrete. In reality, diffusing moisture in concrete carries chloride with it and thus, the moisture diffusion affects the distribution of chloride in concrete. On the other hand, the difference in the chloride concentration (i.e. the chloride concentration gradient) drives the movement of moisture in saturated concrete, which means that the chloride transport influences the moisture diffusion in concrete. To characterize the coupled transport processes, Suwito et al (2006) developed a prediction model based on coupled moisture diffusion and chloride transport in concrete. The coupled governing equations for moisture and chloride transport were solved by a parallel finite element code based on non-overlapping domain decomposition method.

The purpose of this study is to further extend the research and develop a parallel finite element program with overlapping domain decomposition method and predict the chloride and moisture distributions in concrete for long term durability in non-saturated concrete. First, the basic formulation of the coupled transport problem will be introduced. Following, the material models used in the basic equations will be presented, and the finite element method and advantages of the overlapping domain decomposition method will be also discussed. Finally, the numerical prediction will be compared with available test data.

3.2. BASIC FORMULATION AND GOVERNING PARTIAL DIFFERENTIAL EQUATION

The two fully-coupled partial differential equations governing the coupled chloride and moisture diffusion through non-saturated concrete are simply derived by employing the mass balance equations and Fick's law (Xi,1999; Ababneh,2003).

First of all, the flux of chloride ions (J) through a unit area of porous media depends on the gradient of chloride ions as well as the gradient of moisture.

$$J_{cl} = -(D_{cl}\nabla C_f + \varepsilon D_H\nabla H) \quad \text{Eq.(1-1)}$$

$$J_H = -(\delta D_{cl}\nabla C_f + D_H\nabla H) \quad \text{Eq.(1-2)}$$

Where, D_{cl} = chloride diffusion coefficient (cm²/day),

C_f = free chloride concentration (in gram of free chloride per gram of concrete, g/g),

D_H = humidity diffusion coefficient,

H = pore relative humidity and

ε = humidity gradient coefficient, which represents the coupling effect of moisture diffusion on chloride penetration,

δ = chloride gradient coefficient, which represents the coupling effect of chloride ions on moisture diffusion.

When chloride ions diffuse into the concrete, some of them will be bound to the internal surface of the cement paste and aggregate, which are called bound chlorides. These diffuse freely through the concrete. Steel corrosion is related only to the free chloride content but not to the total chloride content (Xi et al, 1999).

The mass balance of chloride ions and moisture can be expressed using Fick's second law as following,

$$\frac{\partial C_t}{\partial t} = \frac{\partial C_t}{\partial C_f} \cdot \frac{\partial C_f}{\partial t} = -\text{div}(J_{Cl}) = \text{div}(D_{Cl}\nabla C_f + \varepsilon D_H\nabla H) \quad \text{Eq.(1-3)}$$

$$\frac{\partial w}{\partial t} = \frac{\partial w}{\partial H} \cdot \frac{\partial H}{\partial t} = -\text{div}(J_H) = \text{div}(\delta D_{Cl}\nabla C_f + D_H\nabla H) \quad \text{Eq.(1-4)}$$

Where, C_t = total chloride concentration (in gram of free chloride per gram of

concrete, g/g),

w = water content,

$\frac{\partial C_t}{\partial C_f}$ =chloride binding capacity,

$\frac{\partial w}{\partial H}$ =moisture binding capacity,

Eq.(1-3) and Eq.(1-4) can be rewritten as,

$$\frac{\partial C_t}{\partial C_f} \cdot \frac{\partial C_f}{\partial t} = \nabla \cdot (D_{Cl} \nabla C_f + \varepsilon D_H \nabla H) = \nabla \cdot (D_{Cl} \nabla C_f + D_\varepsilon \nabla H) \quad \text{Eq.(1-5)}$$

$$\frac{\partial w}{\partial H} \cdot \frac{\partial H}{\partial t} = \text{div}(\delta D_{Cl} \nabla C_f + D_H \nabla H) = \nabla \cdot (D_\delta \nabla C_f + D_H \nabla H) \quad \text{Eq.(1-6)}$$

Where, D_ε = coupling parameter, εD_H

D_δ = coupling parameter, δD_{Cl}

The general boundary conditions are as below,

$$C_f = C_0 \quad \text{on} \quad \Gamma_1 \quad \text{Eq.(1-7)}$$

$$D_{cl} \frac{\partial C_f}{\partial n} + J_{Cl} + D_\varepsilon \frac{\partial H}{\partial n} + \alpha_{cl}(C_f - C_{fa}) = 0 \quad \text{on} \quad \Gamma_2 \quad \text{Eq.(1-8)}$$

$$H = H_0 \quad \text{on} \quad \Gamma_3 \quad \text{Eq.(1-9)}$$

$$D_H \frac{\partial H}{\partial n} + J_H + D_\delta \frac{\partial C_f}{\partial n} + \alpha_H(H - H_a) = 0 \quad \text{on} \quad \Gamma_4 \quad \text{Eq.(1-10)}$$

Where, α_{Cl} = convective chloride coefficient,

α_H = convective relative humidity coefficient,

C_{fa} = ambient chloride ions,

H_a = ambient relative humidity.

Γ_1 and Γ_3 are the part of boundary with a constant chloride ions and relative humidity and Γ_2 and Γ_4 are the part of boundary subjected to a specified chloride ions and relative humidity flux, respectively. Γ_1 and Γ_2 form the complete boundary surface for the chloride ions diffusion problem, and Γ_3 and Γ_4 for the moisture diffusion problem (Suwito et al, 2006).

3.3. MATERIAL PARAMETERS

In order to numerically solve the chloride diffusion problem, many material parameters must be determined; the moisture capacity ($\partial w/\partial H$), chloride binding capacity ($\partial C_t/\partial C_f$), humidity diffusion coefficient (D_H), and chloride diffusion coefficient (D_{Cl}) in Eq. (1-5) and Eq. (1-6) (Ababneh et al, 2003).

3.3.1. *Moisture capacity ($\partial w/\partial H$) and chloride binding capacity ($\partial C_t/\partial C_f$)*

3.3.1.1. *Moisture capacity ($\partial w/\partial H$)*

The moisture capacity of the concrete was developed based on the multiphase and multiscale model (Xi et al, 2000). Assuming that the effect of the shrinkage of concrete can be evaluated simply by the average of the moisture capacities of the aggregate and the cement paste,

$$\frac{\partial w}{\partial H} = f_{agg} \left(\frac{\partial w}{\partial H} \right)_{agg} + f_{cp} \left(\frac{\partial w}{\partial H} \right)_{cp} \quad \text{Eq.(1-11)}$$

Where, f_{agg} and f_{cp} = weight percentages of the aggregate and cement paste,

$\left(\frac{\partial w}{\partial H} \right)_{agg}$ and $\left(\frac{\partial w}{\partial H} \right)_{cp}$ = moisture capacities of aggregate and cement paste, which can

be calculated based on the model developed (Xi et al. 1994a, b) and Xi (1995a, b).

3.3.1.2. Chloride binding capacity ($\partial C_i / \partial C_f$)

A modified relationship between the bound chloride C_b , and the free chloride C_f , was established by Tang and Nilson (1993) based on Freundlich isotherm, and was proposed by Xi and Bazant (1999);

$$C_b = \frac{\beta_{C-S-H}}{1000} \left(\frac{C_f}{35.45 \beta_{sol}} \right)^A 10^B \quad \text{Eq.(1-12)}$$

Which is differentiated with respect to C_f and then one would obtain the chloride binding capacity of concrete as defined by Xi and Bazant (1999) to be;

$$\frac{\partial C_f}{\partial C_i} = \frac{1}{1 + \frac{A \cdot 10^B \cdot \beta_{C-S-H}}{35450 \beta_{sol}} \left(\frac{C_f}{35.45 \beta_{sol}} \right)^{A-1}} \quad \text{Eq.(1-13)}$$

Where, A and B = chloride adsorption related constants, 0.3788 and 1.14,

β_{sol} = ratio of pore solution volume to concrete weight, *Liters / g*,

β_{C-S-H} = weight ratio of C-S-H gel to concrete (g/g),

Based on the definition of β_{sol} , the following equation can be easily derived;

$$\beta_{sol} = \frac{f_{cp} n_{cp} + f_{agg} n_{agg}}{\rho_{sol}} \quad \text{Eq.(1-14)}$$

Where, f_{cp} and f_{agg} = weight percentages of cement paste and aggregate in concrete mix (g/g)

n_{cp} = Cement paste adsorption isotherm,

n_{agg} = aggregate adsorption isotherm,

ρ_{sol} = density of pore solution measured in (*g / liter*),

Specific gravities of concrete and C-S-H are similar, therefore, Xi and Bazant (1999) assumed that the

weight fraction of C-S-H in concrete, β_{C-S-H} , is equal to the volume fraction of C-S-H in concrete, f_{C-S-H} , then,

$$\beta_{C-S-H} = f_{C-S-H} = \frac{V_{total} - V_1 - V_{cp}}{V_{total}} = 1 - f_1 - f_{cp} \quad \text{Eq.(1-15)}$$

Where, f_1 = volume fraction of anhydrous cores of cement particles,

f_{cp} = volume fraction of cement paste capillary pores.

3.3.2. *Moisture diffusion coefficient (D_H) and chloride diffusion coefficient (D_{cl})*

3.3.2.1. *Moisture diffusion coefficient (D_H)*

The humidity diffusion coefficient of concrete depends on the diffusion coefficient of aggregate and the diffusion coefficient of cement paste. Using the composite theory (Christensen, 1979), the effective diffusion coefficient of concrete can be evaluated as following,

$$D_H = D_{Hcp} \cdot \left(1 + g_i \left/ \left[\frac{(1-g_i)}{3} + 1 \left/ \left(\frac{D_{Hagg}}{D_{Hcp}} - 1 \right) \right] \right] \right) \quad \text{Eq.(1-16)}$$

Where, g_i = aggregate volume fraction,

D_{Hcp} = humidity diffusion coefficient of the cement paste,

D_{Hagg} = humidity diffusion coefficient of the aggregates.

The humidity diffusion coefficient of aggregates in concrete is very small due to the fact that the pores in aggregates are discontinuous and enveloped by cement paste and so it can be neglected. The humidity diffusion coefficient of cement paste can be predicted by using the empirical formula described

in Xi et al (1994b).

3.3.2.2. Chloride diffusion coefficient (D_{cl})

Chloride diffusion coefficient in saturated concrete was studied by Xi and Bazant(1999) as following,

$$D_{cl} = f_1(w/c, t_0) \cdot f_2(g_i) \cdot f_3(H) \cdot f_4(T) \cdot f_5(C_f) \quad \text{Eq.(1-17)}$$

In Eq.15, functions represent the chloride ion diffusivity dependence upon the concrete curing time (t_0), gravel volume fraction (g_i), relative humidity (H), temperature (T), and free chloride concentration (C_f), respectively.

First factor of chloride diffusion coefficient accounts for the effect of the water-cement ratio (w/c) and curing time (t_0),

$$f_1(w/c, t_0) = \frac{28 - t_0}{62500} + \left(\frac{1}{4} + \frac{(28 - t_0)}{300} \right) (w/c)^{6.55} \quad \text{Eq.(1-18)}$$

In Eq.(1-18), the second influence factor is to account for the effect of composite action of the aggregate and the cement paste,

$$f_2(g_i) = D_{cp} \left(1 + \frac{g_i}{[1 - g_i]/3 + 1/[(D_{agg}/D_{cp}) - 1]} \right) \quad \text{Eq.(1-19)}$$

Where, g_i = volume fraction of aggregate in the concrete,

D_{agg}, D_{cp} = chloride diffusion coefficient of aggregate and cement paste.

The third factor, $f_3(H)$ is to consider the effect of relative humidity level on the chloride diffusion coefficient. A model proposed by Bazant et al (1972) can be used, which was developed initially for moisture diffusion.

$$f_3(H) = \left[1 + \left(\frac{1-H}{1-H_c} \right)^4 \right]^{-1} \quad \text{Eq.(1-20)}$$

Where, H_c =critical humidity level , 0.75,

Arrhenius law was used by Xi and Bazant(1999) to introduce the temperature effect of the forth factor in chloride diffusion coefficient,

$$f_4(T) = \exp \left[\frac{U}{R} \left(\frac{1}{T_0} - \frac{1}{T} \right) \right] \quad \text{Eq.(1-21)}$$

Where, T_0 and T = reference and current temperatures in Kelvin, $T_0 = 296K$,

R = gas constant, 8.314 J/mole.K,

U= diffusion process activation energy, depending on w/c ratio.

The detail description of diffusion process activation energy, U can be found in the paper of Ababneh et al (2003).

The dependence of chloride diffusion coefficient on free chloride concentration C_f for the fifth factor is presented;

$$f_5(C_f) = 1 - k_{ion} (C_f)^m \quad \text{Eq.(1-22)}$$

Where, k_{ion} and $m = 8.333$ and 0.5 , respectively, by Xi and Bazant (1999).

3.4. FINITE ELEMENT FORMULATION

In order to solve the time-dependent coupled moisture and the chloride diffusion problem, a large linear system equation was derived with finite element method. The finite element formulation will be briefly introduced in this section. The continuous variables in the coupled chloride and moisture diffusion equations, free chloride (C_f) and relative humidity (H_m) are spatially discretized over the space domain,

Ω . The domain discretization can be described,

$$\Omega = \bigcup_{e=1}^{nel} \Omega^e \quad \text{Eq.(1-23)}$$

in which nel is the total number of elements in space domain and Ω^e is an element. It is also defined $\partial\Omega$ as the boundary of computational domain and $\partial\Omega^e$ the boundary of subdomain.

The unknown variables is defined in terms of nodal values, $\{C_f\}$ and $\{H_m\}$,

$$C_f \simeq [N] \left\{ \hat{C}_f \right\} \quad \text{Eq.(1-24)}$$

$$H_m \simeq [N] \left\{ \hat{H}_m \right\} \quad \text{Eq.(1-25)}$$

Where, $[N]$ is the triangle element shape function. The notations $[]$ and $\{ \}$ are row and column vectors, respectively. The element shape functions are expressed as following,

$$[N] = [N_1 \ N_2 \dots \ N_n] \quad \text{Eq.(1-26)}$$

in which N_i is the shape function for node i and n is the total numbers of nodes in an element. The unknown vectors of free chloride $\{\hat{C}_f\}$ and relative humidity $\{\hat{H}_m\}$, can be defined,

$$\{\hat{C}_f\} \equiv \{\hat{C}_1, \hat{C}_2, \hat{C}_3, \dots, \hat{C}_n\} \quad \text{Eq.(1-27)}$$

$$\{\hat{H}_m\} \equiv \{\hat{H}_1, \hat{H}_2, \hat{H}_3, \dots, \hat{H}_n\} \quad \text{Eq.(1-28)}$$

The nodal free chloride concentrations and relative humidity are solved by substituting the approximated values of Eq.(1-24) and Eq.(1-25) into governing equations of Eq.(1-5) and Eq. (1-6), and applying the Galerkin procedure to the weak forms, then the finite element matrix can be obtained as

follows:

$$\frac{d}{dt} \left(\left[C_e(\hat{\phi}) \right] \left\{ \hat{\phi} \right\} \right) = \left[K_e(\hat{\phi}) \right] \left\{ \hat{\phi} \right\} \quad \text{Eq.(1-29)}$$

Where, the element matrices and vector are as follows,

$$[C_e] = \begin{bmatrix} C_c & 0 \\ 0 & C_h \end{bmatrix} \quad \text{Eq.(1-30)}$$

$$[K_e] = \begin{bmatrix} K_{cc} & K_{ch} \\ K_{hc} & K_{hh} \end{bmatrix} \quad \text{Eq.(1-31)}$$

$$\left\{ \hat{\phi} \right\} = \left[\hat{C}_f \hat{H}_m \right] \quad \text{Eq.(1-32)}$$

In detail, the components in element matrices are as below,

$$[K_{cc}] = - \int_{\Omega_e} \nabla [N_c]^T D_{cf} \nabla [N_c] d\Omega + \int_{\partial\Omega_e} [N_c]^T D_{cf} \nabla [N_c] d\Gamma \quad \text{Eq.(1-33)}$$

$$[K_{ch}] = - \int_{\Omega_e} \nabla [N_c]^T D_\varepsilon \nabla [N_h] d\Omega + \int_{\partial\Omega_e} [N_c]^T D_\varepsilon \nabla [N_h] d\Gamma \quad \text{Eq.(1-34)}$$

$$[K_{hc}] = - \int_{\Omega_e} \nabla [N_h]^T D_\delta \nabla [N_c] d\Omega + \int_{\partial\Omega_e} [N_h]^T D_\delta \nabla [N_c] d\Gamma \quad \text{Eq.(1-35)}$$

$$[K_{hh}] = - \int_{\Omega_e} \nabla [N_h]^T D_{Hm} \nabla [N_h] d\Omega + \int_{\partial\Omega_e} [N_h]^T D_{Hm} \nabla [N_h] d\Gamma \quad \text{Eq.(1-36)}$$

$$[C_c] = \int_{\Omega_e} [N_c]^T C_c [N_c] d\Omega \quad \text{Eq.(1-37)}$$

$$[C_h] = \int_{\Omega_e} [N_h]^T C_h [N_h] d\Omega \quad \text{Eq.(1-38)}$$

Finally, Eq.(1-29) is also discretized in time space with time interval $\Delta t = t^{\varepsilon+1} - t^\varepsilon$ as following,

$$\left[\left[C_e(\hat{\phi}) - \theta \cdot \Delta t \cdot K_e(\hat{\phi}) \right] \left\{ \hat{\phi} \right\} \right]^{\xi+1} = \left[\left[C_e(\hat{\phi}) - (1-\theta) \cdot \Delta t \cdot K_e(\hat{\phi}) \right] \left\{ \hat{\phi} \right\} \right]^{\xi} \quad \text{Eq.(1-39)}$$

The value of parameter θ is related to the solution method adopted in the program. Typical values of θ are 0, 1/2 and 1 that correspond to fully explicit, semi-implicit and fully implicit methods, respectively. The semi-implicit method called Crank-Nicholson method is used in this study.

Eq.(1-39) is simplified as linear system equation.

$$[A]^{\xi+1} \left\{ \hat{\phi} \right\}^{\xi+1} = \{b\}^{\xi} \quad \text{Eq.(1-40)}$$

Where,

$$[A]^{\xi+1} = \left[C_e(\hat{\phi}) - \theta \cdot \Delta t \cdot K_e(\hat{\phi}) \right]^{\xi+1} \quad \text{Eq.(1-41)}$$

$$\{b\}^{\xi} = \left[\left[C_e(\hat{\phi}) - (1-\theta) \cdot \Delta t \cdot K_e(\hat{\phi}) \right] \left\{ \hat{\phi} \right\} \right]^{\xi} \quad \text{Eq.(1-42)}$$

3.5. IMPLEMENTATION OF PARALLEL FINITE ELEMENT METHOD

3.5.1. Various programs adapted in parallel finite element program

In order to implement the parallel finite element program in the coupled moisture and chloride diffusion problem, various programs are employed such as Triangle for mesh generation, Parmetis, PETSc, and MPI (Balay et al, 2008; MPI Forum 1994 and 1998; MPICH, 2004; Karypis, 1996-2005; Dalc'in et al, 2005).

In this study, Triangle is used for the mesh generation of triangle element, which is created at Carnegie Mellon University. Triangle generates exact delaunay triangulations, and are suitable for finite element analysis (www.cs.cmu.edu/~quake/triangle.html).

PETSc (3.0.0 p8) is a large and versatile package integrating distributed vectors, distributed matrices in several sparse storage formats, Krylov subspace methods, preconditioners, and Newton-like

nonlinear methods with built-in trust region or linesearch strategies and continuation for robustness. It is designed to provide the numerical infrastructure for application codes involving the implicit numerical solution of PDEs, and it uses on MPI for portability to most parallel machines. The PETSc library is written in C, but may be accessed from user codes written in C, Fortran, and C++.

MPI (Message Passing Interface) is a standardized and portable message-passing system designed to function on a wide variety of parallel computers. The standard defines the syntax and semantics of library routines (MPI is not a programming language extension) and allows users to write portable programs in the main scientific programming languages (Fortran, C, or C++).

Since its release, the MPI specification has become the leading standard for message-passing libraries in the world of parallel computers. Implementations are available from vendors of high-performance computers as a component of the system software, and also from well known open source projects like MPICH.

MPI follows an object oriented design. Among the different abstractions introduced, the communicators play the most important role. Basically, the communicators specify a communication domain between an ordered set of processes or group. This abstraction enables division of processes, and this avoids message conflicts between different modules, and permits extensibility by users.

ParMETIS extends the functionality of METIS and includes routines based on a parallel graph-partitioning algorithm that are especially suited for parallel computations and large-scale numerical simulations involving unstructured meshes.

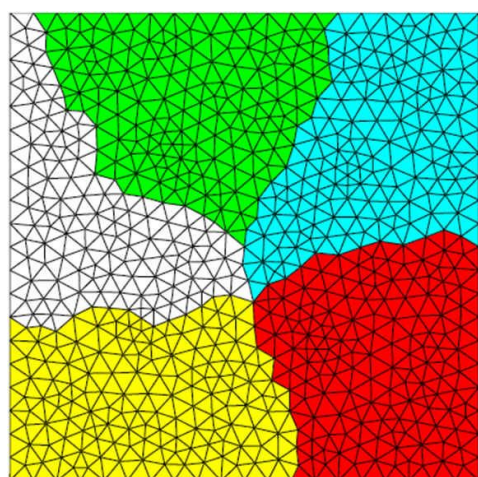
In typical FEM computations, ParMETIS dramatically reduces the time spent in interprocess communication by computing mesh decompositions such that the number of interface nodes/elements is minimized. In particular, ParMETIS provides functionalities for graph and mesh partitioning, dual graph construction, graph repartitioning, partitioning refinement, and sparse matrix reordering.

3.5.2. *Overlapping domain decomposition with additive Schwarz preconditioner*

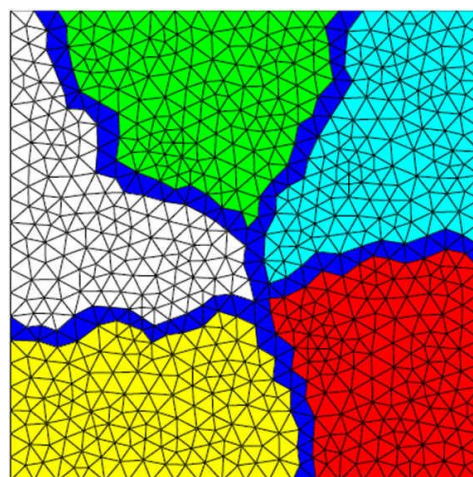
A parallel program is typically developed by dividing the program into multiple fragments that

can execute simultaneously, each on its own processor. In the finite element analysis, this can be accomplished by applying a domain decomposition method. Domain decomposition method is the method usually used for solving large scale system equations and it is also suitable for parallel programming because of data locality (Suwito et al, 2006). There are two types of domain decomposition methods, overlapping and non-overlapping methods as shown in Fig.3.1. In this study, the overlapping method is employed to solve the linear sparse matrix. That is because the advantage of overlapping domain decomposition is easier to setup in algebraic approach and faster convergence than non-overlapping domain decomposition. Furthermore, the boundaries of extended subdomains are smoother than non-overlapping subdomains.

Iterative solver must be used in the iterative domain decomposition method. For this study, the iterative solver GMRES (Generalized Minimal Residual method) was chosen for both global and local matrix. GMRES is mainly chosen because of its ability to solve non-symmetric linear system as in the case of our problem. To improve the convergence of this problem, the additive Schwarz method preconditioner was applied. Fig. 3.2 and 3.3 show the flow chart of parallel pre-process and FE solver.



(a) Non-overlapping domain decomposition



(b) Overlapping domain decomposition with one overlap element

Fig.3.1 Two types of domain decomposition method

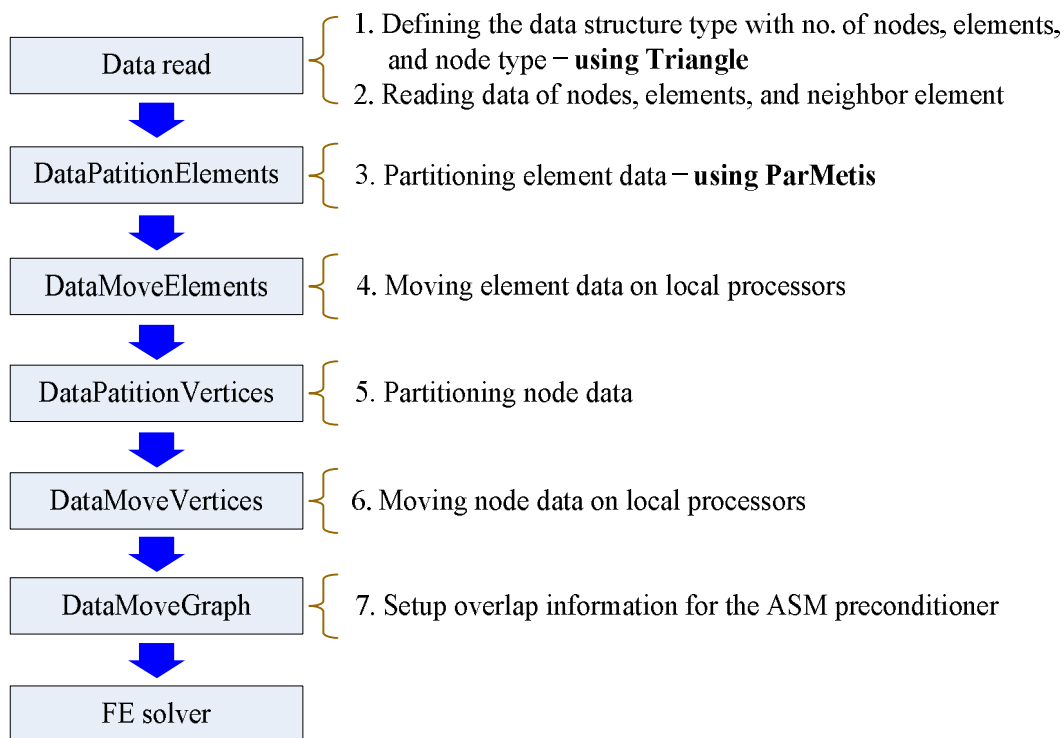


Fig.3.2 Flow chart for parallel pre-process.

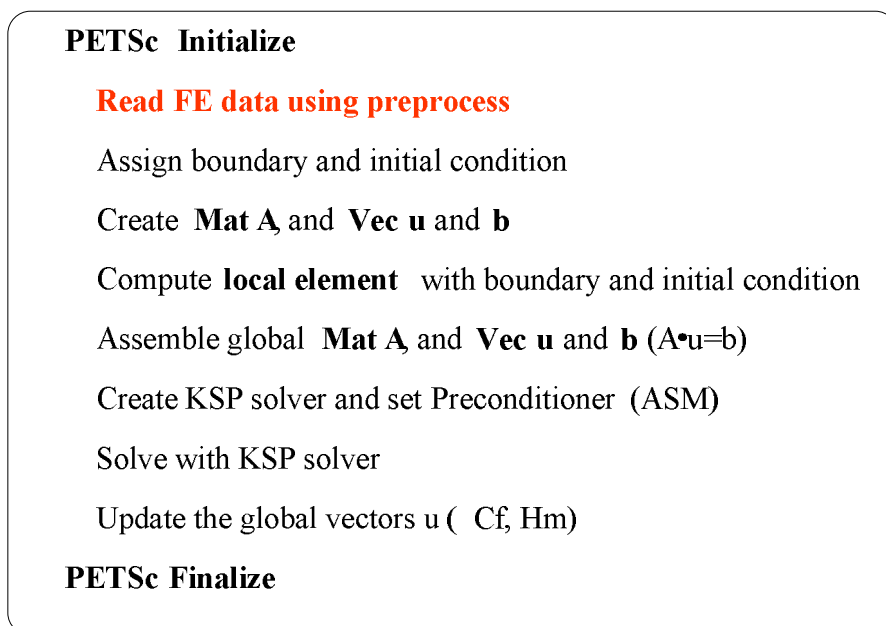


Fig.3.3 Framework of parallel FE method based on PETSc.

3.6. NUMERICAL EXAMPLE

3.6.1. *Validation of parallel finite element program*

The physical model used in the present study is shown in Figure 3.4. It is a concrete slab of 15 cm by 30 cm. The concrete slab contains initially no chloride ions and it has 60% relative humidity (RH). The concrete slab is exposed to 3% NaCl and 100% RH on the top surface. The other boundaries are assumed to be sealed.

Obviously, this example is not to simulate the concrete under service condition, but to simulate the commonly used long-term pond test. With these initial and boundary conditions, one can speculate that the chloride and the moisture diffusions are in the same direction. The material parameters used in the example are shown in Table 3.1. Total analysis time in numerical parameter is one and half year and time step is 0.5 day. There are two stopping condition used in this program; relative tolerance, $Rtol=10^{-4}$ and absolute tolerance, $Atol=10^{-10}$. As previously mentioned, KSP GMRES with additive schwarz preconditioner is used to solve linear large sparse matrix.

Figure 3.5 and 3.6 show the typical finite element mesh used in the analysis and the typical mesh partitioned into 4 and 8 sub-meshes. The mesh is partitioned, and thus each sub-mesh has almost the same number of elements. Also, the number of nodes on sub-mesh boundaries is at its minimal. Approximately 3000 triangle elements are used for the numerical analysis.

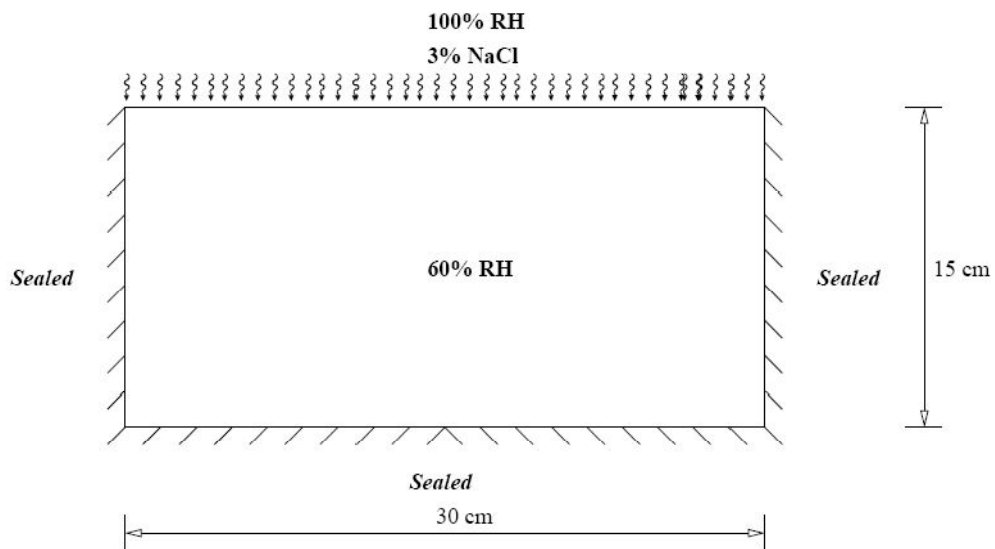


Fig.3.4 The physical model for chloride ion penetration and moisture diffusion in a concrete slab

Table.3.1 Material parameters used in the analysis

Material parameters	value
Water-cement ratio (w/c)	0.55
Curing time (to)	28
Volume fraction of aggregate (gi)	0.65
Cement type	I
Humidity gradient coefficient (ϵ)	0.028
Chloride gradient coefficient (δ)	0.2

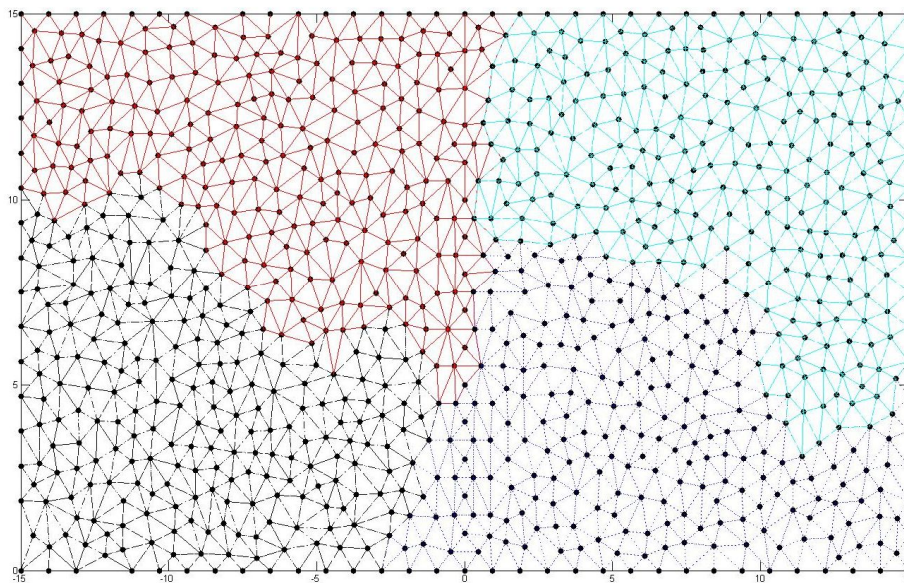


Fig.3.5 An example of mesh partitioning (partitioned into 4 sub-domains)

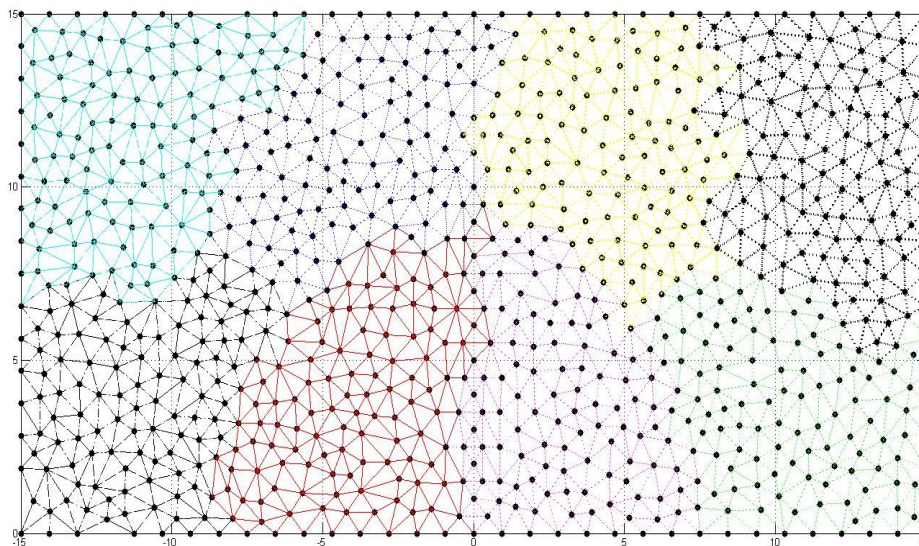


Fig.3.6 An example of mesh partitioning (partitioned into 8 sub-domains)

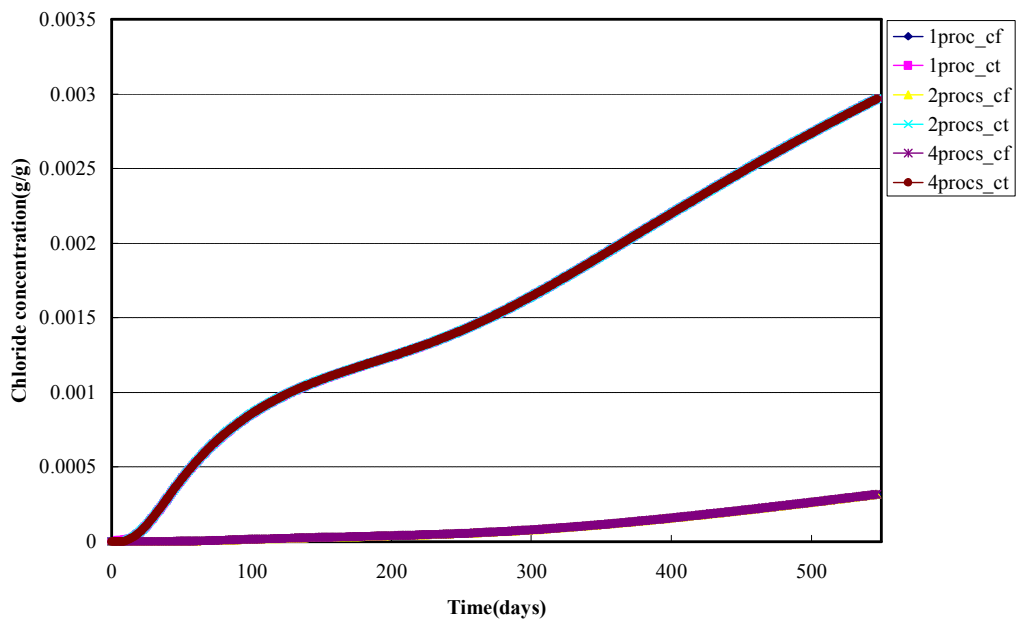


Fig.3.7 chloride concentrations profile in 5cm depth according to no. of processors

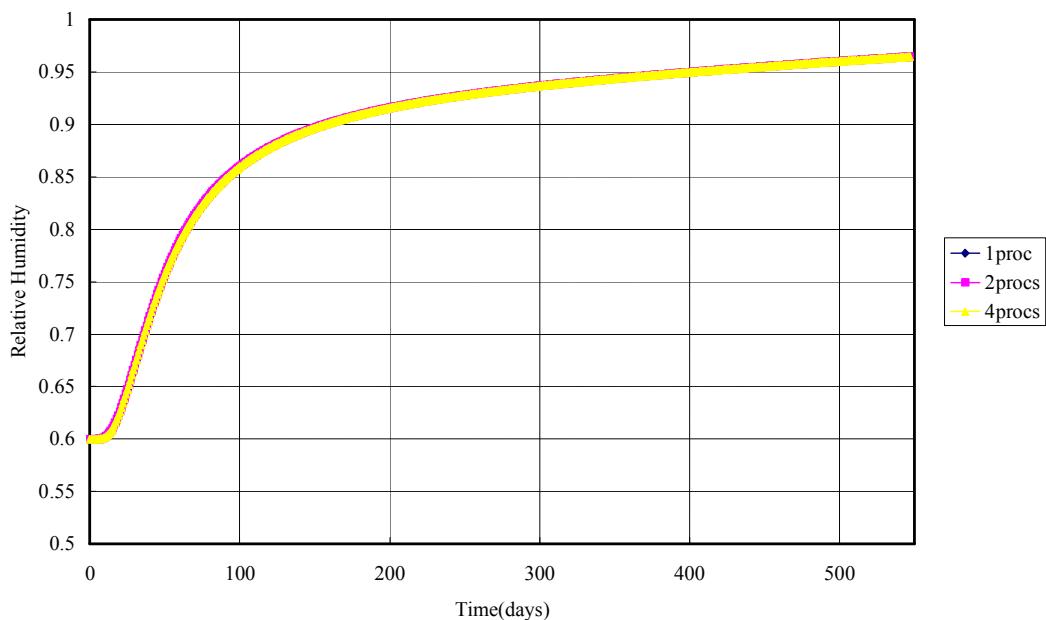


Fig.3.8 relative humidity profile in 5cm depth according to no. of processors

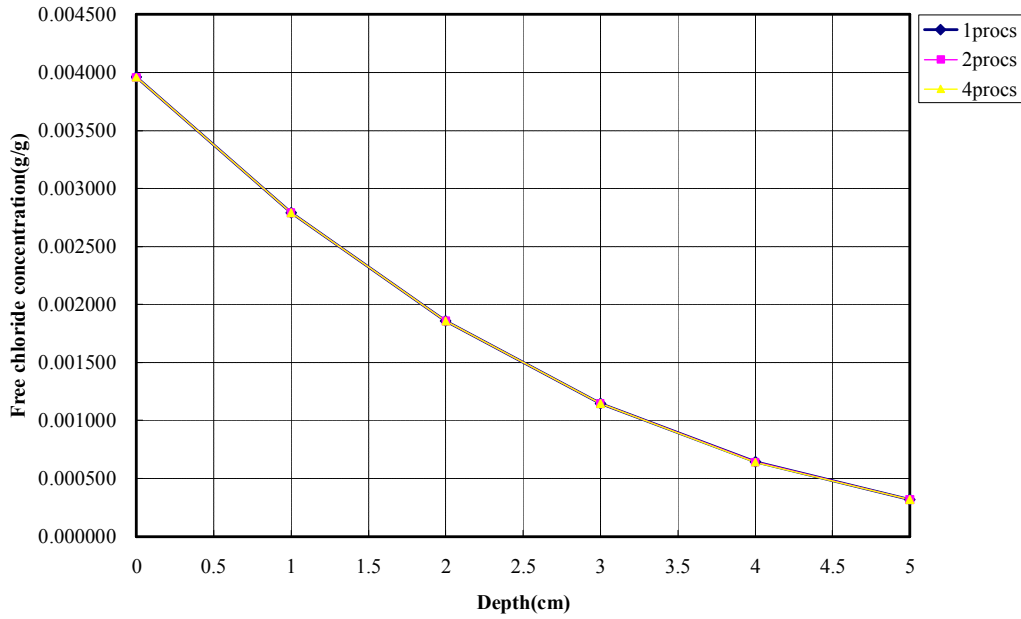


Fig.3.9 Free chloride concentration profile in 5cm depth according to no. of processors

In order to verify the parallel finite element program, the chloride concentrations and the relative humidity according to the number of processors are compared as shown in Figure 3.7 and 3.8. Also, Figure 3.9 shows the free chloride concentrations profile at different depth and 550days.

3.6.2. Speed up and Efficiency

Speed-up and efficiency are necessary to measure the performance of the parallel implementation of the finite element program. The speed-up can be defined as the ratio between the time taken by the code to execute on a single processor, $T_s(n)$, and the time taken for the same code to execute on p processors, $T_p(n)$, as shown,

$$S_p(n) = \frac{T_s(n)}{T_p(n)} \quad \text{Eq.(1-42)}$$

Parallel efficiency can be expressed as the ratio between speed-up and the number of processors,

$$E_p(n) = \frac{S_p(n)}{P} \quad \text{Eq.(1-43)}$$

Four kinds of meshes with the numbers of nodes of 3000, 6000, 12000 and 24000 were analyzed. In addition, the speed of the network plays the important role in the parallel computing. Up to 64 processors were used in the example.

As the number of processors used in the analysis increases, the size of problem solved by each processor decreases. Thus, the speed-up increases with increasing number of processors, as shown in Fig. 3.10. This simply means that the time required for solving the problem becomes shorter when more processors are used in the analysis. But, with more processors, the communication between the processors increases.

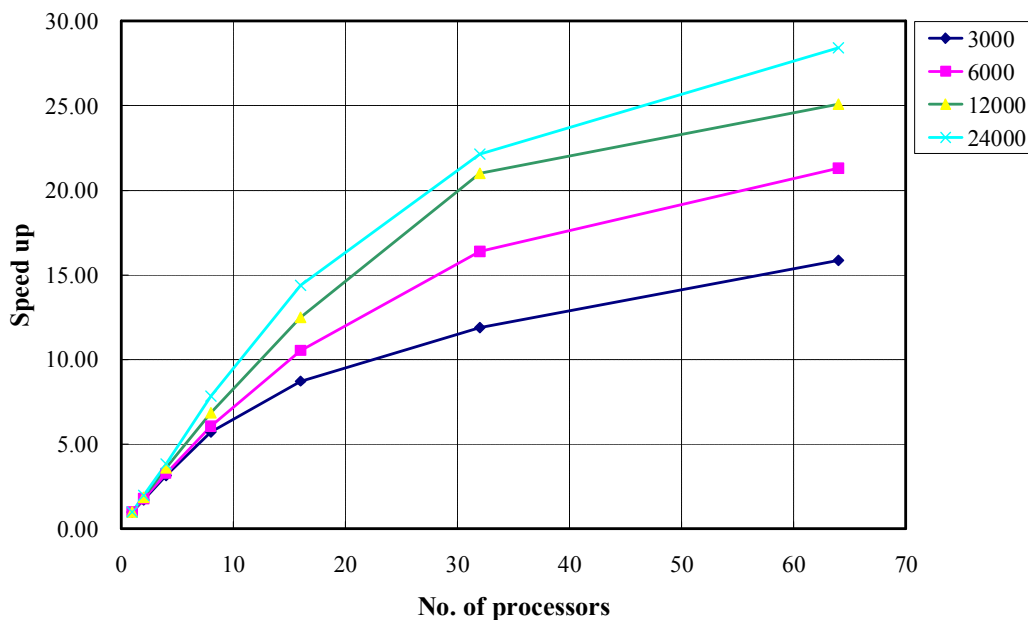


Fig.3.10 Speed up over a number of processors used in the analysis

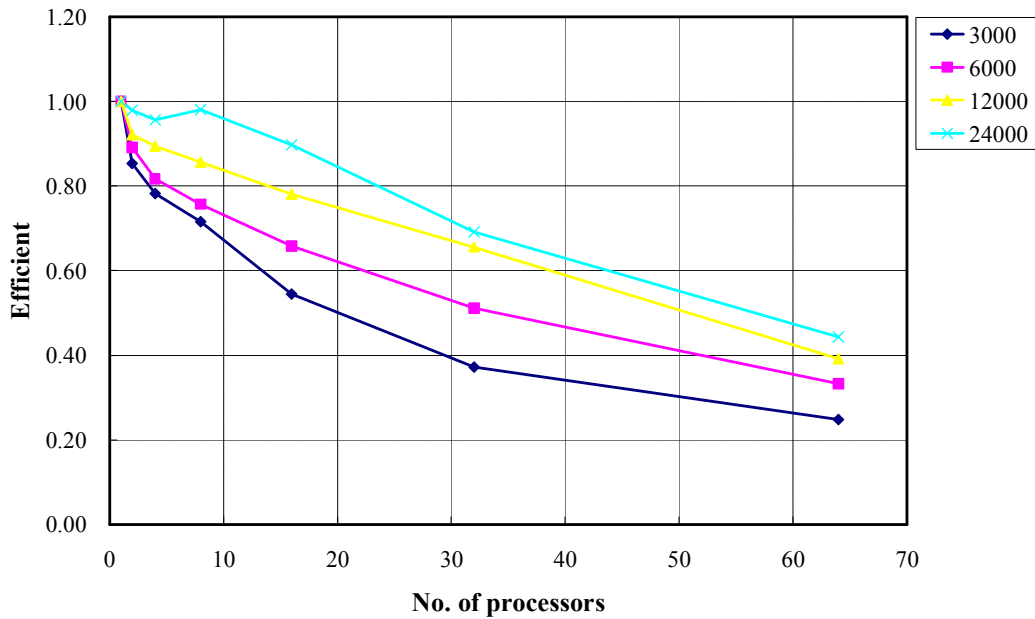


Fig.3.11 Efficiency over a number of processors used in the analysis

3.7. CONCLUSIONS

1. The parallel finite element program is developed based on the robust mathematical material model. The program is used to simulate the coupled moisture and chloride penetration into non-saturated concrete structures. Deicing salts are the sources of chloride ions, which can cause the steel corrosion in reinforced concrete structures. The material parameters related to chloride and moisture diffusion in concrete are taken into account. These parameters include chloride and moisture diffusion coefficients, moisture capacity, and chloride binding capacity.

2. For the implementation of parallel FE analysis, Triangle for mesh generation, ParMetis, PETSc, and MPI are employed. This program also used the overlapping domain decomposition method with additive schwarz preconditioner. As the result of simulation, the computation time is decreased when the number of processors is increased. But, with the more number of processors, the communication between the processors increases.

3. The present model can be used to simulate the non saturated concrete structures subjected to other aggressive chemicals from de-icing salt. The framework of present model can be extended to simulate the multi-species de-icing salts ingress into non-saturated concrete structures in future work. The parallel finite element method is an effective tool and widely used for solving the partial differential equations of mass diffusion.

CHAPTER 4

APPLICATION OF PARALLEL FINITE ELEMENT METHOD OF COUPLED DIFFUSION PROCESSES IN LARGE SCALE CONCRETE STRUCTURES

4.1. INTRODUCTION

The chloride penetration and susceptibility of the reinforced concrete have a considerable impact on the durability of reinforced concrete structures, caused from the induction of the chloride corrosion. About 20% of those structures are exposed to severe environment such as deicing salt or marine condition. Once the chloride content on the surface of steel reinforcement reaches a threshold value and the moisture and oxygen are sufficiently provided, the corrosion of steel bar will be initiated (Ali, 2010; Masi et al. 1997). The corrosion initiation period is the time during which substances such as water, chloride ions, and carbon dioxide flow through the concrete cover. The period depends on the chemical reactions (Conciatori et al., 2008; Conciatori et al., 2010);

In real large concrete bridges, there are various moisture and chloride ion concentrations on the top surface due to weather effect and the use of de-icing salt. Moisture and chloride concentrations will have spatial distributions and seasonal variations. The service life of concrete is not a material property but it follows a combination of material properties and certain microclimatic parameters of the environment. The microclimate is a term for the climatic conditions at the concrete surface or very close to the surface. This condition at a surface has a more decisive effect on the conditions inside the concrete than most other parameters (Nilsson, 1995). The model of microclimate such as environmental humidity

and temperature was proposed by Bazant et al. (1993).

To simulate more realistic structural performance of concrete bridges, complex scientific methods such as finite element method including finite difference method, and finite volume method and more accurate and elaborate material model are needed. In order to predict realistic results of corrosion initiation time and to describe the thin layer from concrete surface to reinforcement, large FE mesh is needed. For large meshes, parallel algorithm and more processor units should be employed, up to 2000 processors.

To consider more realistic boundary conditions on a bridge structure, humidity model applied with random stochastic process is employed and approximately 1.5 million nodes and 3 million elements is used. The previous parallel program handles only constant boundary conditions. In this chapter, multi-boundary condition to describe the actual chloride concentration and humidity diffusion will be handled instead of only constant boundary condition.

4.2. APPLIED BRIDGE OVERVIEW

The bridge is located on Highway 83 at the edge of Castlewood Canyon State Park in the Black Forest of central Colorado. The original two-lane reinforced concrete arch bridge was built in 1946. The arches are 6'-4" wide by 5'-10" deep at the base with the depth tapering down to 3'-4" at the highest point. This bridge was severely dilapidated and is in need of repairing, enlarging, and strengthening. Parts of the soft concrete had spalled off of the deck, columns, and arches, and the steel rebar under concrete were severely rusted. In 2003, the original arch was repaired, the spandrel columns were replaced, the bridge deck was replaced and widened from about 35' to 43' including railings, and the overall length was increased from 373'-6" to 404'-5" as follows.

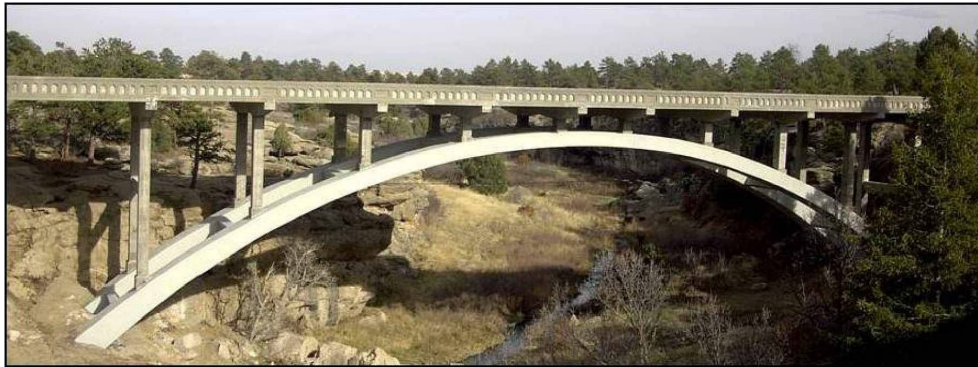


Fig.4.1 Castlewood Canyon bridge, Franktown, Colorado

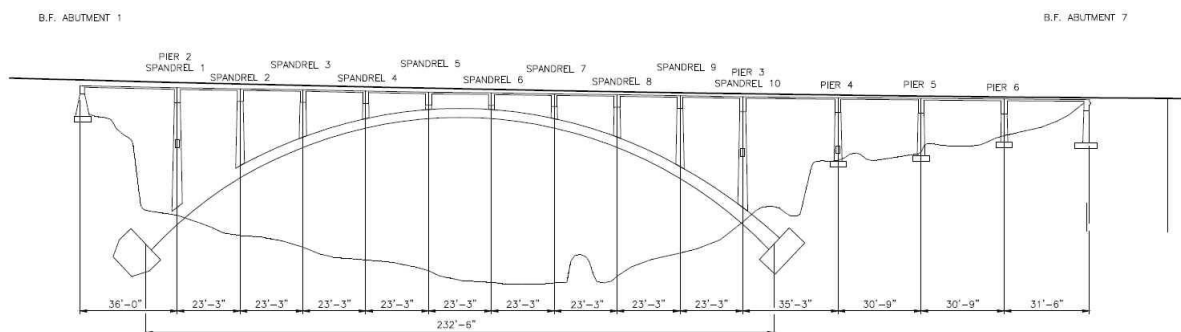


Fig.4.2 Geometry of Castlewood Canyon bridge

4.3. PARALLEL FINITE METHOD OF LARGE-SCALE CONCRETE STRUCTURE

4.3.1. *Modeling of Castle wood canyon bridge with large meshes*

In order to analyze the penetration of chloride and humidity in a real bridge, a large number of meshes is needed to capture the penetration phenomenon within thin layer from concrete top surface to steel rebar. In previous chapter, the number of nodes and elements was generated. Triangle as mesh generator was used. Triangle is specialized for creating two-dimensional finite element meshes, but can also perform simpler related tasks such as forming Delaunay triangulations. For castle wood canyon bridge, about 1.5 million nodes and 3 million elements were generated for input files as shown in Fig.4.3. To visualize and check the mesh size and shape, ParaView was employed as illustrated in Fig. 4.4. ParaView is an open-source, multi-platform data analysis and visualization application. It is easy to build visualizations in a short period of time to analyze their data using qualitative and quantitative techniques. ParaView was developed to analyze extremely large datasets using distributed memory computing resources. It can be run on supercomputers to analyze datasets of terascale as well as on laptops for smaller data. ParaView can read the VTK file format. The simplest are the legacy, serial formats that are easy to read and write either by hand or programmatically. This file format is automatically created when the program runs. For partitioning origin meshes, Parmetis was used to be embedded in the parallel program to automatically partition. ParMETIS is an MPI-based parallel library that implements a variety of algorithms for partitioning unstructured graphs, meshes, and for computing fill-reducing orderings of sparse matrices. ParMETIS extends the functionality provided by METIS and includes routines that are especially suited for parallel AMR computations and large scale numerical simulations. The algorithms implemented in ParMETIS are based on the parallel multilevel k -way graph-partitioning, adaptive repartitioning, and parallel multi-constrained partitioning schemes developed.

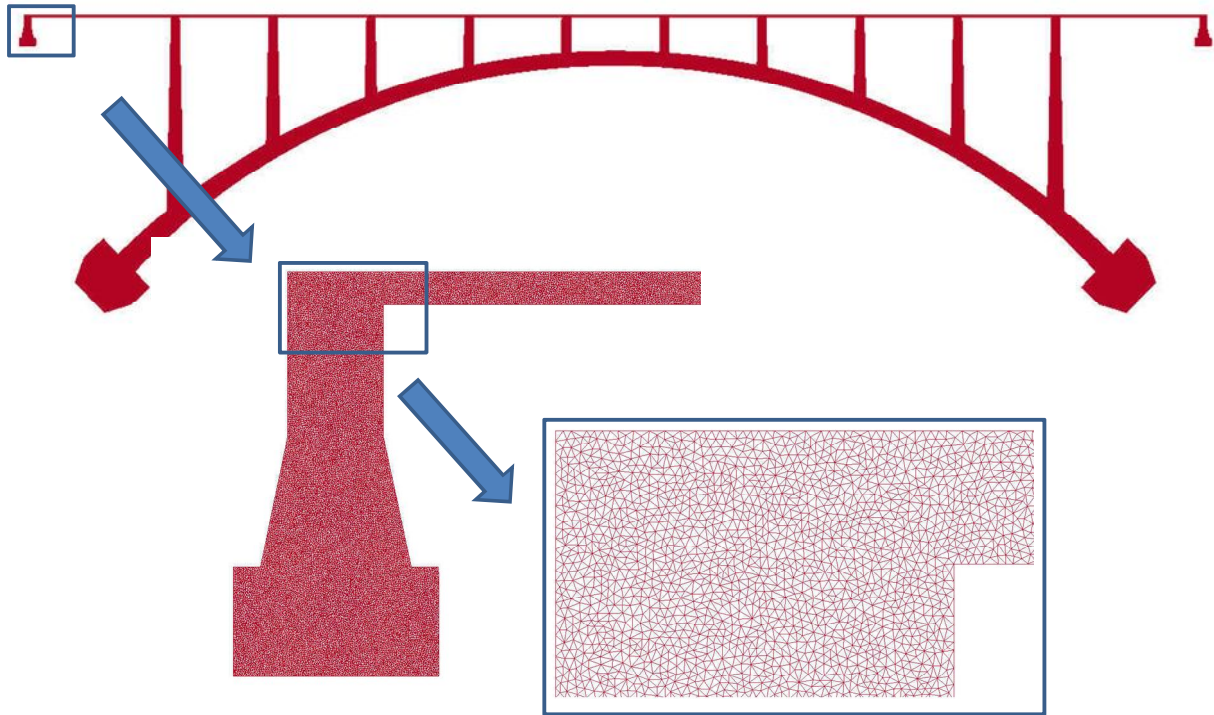


Fig.4.3 Modelling of Castlewood Canyon bridge

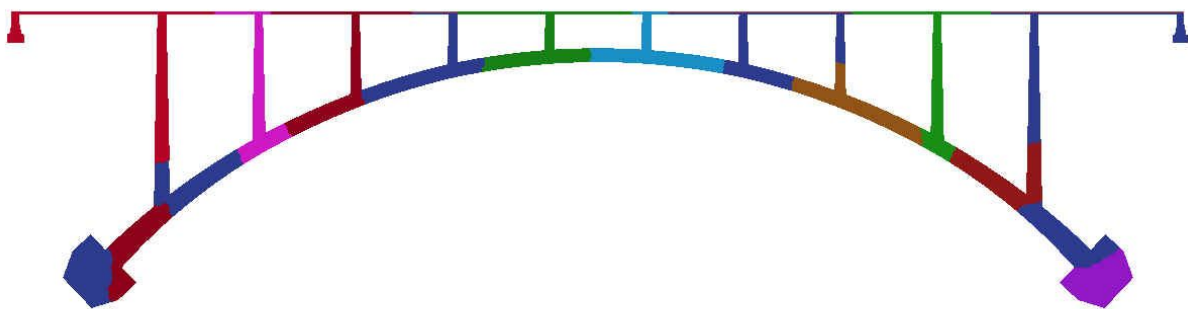


Fig.4.4 Partitioning of Castlewood Canyon bridge with 16 processors

4.3.2. *Environmental humidity model*

Environmental humidity model plays an important role of diffusion of chloride in concrete. The humidity model used in this study was proposed by Bazant and Xi (1993). Even though the moisture and temperature transport in concrete are coupled, humidity fluctuation was considered and temperature was assumed to be constant during analysis time. To establish a practicable but realistic humidity input model, the comparison of real climate record is needed as shown in Fig.4.5.

The environmental total input humidity model, consists of three different components as shown in Eq.(4-1): First, H_1 is the mean value, standing for the stable horizontal trend. Second, H_2 is a random phase process corresponding to the harmonic variation of humidity. Third, H_3 is a random normal distribution with a specific mean and variance (Bazant et al.,1993).

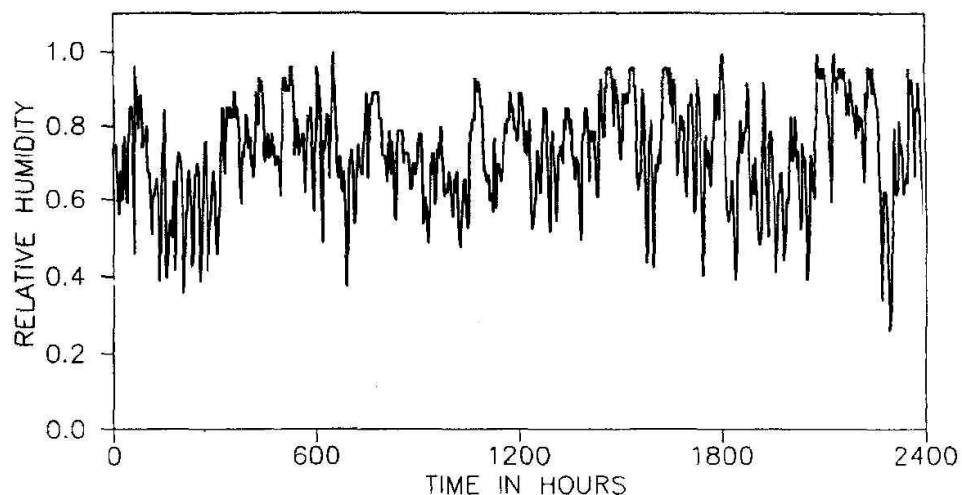
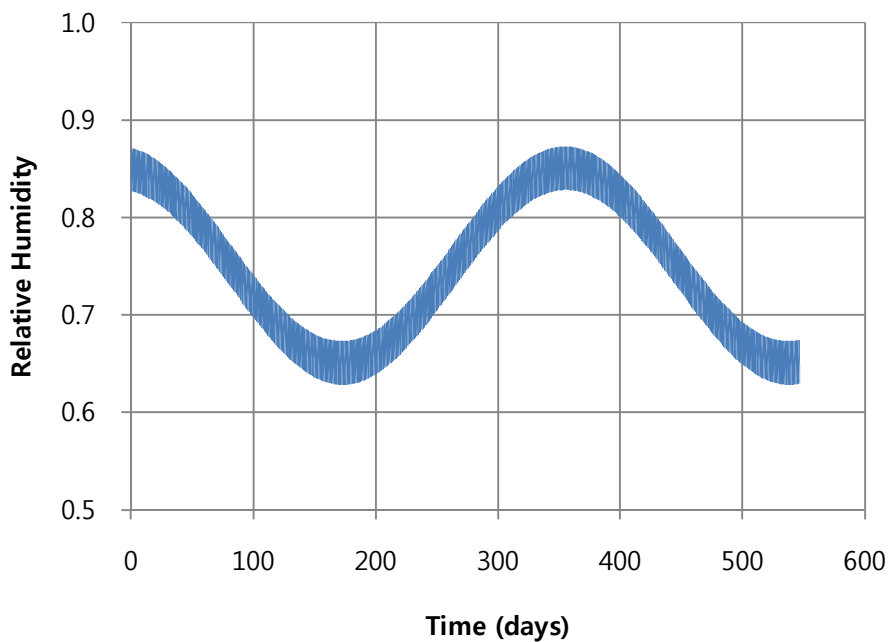
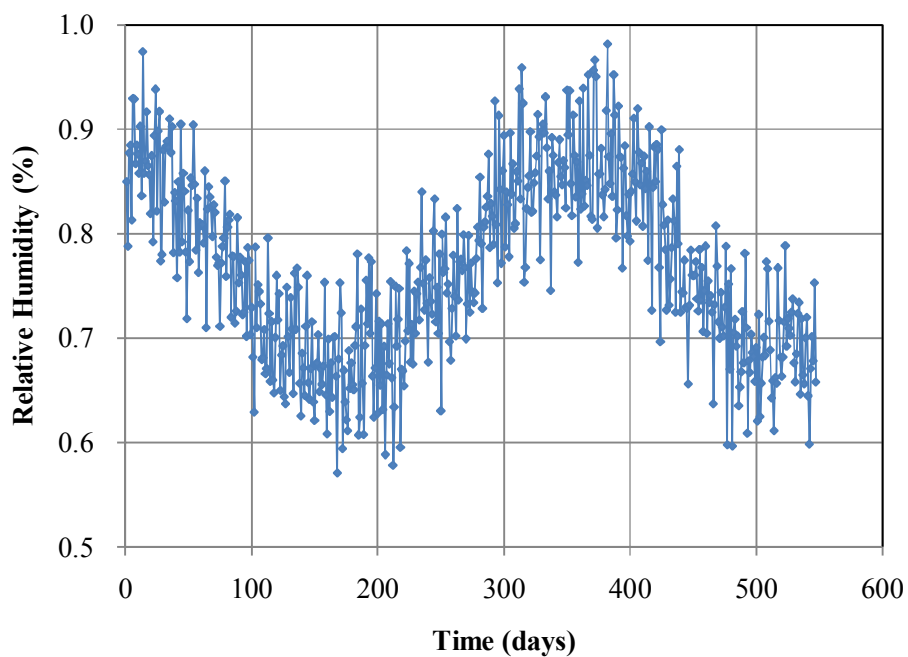


Fig.4.5 Environmental humidity Record, midway station, Chicago (Bazant et al,1993)



(a) Humidity model without random noise



(b) Humidity model with three components (including random noise)

Fig.4.6 Environmental humidity model

$$H = H_1 + H_2 + H_3 \quad \text{Eq.(4-1)}$$

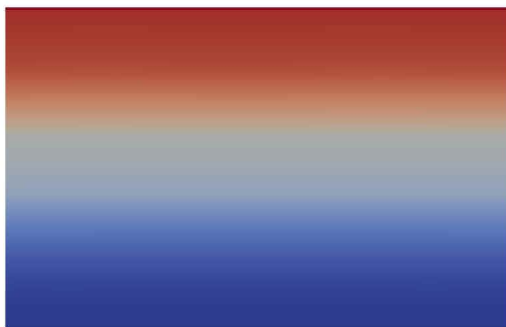
Where, $H_1 = \bar{H}$, mean value of environmental model

$H_2 = A_1 \cos(2\pi t + \varphi_1) + A_{365} \cos(2\pi t + \varphi_{365})$, the random phase process of a one day period with $A_1=0.1$ and the random phase process of a one year period with $A_{365}=0.08$, φ_1 and φ_{365} have uniform distributions with constant density $\frac{1}{2\pi}$,

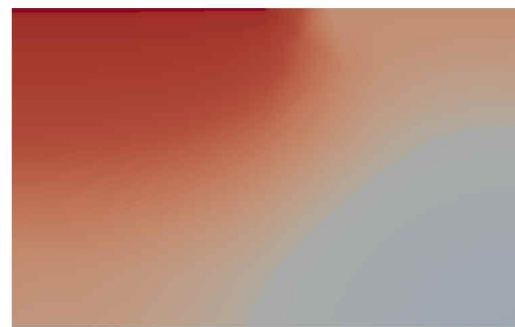
$$H_3 = \frac{1}{\sqrt{2\pi\sigma^2}} e^{-\left[\frac{(x-\mu)^2}{2\sigma^2}\right]}, \text{ normally distributed random numbers are generated with}$$

specific mean and variance, 0.0046 (Bazant et al., 1993).

For the chloride concentration on the top surface of concrete, various boundary conditions were used to actualize the realistic boundary condition as illustrated in Fig.4.7. One can see that the interference between the interfaces of different concentration.



(a)Single boundary condition



(b)Two boundary condition

Fig.4.7 Comparison of single and various boundary condition

4.4. NUMRERICAL RESULTS AND DISCUSSION

4.4.1. *Speed up*

In order to measure the performance of the parallel implementation of finite element program, Speed-up and efficient are needed in accordance to the number of processors. The definition of speed up and efficient was mentioned in the previous chapter. In this chapter, the mesh with the number of about 1.5 million nodes was analyzed for speed up and the number of processors was used from 8 processors to 2048 processors. When using up to 8 processors, the program was not operated due to memory capacity, which can be assigned input data on each memory.

As the number of processors used in the analysis increases, speed up is improved up to 512 processors, which means that speed up is better than ideal condition. After more processors are used in the analysis, speed up gradually increased, which means that the communication time between the processors increases. As shown in Fig.4.8, one can see the optimum point of number of processors.

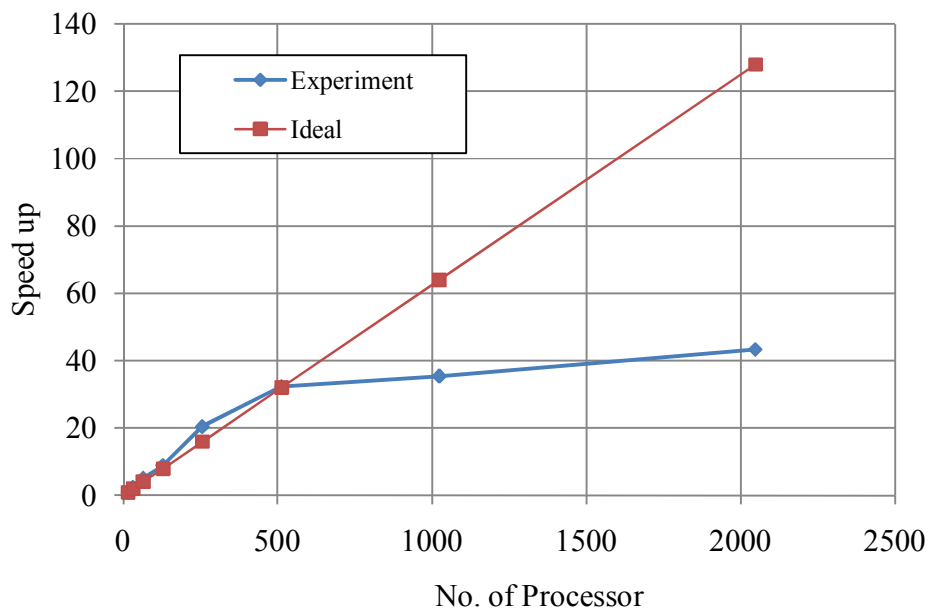


Fig.4.8 Speed up over number of processors

4.4.2. *Effect of Boundary Condition*

4.4.2.1. *Constant boundary condition*

The physical and material model used in the present study was mentioned in previous chapter. The castle wood canyon bridge is the concrete model mentioned in Fig.4.1 and 4.3. The concrete bridge contains initially no chloride ions and has 60% relative humidity (RH). The top surface of concrete bridge is exposed to 3% NaCl and 100% RH. To analyze the diffusion of coupled chloride and humidity, from 8 to 2048 processors and about 1.5 million nodes are used with parallel finite element method.

Obviously, this example is not to simulate the concrete under service condition. With these initial and boundary conditions, one can speculate that the chloride and the moisture diffusions are in the same direction. The material parameters used in the example are shown in Table 3.1. The typical finite element mesh used in the analysis and the typical mesh partitioned into 16 sub-meshes are shown in Fig.4.3 and 4.4. The mesh is partitioned by ParMetis so that each sub-mesh has almost the same number of elements.

Fig.4.9 and 4.10 show the contour of chloride and humidity distribution into the entire domain. The total and free chloride concentration at 50mm below from top surface of concrete is Fig.4.11 and the relative humidity is Fig.4.12 over time up to 550 days. As the result of analysis, the concentration of chloride and humidity is continuously accumulated inside concrete. Specially, the variation of humidity inside concrete might not be increased in reality due to the seasonally change of the humidity distribution, so that periodic humidity model should be applied to the boundary condition.

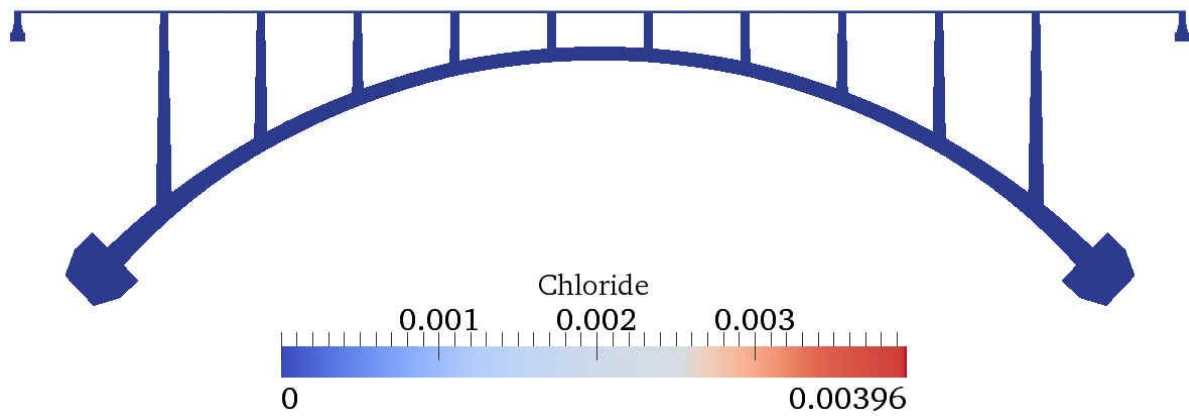


Fig.4.9 Contour of chloride distribution

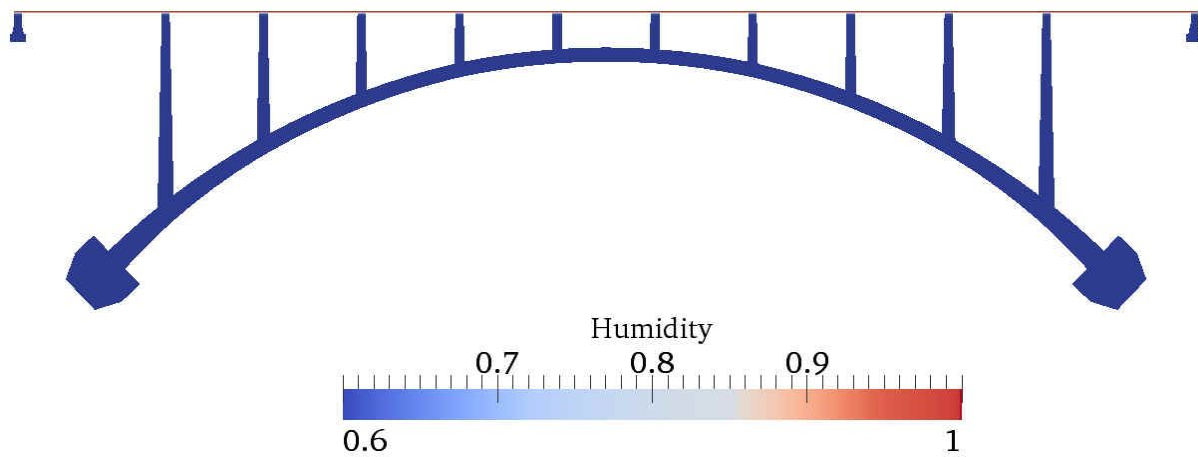


Fig.4.10 Contour of humidity distribution

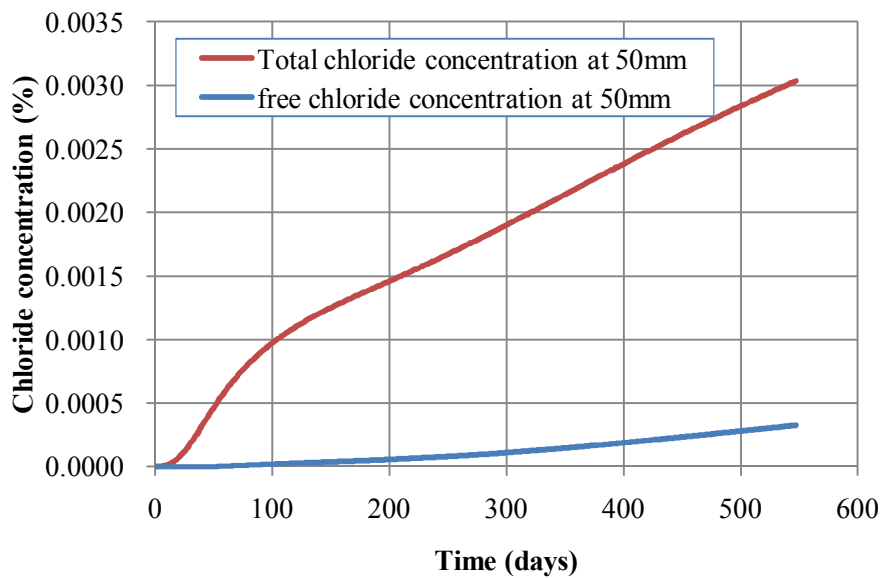


Fig.4.11 Chloride concentration over time at 50mm depth

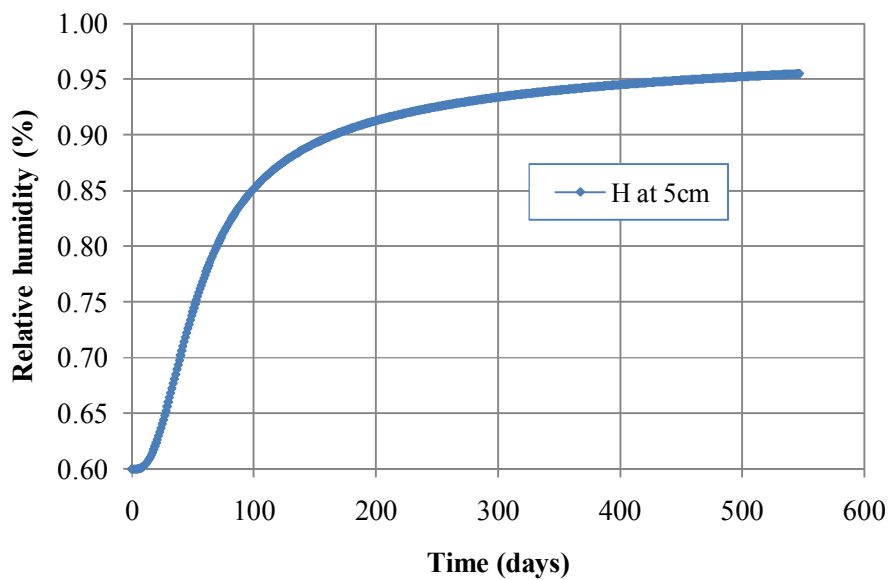


Fig.4.12 Humidity over time at 50mm depth

4.4.2.2. *Periodic boundary condition*

In order to simulate the real diffusion phenomenon in concrete, the periodic boundary condition is should required. Fig.4.13 and 4.14 show the result of chloride concentration and relative humidity at different depth over time. As shown in Fig.4.13, total concentration is gradually increasing until almost one year. That is because the chloride concentration was affected by the periodic humidity boundary condition. After one year it suddenly increased caused by the influence of the constant chloride initial condition. However, the total chloride concentration at 50mm was reduced up to 15% rather than the concentration using constant boundary. In order to predict and demonstrate the realistic and seasonal chloride diffusion through concrete cover, seasonal change information of chloride concentration on the top surface of concrete deck.

In Fig.4.13, the change of humidity distribution is influenced from the humidity model inputted as boundary condition. The short period random noise can only reach a shallow portion near the top surface of concrete deck. As the concrete depth is increased, the effect of short period random noise decreases. However, the seasonal change of humidity concentration has an influence on 50mm depth of concrete deck. At the 50mm from the top surface of concrete deck, the maximum value of humidity is about 77%, which is decreasing up to 20% comparing with constant boundary condition. Also, the result about 500 days shows that the humidity trend is reversed between 10mm and 50mm, which means that evaporation of humidity just near concrete surface is easier than evaporation at 50mm. Therefore, this prediction model is reasonable and effective to observe the diffusion of chloride and humidity.

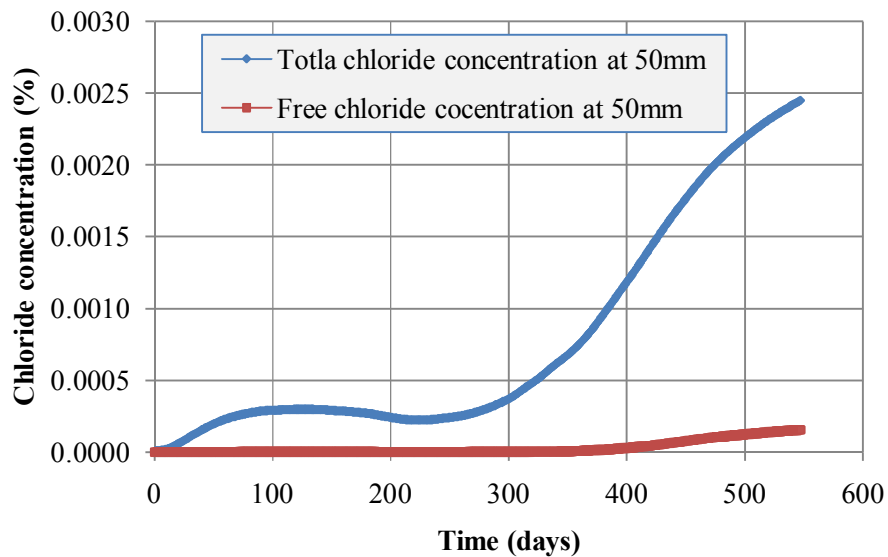


Fig.4.13 Chloride concentration over time at 50mm depth

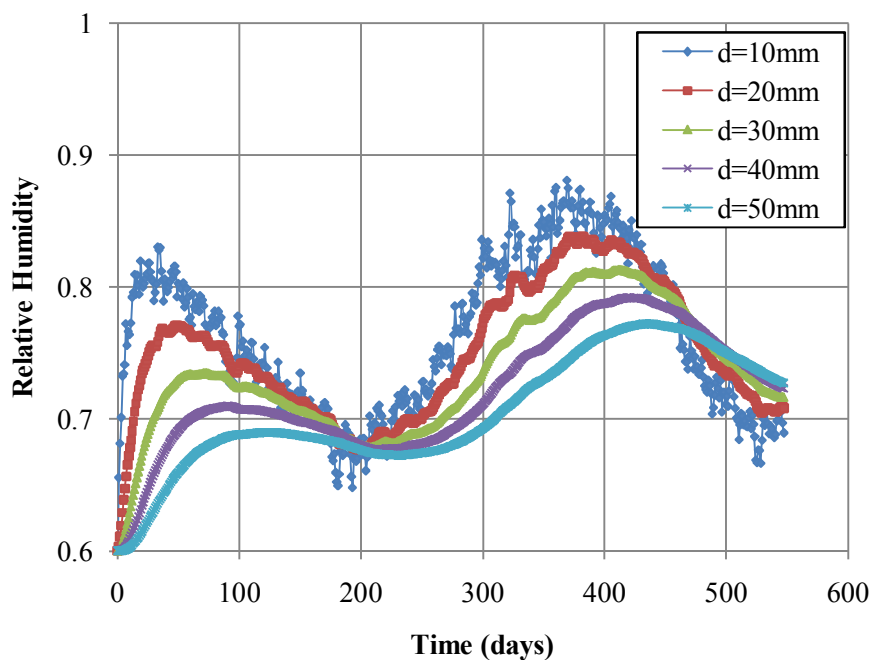


Fig.4.14 Humidity over time according to depth

4.5. CONCLUSIONS

In order to simulate more realistical structural performance of concrete bridges, the parallel finite element program was developed based on the handling of large scale meshes and number of processor, associating with the overlapping domain decomposition method with additive schwarz preconditioner.

1. In order to measure the performance of the parallel implementation of finite element program, Speed-up was investigated in order to solve the optimum number of processors with about 1.5 million nodes. When using up to 8 processors, the program was not operated due to memory capacity. As increasing the number of processors, however, speed up is improved up to 512 processors. After more processors are used in the analysis, speed up gradually increased, which means that the communication time between the processors increases. The optimum number was 256 processors.

2. In order to actualize the numerical model and observe the effect of boundary condition, the constant and periodic boundary conditions were used to comparing the diffusion of chloride and humidity within concrete. Temperature effect was assumed as constant in this study. The concentration of chloride and humidity is continuously accumulated and increased inside concrete. Due to the seasonally change of the humidity distribution, relative humidity inside concrete might not be continuously increased in reality, so that periodic humidity model should be applied to the boundary condition.

3. Environmental humidity model associated with random process was used as boundary condition. At the 50mm from the top surface of concrete, the maximum value of humidity is decreased up to 20% comparing with using constant boundary condition. Also, the result about 500 days indicates that the humidity trend is reversed between 10mm and 50mm and humidity easily is exchanged near concrete surface. Therefore, this prediction model is reasonable and effective to observe the diffusion of chloride and humidity and to predict the chloride initial time on reinforcement. The parallel finite element method is an effective tool and widely used for solving the partial differential equations of mass diffusion in large scale concrete structure.

CHAPTER 5

MULTI SPECIES TRANSPORT PROCESS IN NON-SATURATED CONCRETE STRUCTURES

5.1. INTRODUCTION

Concrete is the most widely used infrastructure material in the world due to its relatively low cost and good performance. Among industrial byproducts with concrete, reinforced concrete is one of the main construction materials. However, the reinforced concrete structures actually undergo deterioration in many severe situations such as marine environment and nuclear power plant. There are three main causes for reinforced concrete deterioration: chemical reaction involving concrete components, physical actions, and electrochemical reactions at the interface steel and concrete causing reinforcement corrosion. From these three deterioration causes of reinforced concrete, the corrosion of steel rebar in concrete is, undoubtedly, one of the most important causes and chloride-induced corrosion of reinforcement embedded in concrete has occurred most frequently in the world. Therefore, in order to understand the corrosion mechanisms and predict the long-term durability performance of the concrete structure, mathematical models characterizing the deterioration process need to be developed. For the needs, it is important to reveal chloride (Cl^-) penetration mechanism in concrete. However, chloride is not the only ions diffusing in concrete. The effect of other ions (Na^+ , Ca^{2+} , K^+ , OH^-) in concrete needs to be disclosed as well. In this chapter, chloride ingress and multi-ions transport will be mentioned and simulated based on mathematical model and numerical techniques.

One of the major sources of chloride ions is the deicing salts such as sodium chloride (NaCl),

calcium chloride (CaCl_2), and magnesium chloride (MgCl_2), which is commonly used on highway roads and reinforced concrete bridges (Han, 2007; Song et al, 2008; Tamimi et al, 2007). In order to control snow and ice, frequently, different types of deicers can be applied to the same area at the same time.

For a couple of decades, many researchers have studied the ingress of various ions into concrete. Fick's laws of diffusion are very famous for analyzing data on the migration through the material. For general problems in electro-chemistry, the solution of system was studied by Plank (Chatterji, 1994). Li et al (1998) presented the mathematical model and numerical results for the simulation of electrochemical chloride in saturated concrete. In electrical field, the concentration profile of ionic species charged by various current densities was demonstrated with considering the activity of ions in concentration solution. Later on, Li et al (2000) simulated the transport behavior of ions in saturated concrete with a finite element model. This model was developed based on the Nernst-Planck equation related to the ionic interaction of multi-ions in concrete pore solution. The study of influences of boundary conditions, current density, diffusion coefficient of concrete was incorporated in the model. Furthermore, Truc et al (2000), Lorente et al (2003), and Nguyen et al (2006) developed the multi-species numerical model, applying the Nernst-plank equation in order to simulate the transport of several ionic species in saturated concrete. Wang et al. (2001, 2005) also proposed the model of the electrochemical chloride removal from concrete, which involved consideration of the effect of electrostatic coupling of charged ions, adsorption, porosity, and tortuosity of pore structure. Samson et al. (1999) presented the mathematical model of ions diffusion in porous media. This model based on Nernst-Planck equation involved poisson's equation to evaluate the electrical coupling between ions. Then, Samson and Marchand (1999) extended the model to consider the chemical activity effects by considering ions in non-ideal solution. The mathematical model was developed by taking into account the chemical activity terms in the governing equation. Lately, Samson and Marchand (2007) researched the transport model of ions in non-saturated cement-based materials related to external sulfate or calcium and hydroxide leaching. The mathematical model was developed based on the set of Nernst-Planck/Poisson equation by taking into account the diffusion, electrical coupling, chemical activity, and advection mechanisms in the isothermal condition. Recently,

Nielsen et al (2003) studied the chloride diffusion coefficient in partially saturated cementitious material with combining the composite theory and Power's model, instead of Nernst-plank equation.

In this study, mathematical models of the transport theory of multi-species due to de-icing salts will be presented. The model involves not only the effect of diffusion mechanism but also the influence of interaction of ionic species. Furthermore, the coupled effect of moisture and multi-ions diffusion has been incorporated in the model. The numerical results are solved by parallel finite element method with extending the mathematical model used in the chapter 3 and 4 and compared and verified with the experimental results in saturated concrete.

5.2. BASIC FORMULATION OF GOVERNING EQUATIONS

Concrete can consist of three physical phase including aggregate, paste/mortar, and porosity. The diffusivities of ionic species are negligible in aggregate because of dense and hard material in concrete. However, pore system provides the diffusion path to migrate ionic species. This multi-species (Cl^- , Na^+ , Ca^{2+} , K^+ , OH^-) depend on cement types and additive varieties and can be present in pore solutions. Total chloride is the sum of bound and free chloride. The free chlorides are water-soluble and the threshold amount of it can attack the passive film on the reinforced rebar surface. And in traditional method to predict the service life of concrete structure, only chloride ions are taken into account. Even though this way is simple and easy, it fails to clarify concrete deterioration due to ionic and mineral interactions. Thus, in order to present the diffusion of ionic species in the system, the mathematical model to reflect the real phenomena can be needed.

To describe the ionic transport process in a porous media, the governing equation of multi species diffusion in partially saturated concrete affected by moisture gradient can be written as follows.

For the flux of each species in the pore solution of saturated concrete, the Nernst-Plank equation is employed.

$$J_i = - \left[D_i \nabla C_{f-i} + Z_i D_i \left(\frac{F}{RT} \nabla \phi \right) C_{f-i} \right] \quad \text{Eq.(5-1)}$$

where J_i is the flux of ions, D_i is the diffusion coefficient, C_{f-i} is the concentration of multi-species (Na^+ , Ca^{2+} , K^+ , OH^- , Cl^-), z_i is the charge number, F is the Faraday's constant, R is the gas constant, T is the temperature, ϕ is the electrostatic potential, and index i represents for i -th species.

Under an internally-induced electric field, all the ionic species in the pore solution have effect on the electro-neutrality condition. In order to solve the system of equations, a supplemental relation is needed to consider the electrical potential due to inherently caused by the movement of all species. There are three methods to determine the magnitude of ϕ .

- Electroneutrality

$$\sum Z_i C_i = 0 \quad \text{Eq.(5-2)}$$

- Null current

$$\sum Z_i J_i = 0 \quad \text{Eq.(5-3)}$$

- Poisson equation

$$\sum Z_i C_i = -\epsilon \nabla \cdot \nabla \phi \quad \text{Eq.(5-4)}$$

Where ϵ is the dielectric constant. These three equations are taken over all ionic species in the ionic solution. Nguyen et al. (2006) found that electrostatic potential can be evaluated in terms of electroneutrality which can simplify the numerical simulation shown in Eq.(5-2). The electrostatic potential equation based on null current in Eq.(5-3) was mentioned by Li and Page (2000), Truc et al. (2000), and Wang et al. (2005). Poisson's equation showing in Eq.(5-4) was used by Samson and Marchand (1999, 2007) to calculate the electrostatic potential. In this study, the null current flux assumption was employed for solve Eq.(5-1). For the electro potential ϕ , Eq.(5-3) is substituted into Eq.(5-1).

$$\nabla \phi = \frac{RT}{F} \frac{\sum_{i=1}^N Z_i D_i \nabla C_i}{\sum_{i=1}^N Z_i^2 D_i C_i} \quad \text{Eq.(5-5)}$$

Finally, the flux of multi species in non-saturated concrete is,

$$J_i = - \left[D_i \nabla C_{f-i} + Z_i D_i \left(\frac{F}{RT} \nabla \phi \right) C_{f-i} + D_{i-H} \nabla H \right] \quad \text{Eq.(5-6)}$$

The mass balance equations for each ionic species can be expressed as

$$\frac{\partial C_{t-i}}{\partial t} = -\nabla J_i \quad \text{Eq.(5-7)}$$

By substituting Eq. (5-1) into Eq. (5-4), yields

$$\frac{\partial C_{t-i}}{\partial t} = -\nabla \left[D_i \nabla C_{f-i} + Z_i D_i \left(\frac{F}{RT} \nabla \phi \right) C_{f-i} + D_{i-H} \nabla H \right] \quad \text{Eq.(5-8)}$$

$$\text{Where, } \frac{\partial C_{t-i}}{\partial t} = \frac{\partial C_{t-i}}{\partial C_{f-i}} \cdot \frac{\partial C_{f-i}}{\partial t} + \frac{\partial C_{t-i}}{\partial H} \cdot \frac{\partial H}{\partial t}$$

The moisture transport can be described,

$$J_H = - \left[D_{H-i} \nabla C_{f-i} + D_H \nabla H \right] \quad \text{Eq.(5-9)}$$

Where J_H is the flux of relative humidity, D_H is the diffusion coefficient, H is relative humidity.

In the same way, the mass balance equations for moisture is

$$\frac{\partial w}{\partial t} = -\nabla J_H = -\nabla [D_{H-i} \nabla C_{f-i} + D_H \nabla H] \quad \text{Eq.(5-10)}$$

$$\text{Where, } \frac{\partial w}{\partial t} = \frac{\partial w}{\partial C_{f-i}} \cdot \frac{\partial C_{f-i}}{\partial t} + \frac{\partial w}{\partial H} \cdot \frac{\partial H}{\partial t}$$

Finally, Eq. (5-8) and (5-10) can be combined and simplified into matrix form,

$$\begin{bmatrix} \frac{\partial w}{\partial H} & \frac{\partial w}{\partial C_{f-i}} \\ \frac{\partial C_{t-i}}{\partial H} & \frac{\partial C_{t-i}}{\partial C_{f-i}} \end{bmatrix} \cdot \begin{bmatrix} \frac{\partial H}{\partial t} \\ \frac{\partial C_{f-i}}{\partial t} \end{bmatrix} = \nabla \begin{bmatrix} D_{H-H} & D_{H-i} \\ D_{i-H} & D_{i-i} \end{bmatrix} \cdot \begin{bmatrix} \nabla H \\ \nabla C_{f-i} \end{bmatrix} \quad \text{Eq.(5-11)}$$

Where, C_{f-i} is the concentration of multi species (Na^+ , Ca^{2+} , K^+ , OH^- , Cl^-). Total degree of freedom in this matrix form is 6 unknowns.

5.3. MATERIAL MODEL

5.3.1. Capacity and diffusivity coefficients of multi species in non-saturated concrete

The moisture capacity ($\partial w / \partial H$) of concrete can be determined by the average of the moisture capacities of cement paste and aggregate as proposed by Xi et al. (2000). The chloride binding capacity ($\partial C_{t-cl} / \partial C_{f-cl}$) is defined as the ratio between the change of free chloride content and total chloride content. Recently it was developed by Xi and Bazant (1999). The other species (Na^+ , Ca^{2+} , K^+ , OH^-) capacity is employed as 1.

$$\begin{bmatrix} \frac{\partial w}{\partial H} & \frac{\partial w}{\partial C_{f-i}} \\ \frac{\partial C_{t-i}}{\partial H} & \frac{\partial C_{t-i}}{\partial C_{f-i}} \end{bmatrix} = \begin{bmatrix} \frac{\partial w}{\partial H} & 0 & 0 & 0 & 0 & 0 \\ 0 & \frac{\partial C_{t-cl}}{\partial C_{f-cl}} & 0 & 0 & 0 & 0 \\ 0 & 0 & 1 & 0 & 0 & 0 \\ 0 & 0 & 0 & 1 & 0 & 0 \\ 0 & 0 & 0 & 0 & 1 & 0 \\ 0 & 0 & 0 & 0 & 0 & 1 \end{bmatrix} \quad \text{Eq.(5-12)}$$

The moisture diffusion coefficient (D_{H-H}) of concrete based on composite theory derived by Christensen (1979) can be calculated by the relationship with the diffusion coefficient of aggregate and the diffusion coefficient of cement paste. The diffusion coefficient of chloride ions (D_{cl-cl}) in concrete can be estimated using the multifactor method proposed by Xi and Bazant (1999). It depends on the influence of water-cement ration, composite action of the aggregates, relative humidity, temperature, and free chloride concentration. A detailed derivation of mass balance equation for multi species including electrical coupling term could be referred to appendix A.

$$\begin{bmatrix} D_{H-H} & D_{H-i} \\ D_{i-H} & D_{i-i} \end{bmatrix} = \quad \text{Eq.(5-13)}$$

$$\begin{bmatrix} D_{H-H} & D_{H-cl} & D_{H-Na} & D_{H-K} & D_{H-OH} & D_{H-Ca} \\ D_{cl-H} & D_{cl-cl} & D_{cl-Na} & D_{cl-K} & D_{cl-OH} & D_{cl-Ca} \\ D_{Na-H} & D_{Na-cl} & D_{Na-Na} & D_{Na-K} & D_{Na-OH} & D_{Na-Ca} \\ D_{K-H} & D_{K-cl} & D_{K-Na} & D_{K-K} & D_{K-OH} & D_{K-Ca} \\ D_{OH-H} & D_{OH-cl} & D_{OH-Na} & D_{OH-K} & D_{OH-OH} & D_{OH-Ca} \\ D_{Ca-H} & D_{Ca-cl} & D_{Ca-Na} & D_{Ca-K} & D_{Ca-OH} & D_{Ca-Ca} \end{bmatrix}$$

5.3.2. Coupling parameters

For the influence of between chloride and moisture, Ababneh and Xi (2002) and Abarr (2005) described in their research papers. Ababneh and Xi (2002) conducted an experimental study on the effect of chloride penetration on moisture diffusion in concrete. Based on the result, the effect of chloride penetration on moisture diffusion is significant. Thus, the coupling parameters, D_{H-cl} , is not a constant value, but it depends on chloride concentration. Abarr (2005) investigated the effect of moisture diffusion on chloride penetration in saturated concrete. The results indicate that D_{cl-H} increases with increasing of chloride concentration and D_{cl-H} decreases up to zero when the free chloride concentration is small. Therefore, it can be concluded that D_{cl-H} is chloride concentration dependent. In this study, as the coupling parameters, ε and δ for D_{cl-H} and D_{H-cl} , 0.19 and 0.52 were used.

$$D_{cl-H} = \varepsilon \cdot cl_f \quad \text{Eq.(5-14)}$$

$$D_{H-cl} = \delta \cdot cl_f \quad \text{Eq.(5-15)}$$

However, there have been no experimental data or material models of coupling parameters for other species, Na, Ca, OH, and K. As the first approximation, the coupling parameters of these ionic species can be evaluated proportionally based on the previous research (Ababneh and Xi, 2002; Abarr, 2005). As shown in Eq.(5-16), the parameter considering the effect of moisture on ionic diffusion can be the same as what it was used for chloride, because the moisture movement can carry any other ions as it carries the chloride ions. However, the effect of multi-species on the moisture diffusion cannot be treated in the same way. This is because the effect of the diffusion of a specific ion on the moisture movement varies with the diffusion rate of the ion. Therefore, the coupling parameter, δ , of each species can be estimated by the ratio between a specific ionic species and the chloride ion as shown in Eq.(5-17).

$$D_{i-H} = \varepsilon \cdot cl_f = \varepsilon \cdot cl_i \quad \text{Eq.(5-16)}$$

$$\frac{D_i}{D_{cl}} = \frac{D_{H-c_i}}{D_{H-cl_f}} = \frac{\delta_i \cdot C_i}{\delta \cdot cl_f} \quad \text{Eq.(5-17)}$$

5.4. NUMERICAL MODEL

In order to implement the parallel finite element computation for coupled moisture and multi-species diffusion problem, large sparse matrix should be derived and the continuous variables, relative humidity (H_m) and other 5 species (Na, Ca, OH, K and Cl), in Nernst-plank equations, were spatially discretized over the space domain, Ω . In order to solve the numerical model in time space, the semi-implicit method called Crank-Nicholson method was used in this study.

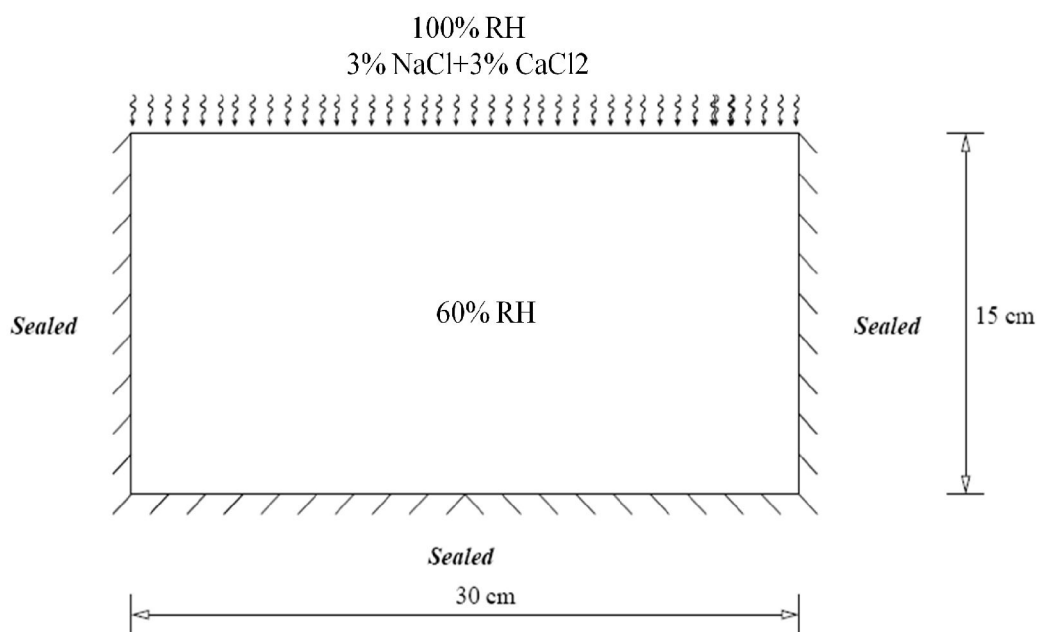
The study focuses on the chloride penetrating into concrete sample from the top surface. The ions in concrete pore solution, Na⁺, K⁺, and OH⁻, are involved in the numerical analysis. The material parameters and input data for numerical simulations related to the governing equations are shown in Table 5.1. These are diffusion coefficients, initial concentration at the top surface, and initial concentration in concrete pore solution of each ionic species, water-to-cement ratio, and volume fraction of aggregate. The concentration of alkali ions in pore solution, Na⁺ and K⁺, are obtained from cement manufacturing company which provides the chemical composition of cement used in experimental study (Damrongwiriyanupap, 2010). The numerical simulations were performed in non-saturated condition. This means that the relative humidity inside and outside of the concrete are different. The units of all ionic concentrations are in mol/l except for the total chloride which is in grams of chloride/gram of concrete weight (g/g).

The geometry of concrete sample used in numerical simulation is shown in Fig. 5.1. It is a 15 cm by 30 cm concrete specimen. The concrete domain was exposed to 3% of NaCl and CaCl₂ solution on the top surface. The other boundaries are assumed to be insulated. The moisture condition inside the concrete block was assumed to be partially saturated, 60% RH. The numerical domain was divided into about

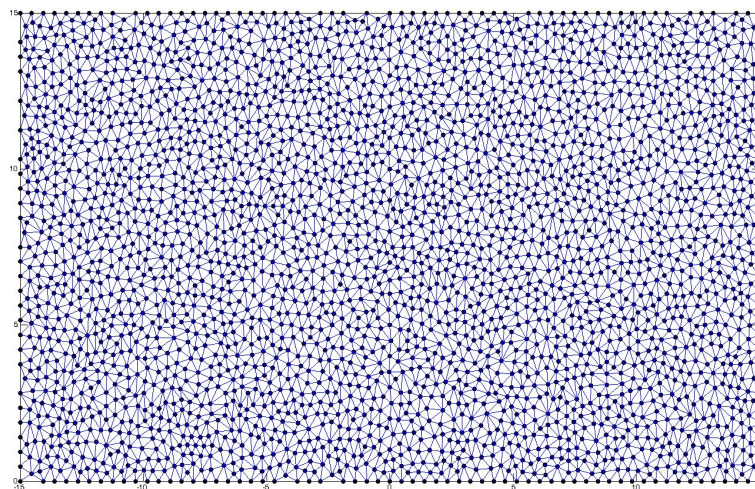
6,000 triangle elements and 3,000 nodes for finite element analysis.

Table.5.1 Material parameters and input data for Numerical analysis

Species	K	Na	Cl	OH	Ca
Charge number	+1	+1	-1	-1	+2
Diffusion coefficient (m ² /s)	4.00E-11	2.80E-11	Refer to Eq.(3-16)	5.30E-10	1.60E-11
Initial condition at top surface (mol/liter)	0	0.531	1.053	0	0.27
Initial condition in pore solution (mol/liter)	0.0995	0.0389	0	0.1384	0
Cement type	I/II				
Water-cement ratio (w/c)	0.55				
Volume fraction of aggregate (g _i)	0.65				
Outside RH (%)	100				
Inside RH (%)	60				



(a) Geometry information for numerical analysis



(b) Meshes for numerical analysis

Fig.5.1 Numerical simulation model

5.5. NUMERICAL RESULTS AND DISCUSSION

5.5.1. *Validation of numerical model in saturated concrete*

The Nernst-Planck equation can be used to explain the penetration of multi-types of deicing solutions into concrete. In order to verify the numerical model, total chloride profiles corresponding to Table 5.2 are compared with numerical results (Damrongwiriyanupap, 2010). As shown in Fig. 5.2 and 5.3, the test results of concrete specimens exposed to chloride solutions with 0.55 and 0.65 water-cement ratio at 15 and 30 days of exposure, respectively, are plotted in comparison with the numerical results obtained from the mathematical model studied above. In reality, not only single type of deicing salt but also the combinations of salts are frequently used at the same location. That is because the combination of 3% of NaCl and CaCl₂ was used as the boundary condition.

Table.5.2 Total chloride profile associated with two different water-cement ratio and time period on depth.

W/C	time(days)	Depth (mm)						
		0-6	6-12	12-18	18-24	24-30	30-36	36-42
0.55	15	0.450	0.125	0.036	0.006	0.003	0.003	0.002
	30	0.599	0.269	0.068	0.014	0.004	0.003	0.002
0.65	15	0.517	0.193	0.085	0.011	0.004	0.002	0.002
	30	0.677	0.31	0.153	0.055	0.008	0.003	0.003

Fig.5.2 and 5.3 show the total chloride profiles obtained from the experiment compared with the numerical results. It is noticed from these figures that numerical results have a good agreement with the total chloride concentrations obtained from the experiment. However, numerical result with 0.55 water-cement ratio is better fit on experimental result than one with 0.65 water-cement ratio. That is because the material model used in numerical model is more proper and effective to predict the penetration of chloride

into concrete made by 0.55 water-cement ratio.

The presented numerical model can be used to simulate not only the chloride diffusion but also other chemical species. As illustrated in Fig. 5.4, the concentration profiles of sodium and potassium, Na^+ and K^+ , predicted by this present model are plotted with the numerical results obtained from concrete specimens with 0.55 water-cement ratio exposed to different chloride solutions at 15 and 30 days of different exposure period. As seen, the trends of sodium and potassium profiles resulting from the prediction model have a good match with the experimental result as shown in Fig. 5.5.

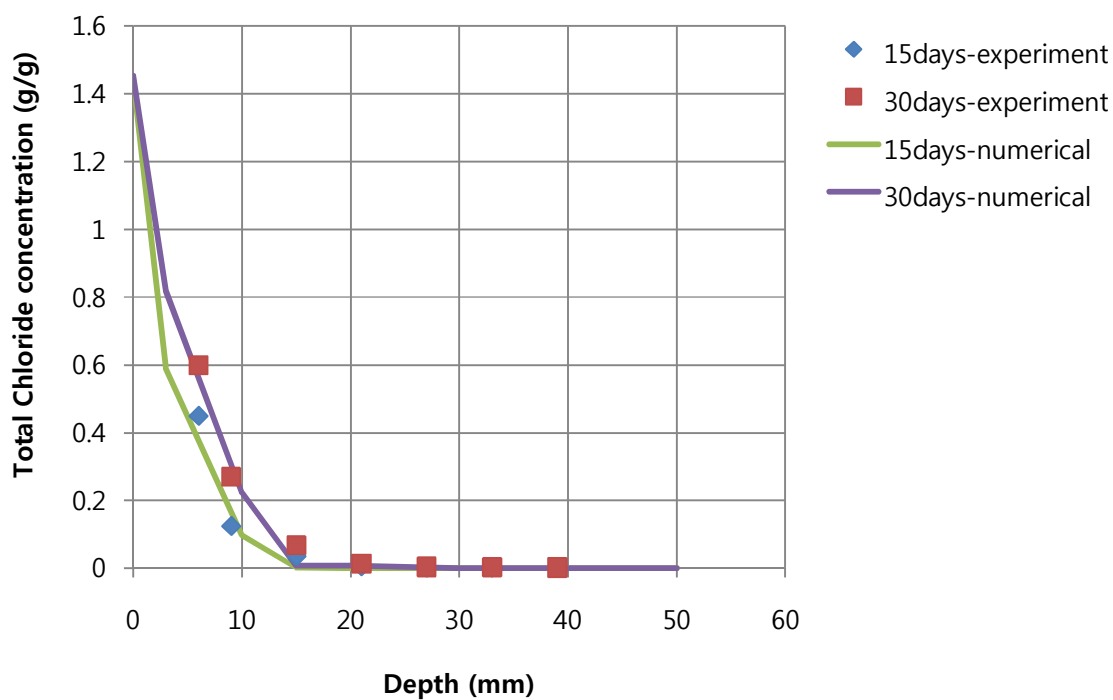


Fig.5.2 Chloride profiles of concrete specimen with 0.55 water-cement ratio

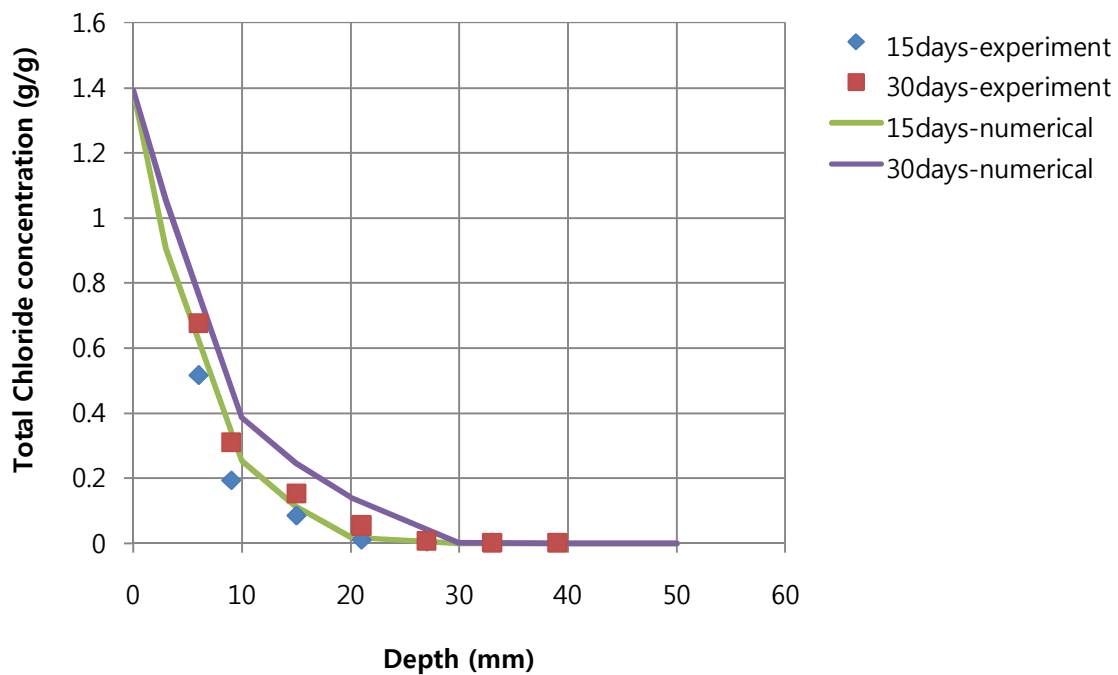


Fig.5.3 Chloride profiles of concrete specimen with 0.65 water-cement ratio

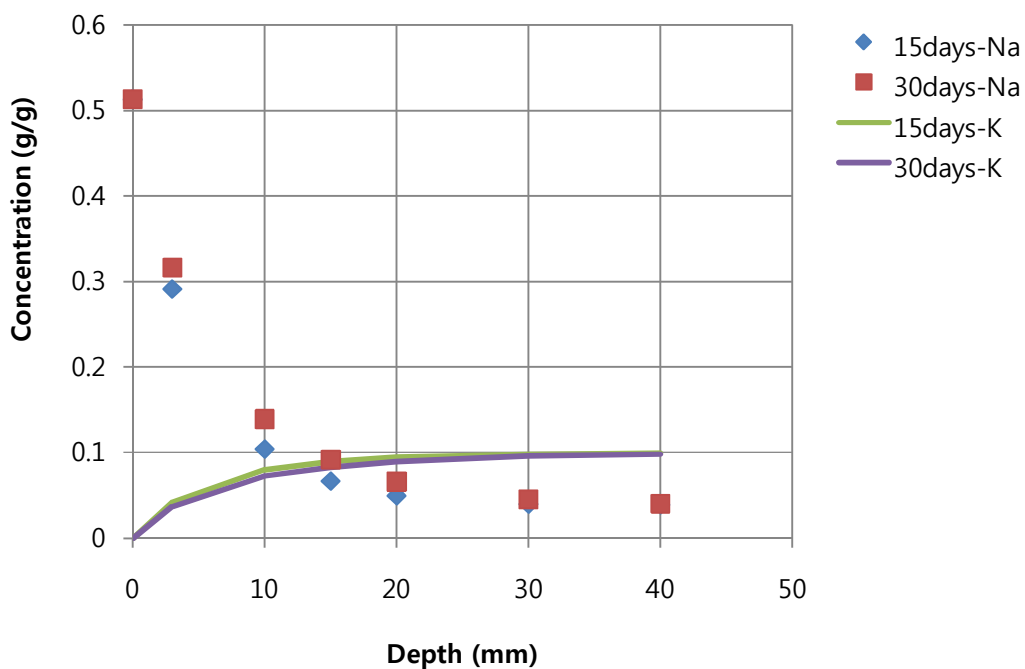


Fig.5.4 Cations profiles of concrete specimen with 0.55 water-cement ratio exposed to 3% of NaCl at 15 days of exposure

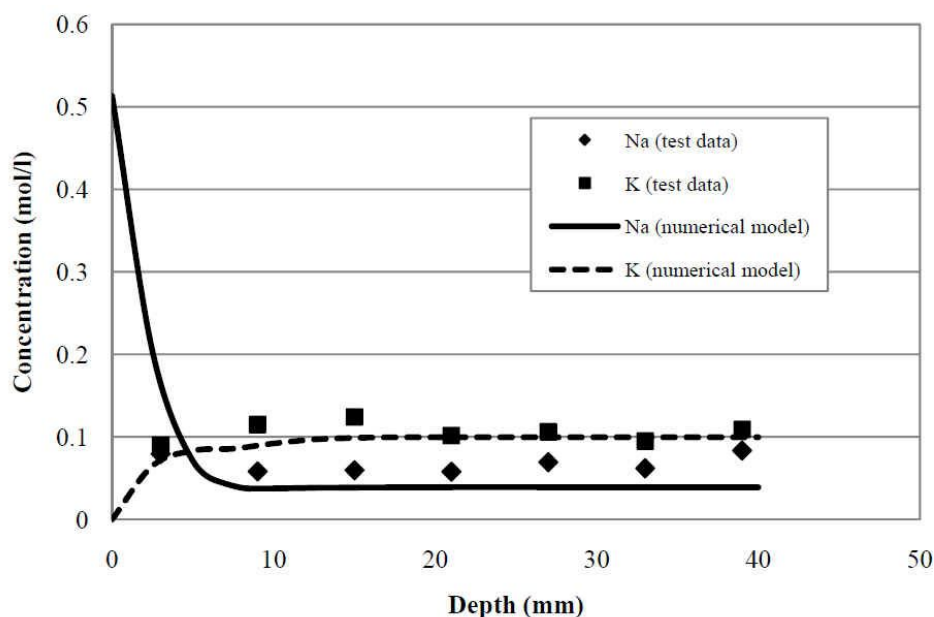


Fig.5.5 A comparison of test and numerical result of specimen exposed to 3% of NaCl at 15 days of exposure

5.5.2. Multi-species diffusion in non saturated concrete

In the non-saturated concrete, the effect of chloride penetration on moisture diffusion is significant (Ababneh and Xi, 2002). For observing the penetration of chloride into concrete from the top surface, the deicing salt combined with NaCl and CaCl₂ was used as a boundary condition. Also, the ions in concrete pore solution, K⁺, Na⁺, and OH⁻, are considered as initial conditions in the numerical analysis. The material parameters and input data for numerical simulations were the same as used in Table 5.1. The numerical simulations are performed in non-saturated condition, which means the moisture gradient (RH = 60% inside and RH = 100% outside of concrete) was considered for its effect on the diffusion of ionic species in concrete. Thus, the moisture gradient is from outside to inside concrete. The concrete model is exposed to 3% NaCl and 3% CaCl₂ solutions on the top surface. The other boundaries are assumed to be insulated. The concrete sample is divided into 6000 triangle elements and 3000 nodes for finite element model as illustrated in Fig.5.1.

Fig. 5.6 shows the humidity profile at 20, 50, 100, 200, and 400 days of exposure. It can be

observed that the moisture gradient moves from the exposed surface to inside of the concrete model and it finally converges and remains the steady state unchanging in time. In fact, the moisture gradient can carry chloride, sodium, and calcium ions and diffuse simultaneously accelerating the penetration rate of these ions.

The profile of total and free chloride concentration at different times of exposure is shown in Fig.5.7. The depth of penetration is measured from the top surface of concrete sample. As seen in Fig.5.7, the total and free chloride concentration decreases with increasing depth from the top surface. As the exposure time goes on, at the same depth, the chloride concentration is getting higher because free and bound chlorides tend to increase with longer times of exposure.

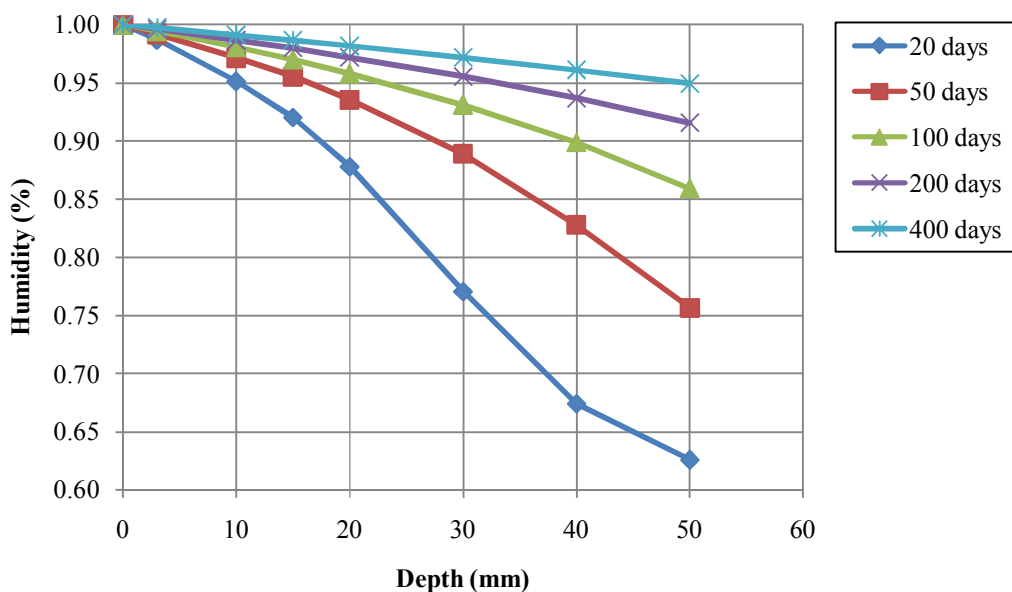
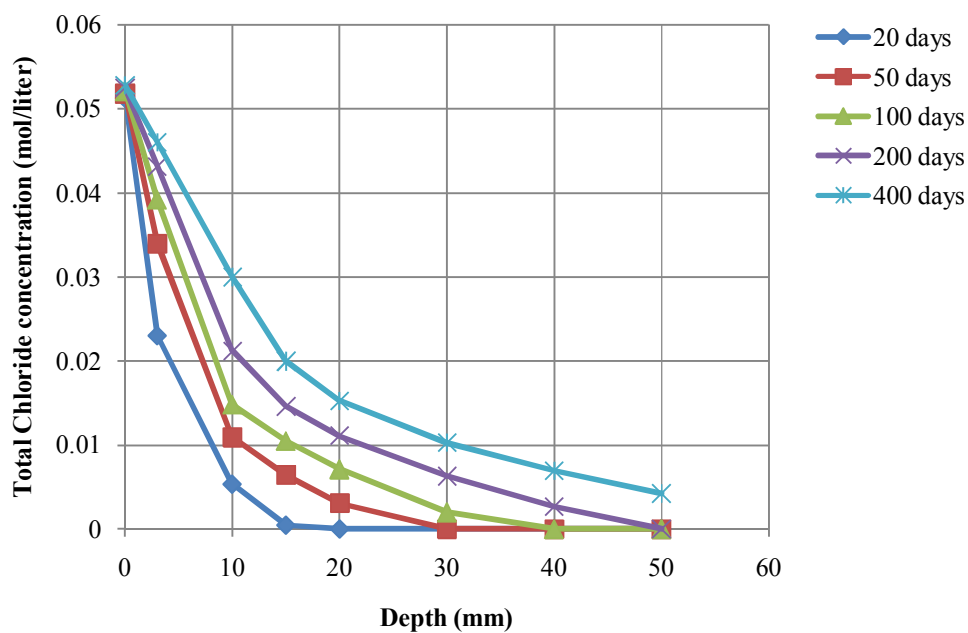
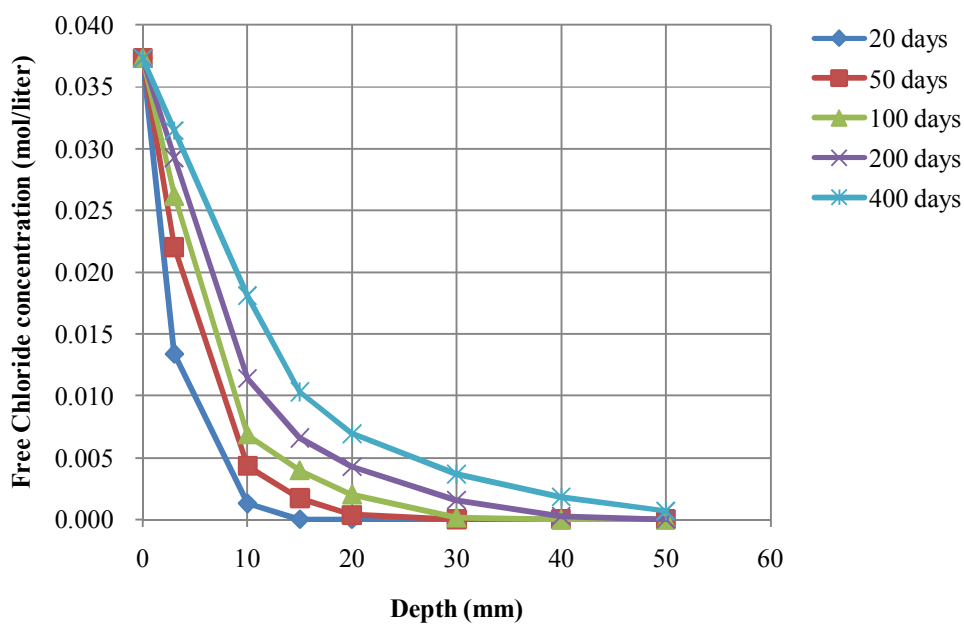


Fig.5.6 Profile of relative humidity at different depth over time



(a) Total chloride concentration profile over time



(b) Free chloride concentration profile over time

Fig.5.7 Profile of chloride concentration at different depth over time

As plotted in Fig.5.8 and 5.9, the trends of sodium and calcium concentration are similar to chloride concentration because they have the same boundary conditions that the concentration at the exposed surface is higher than that inside of the model due to concentration gradient of ions (Cl^- , Na^+ , and Ca^{2+}).

On the contrary of chloride, sodium, and calcium concentration profiles, the trends of concentration gradient of potassium (K^+) and hydroxyl (OH^-) ion are from inside to outside of concrete because the inside concentration is higher than concentration of the exposed surface, which means that any source of potassium and hydroxyl solution was not supplied on the top surface. The variations of potassium and hydroxyl concentration with depth at different times of exposure are shown in Fig. 5.10 and 5.11, respectively.

As shown in Fig.5.10 and 5.11, the concentration of potassium and hydroxyl ions increase with the increase of depth from the top surface. However, these values decrease with increasing of exposure times. The gradient of relative humidity inside and outside concrete is initially high. However, as exposure time goes by, the gradient and slope of between internal and external decrease and nonlinearity is reduced. For instance, the difference in concentration of potassium and hydroxyl at between 20 days and 50 days is much higher and clearer than difference of concentration at between 200 and 400. It is noticed that moisture has influence on the diffusion of multi-ionic species in concrete by accelerating the penetration rate of multi-species.

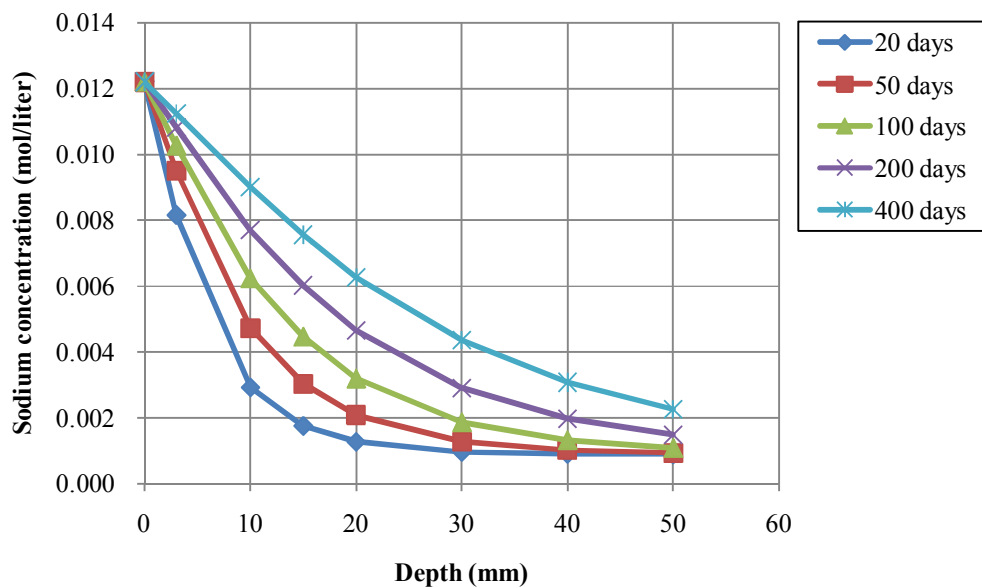


Fig.5.8 Profile of sodium concentration at different depth over time

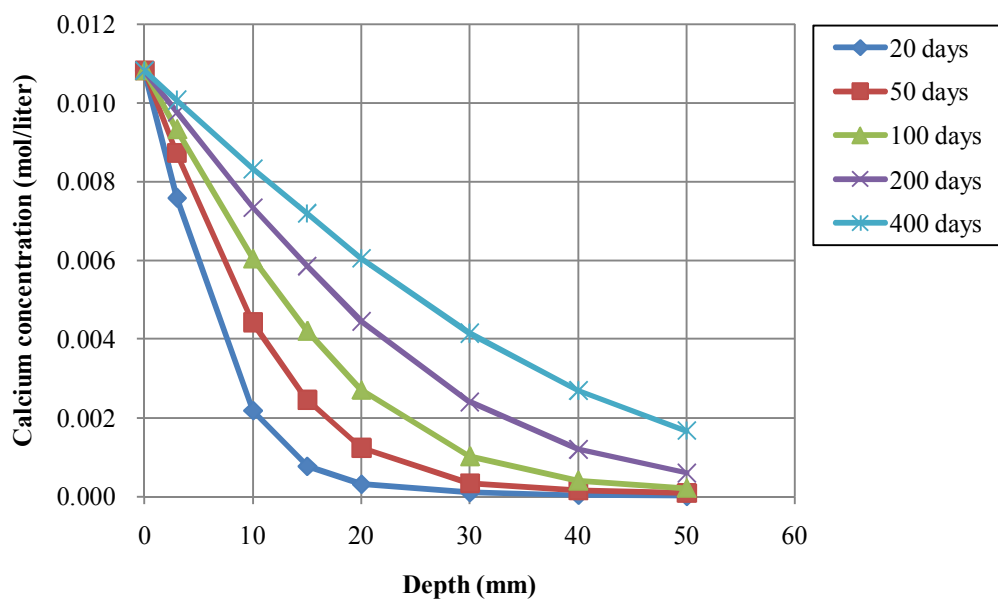


Fig.5.9 Profile of calcium concentration at different depth over time

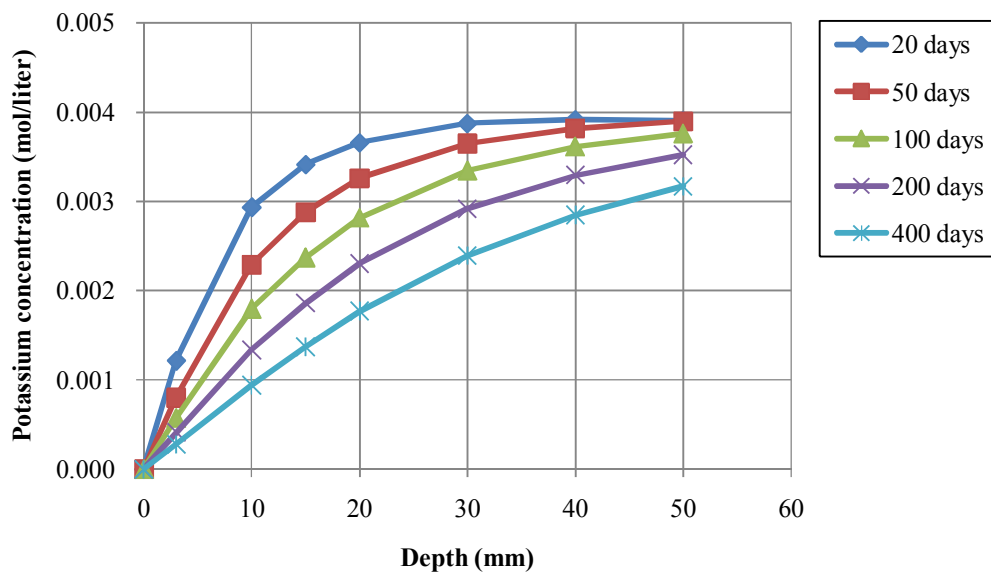


Fig.5.10 Profile of potassium concentration at different depth over time

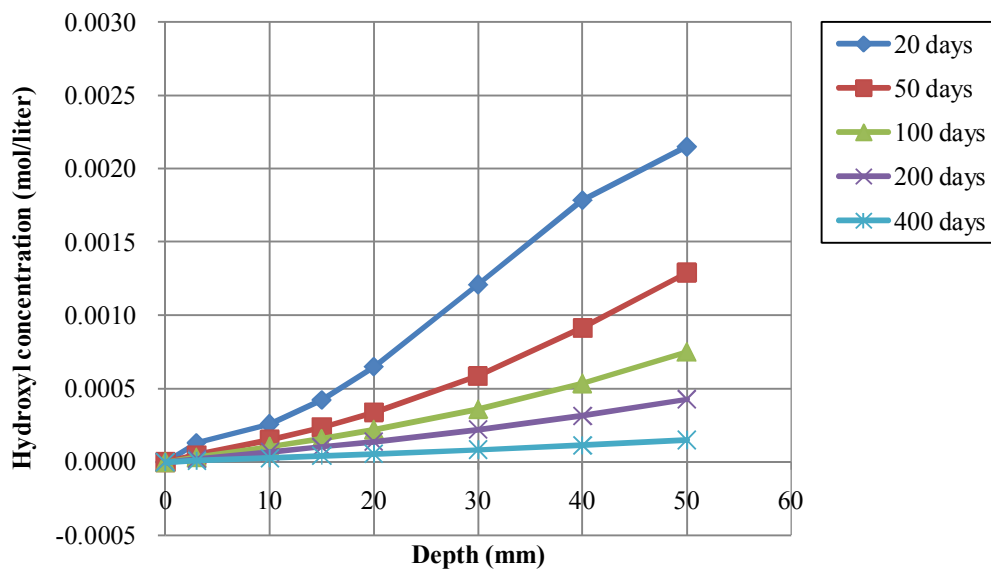


Fig.5.11 Profile of hydroxyl concentration at different depth over time

5.6. CONCLUSIONS

1. A mathematical model is developed based on the Nernst-Planck equation and null current condition to solve the ionic-induced electrostatic potential. This model also includes the material models of diffusion mechanisms in cement paste and aggregate. The model can be used to simulate the multi-species deicing salts penetration into concrete structures by considering the effect of moisture gradient.

2. Moisture diffusion has significant effect on penetration of deicing salts into concrete by accelerating the penetration rate of chloride, sodium, and calcium ions. The coupling parameter was assumed because of no experimental data or material models of coupling parameters for other species. The parameter considering the effect of moisture on ionic diffusion can be assumed by the same as used for chloride due to carrying any other ions as it carries the chloride ions. The coupling parameter of each species can be estimated by the ratio between a specific ionic species and the chloride ion.

3. In order to verify the mathematical model, the numerical simulation was performed using finite element method and the results are compared with an available chloride ponding test data. It was found that the numerical results agree well with the experimental results.

4. The numerical simulation was conducted in non-saturated condition to investigate the diffusion of ionic species such as chloride, sodium, calcium, hydroxyl and potassium. The penetration of chloride, sodium, and calcium increase when time goes by, because the initial concentration outside the concrete is much higher and the moisture gradient has an effect on accelerating the diffusion rate of ions. However, the concentration of hydroxyl and potassium is decreased due to opposite reason. This model can be used satisfactorily to predict the penetration of aggressive chemicals, such as deicing salts into non-saturated condition.

CHAPTER 6

COUPLED CHEMO-HYGRO-THERMAL TRANSPORT PROCESSES IN NON-SATURATED CONCRETE STRUCTURES

6.1. INTRODUCTION

In climates with ice or snow, the extensive utilization of deicing salt during winter is the one of the major causes of deterioration of concrete roads and bridges. Chloride-induced corrosion of reinforcing steel due to chloride-rich environments is a major problem in long-term durability of concrete structures. Once the concentration of chloride ions reaches the critical value, the corrosion of reinforcement can start to rust. The volume expansion of rust formation may cause cracking, spalling, and delaminating of concrete cover. These damages can lead to the reduction of load-bearing capacity of structures.

In saturated concrete, concentration gradient is governing chloride penetration in Fick's law. Similarly, in partially saturated concrete, chloride penetration has an influence on accelerating rate of moisture diffusion (Ababneh and Xi, 2002), and moisture diffusion has a significant effect on the chloride ingress (Ababneh, 2002; Abarr, 2005; Suwito, 2005).

However, the actual conditions of reinforced concrete structures are often exposed to the climate change, which leads to periodic moisture and temperature boundary condition. Furthermore, not only the moisture diffusion but also the temperature variations have effect on the chloride penetration. This effect has already incorporated with BET isotherms and Arrhenius's law (Xi et al, 1994, Chatterji, 1994).

In order to better predict chloride ions transport into concrete material, it is necessary to develop a

robustly mathematical model considering temperature effect. The governing equations will be derived for the chloride ions penetration based on the conditions of non-saturated concrete under thermo effect. This has been investigated by many researchers based on experimental and numerical studies.

Bazant et al. (1978, 1981) and Saetta et al. (1993) mentioned the relationship of temperature and moisture transfer in saturated and non-saturated concrete with mathematical model, experimental data, and numerical program. Especially, Bazant et al. (1978, 1981) proposed some relationships of sorption isotherms, dependence of permeability on temperature, and change of porosity due to dehydration. Sih et al. (1980) simulated the influence of coupled heat and moisture diffusion on transient stresses. Lien et al. (1998) also studied the mass transfer under influence of moisture and thermal gradients. In the result, the existence of a thermal gradient may induce an internal pressure gradient in porous media of sufficiently low permeability. The influence of accelerated hydration at elevated temperatures must be taken into consideration of drying process. Tenchev et al. (2001) and Li et al. (2002) proposed the mathematical model of transient differential equations for coupled heat and mass transfer in heated concrete. They presented the detailed finite element formulation and computational procedures, and several physical quantities based on experimental data and semi-analytical relationship. The pore pressure based on the numerical results well agrees with experimental data and is dominated by low permeability and high initial water content. Isgor et al. (2004) developed the two-dimensional finite element computing program called CONDUR, which considers the coupling effects of moisture, heat, and carbon dioxide transport in concrete. The proposed finite element model and program are capable of handling any geometry including cracks, prescribed initial and boundary conditions and pertinent material nonlinearities. As the result, the existing cracks have a significant effect on the transport properties of concrete. This phenomenon was investigated by Chen et al. (2007).

Generally, concrete structures lie in non-isothermal condition and the temperature variation may affect significantly chemical reaction of ions. That is, temperature gradient is a one of the important driving forces (Samson and Marchand, 2007). Isteita (2009) investigated that the rate of chloride penetration into concrete was accelerated by increasing temperature and proposed coupling parameters of

chloride penetration on temperature effect.

In this study, a mathematical model will be developed to predict the influence of coupled temperature and moisture on multi species penetration into partially saturated concrete structures.

The governing equation of ions is derived based on Nernst-Planck equation, which takes into account the effect of between chloride ions and ions in the concrete pore solution, Na⁺, K⁺, and OH⁻. The governing equations are solved by the parallel finite element method. In order to verify the numerical results obtained from the model, available experimental test data will be used.

6.2. BASIC FORMULATION OF GOVERNING EQUATIONS

The formulation of chloride ions and other species (Na⁺, Ca²⁺, K⁺, OH⁻) in non-saturated concrete is based on the Nernst-Planck equation. The transport of all ionic species is associated with the coupled effect of temperature and moisture in concrete. The heat flow is described by the Fourier's law of heat conduction.

The governing equation of multi species diffusion in partially saturated concrete affected by the coupling of moisture gradient and temperature gradient (soret effect) can be written as follows.

For ion transport,

$$J_i = - \left[D_i \nabla C_{f-i} + Z_i D_i \left(\frac{F}{RT} \nabla \phi \right) C_{f-i} + D_{i-H} \nabla H + D_{i-T} \nabla T \right] \quad \text{Eq.(6-1)}$$

where J_i is the flux of ions, D_i is the diffusion coefficient, C_{f-i} is the concentration of multi-species (Na⁺, Ca²⁺, K⁺, OH⁻, Cl⁻), z_i is the charge number, F is the Faraday's constant, R is the gas constant, T is the temperature, Φ is the electrostatic potential, and index i represents for i -th species. D_{i-H} and D_{i-T} are the coupling parameters of effect of moisture and temperature on ions diffusion, respectively. In Eq. (6-1), the first term in right hand side is the diffusion due to concentration gradient, and the second term is the migration or the electrical coupling between ions.

The moisture and temperature transport can be described,

$$J_H = -[D_{H-i} \nabla C_{f-i} + D_H \nabla H + D_{H-T} \nabla T] \quad \text{Eq.(6-2)}$$

$$J_T = -[D_{T-i} \nabla C_{f-i} + D_{T-H} \nabla H + D_T \nabla T] \quad \text{Eq.(6-3)}$$

Where J_H and J_T are the flux of relative humidity and temperature, D_H and D_T are the diffusion coefficient, H is relative humidity and T , temperature.

The mass balance equations for each ionic species can be expressed as

$$\frac{\partial C_{t-i}}{\partial t} = -\nabla J_i \quad \text{Eq.(6-4)}$$

By substituting Eq. (6-1) into Eq. (6-4), yields

$$\frac{\partial C_{t-i}}{\partial t} = -\nabla \left[D_i \nabla C_{f-i} + Z_i D_i \left(\frac{F}{RT} \nabla \phi \right) C_{f-i} + D_{i-H} \nabla H + D_{i-T} \nabla T \right] \quad \text{Eq.(6-5)}$$

$$\text{Where, } \frac{\partial C_{t-i}}{\partial t} = \frac{\partial C_{t-i}}{\partial C_{f-i}} \cdot \frac{\partial C_{f-i}}{\partial t} + \frac{\partial C_{t-i}}{\partial H} \cdot \frac{\partial H}{\partial t} + \frac{\partial C_{t-i}}{\partial T} \cdot \frac{\partial T}{\partial t}$$

In the same way, the mass balance equations for moisture and temperature are

$$\frac{\partial w}{\partial t} = -\nabla J_H = -\nabla [D_{H-i} \nabla C_{f-i} + D_H \nabla H + D_{H-T} \nabla T] \quad \text{Eq.(6-6)}$$

$$\frac{\partial Q}{\partial t} = -\nabla J_T = -\nabla [D_{T-i} \nabla C_{f-i} + D_{T-H} \nabla H + D_T \nabla T] \quad \text{Eq.(6-7)}$$

$$\text{Where, } \frac{\partial w}{\partial t} = \frac{\partial w}{\partial C_{f-i}} \cdot \frac{\partial C_{f-i}}{\partial t} + \frac{\partial w}{\partial H} \cdot \frac{\partial H}{\partial t} + \frac{\partial w}{\partial T} \cdot \frac{\partial T}{\partial t}$$

$$\frac{\partial Q}{\partial t} = \frac{\partial Q}{\partial C_{f-i}} \cdot \frac{\partial C_{f-i}}{\partial t} + \frac{\partial Q}{\partial H} \cdot \frac{\partial H}{\partial t} + \frac{\partial Q}{\partial T} \cdot \frac{\partial T}{\partial t}$$

Finally, Eq.(6-5), (6-6), and (6-7) can be combined and simplified into matrix form,

$$\begin{bmatrix} \frac{\partial Q}{\partial T} & \frac{\partial Q}{\partial H} & \frac{\partial Q}{\partial C_{f-i}} \\ \frac{\partial w}{\partial T} & \frac{\partial w}{\partial H} & \frac{\partial w}{\partial C_{f-i}} \\ \frac{\partial C_{t-i}}{\partial T} & \frac{\partial C_{t-i}}{\partial H} & \frac{\partial C_{t-i}}{\partial C_{f-i}} \end{bmatrix} \cdot \begin{bmatrix} \frac{\partial T}{\partial t} \\ \frac{\partial H}{\partial t} \\ \frac{\partial C_{f-i}}{\partial t} \end{bmatrix} = \nabla \begin{bmatrix} D_{T-T} & D_{T-H} & D_{T-i} \\ D_{H-T} & D_{H-H} & D_{H-i} \\ D_{i-T} & D_{i-H} & D_{i-i} \end{bmatrix} \cdot \begin{bmatrix} \nabla T \\ \nabla H \\ \nabla C_{f-i} \end{bmatrix} \quad \text{Eq.(6-8)}$$

Where, C_{f-i} is the concentration of multi species (Na^+ , Ca^{2+} , K^+ , OH^- , Cl^-). Total degree of freedom in this matrix form is 7 unknowns.

6.3. MATERIAL MODEL

6.3.1. Capacity and diffusivity coefficients

The moisture capacity ($\partial w / \partial H$) of concrete can be determined by the average of the moisture capacities of cement paste and aggregate as proposed by Xi et al. (2000). The chloride binding capacity ($\partial C_{t-cl} / \partial C_{f-cl}$) is defined as the ratio between the change of the free chloride content and the total chloride content, which was recently developed by Xi and Bazant (1999). The other species (Na^+ , Ca^{2+} , K^+ , OH^-) and temperature capacity is employed as 1. The heat capacity ($\partial Q / \partial T$) of concrete is taken up with constant value of specific heat and density. The change of moisture due to temperature ($\partial w / \partial T$) is not sufficient under normal temperature condition, so that it might be ignored.

$$\begin{bmatrix} \frac{\partial Q}{\partial T} & \frac{\partial Q}{\partial H} & \frac{\partial Q}{\partial C_{f-i}} \\ \frac{\partial w}{\partial T} & \frac{\partial w}{\partial H} & \frac{\partial w}{\partial C_{f-i}} \\ \frac{\partial C_{t-i}}{\partial T} & \frac{\partial C_{t-i}}{\partial H} & \frac{\partial C_{t-i}}{\partial C_{f-i}} \end{bmatrix} = \begin{bmatrix} \frac{\partial Q}{\partial T} & \frac{\partial Q}{\partial H} & 0 & 0 & 0 & 0 & 0 \\ \frac{\partial w}{\partial T} & \frac{\partial w}{\partial H} & 0 & 0 & 0 & 0 & 0 \\ 0 & 0 & \frac{\partial C_{t-cl}}{\partial C_{f-cl}} & 0 & 0 & 0 & 0 \\ 0 & 0 & 0 & 1 & 0 & 0 & 0 \\ 0 & 0 & 0 & 0 & 1 & 0 & 0 \\ 0 & 0 & 0 & 0 & 0 & 1 & 0 \\ 0 & 0 & 0 & 0 & 0 & 0 & 1 \end{bmatrix} \quad \text{Eq.(6-9)}$$

The moisture diffusion coefficient (D_H) of concrete based on composite theory derived by Christensen (1979) can be calculated by the relationship with the diffusion coefficient of aggregate and the diffusion coefficient of cement paste. The diffusion coefficient of chloride ions (D_{cl}) in concrete can be estimated using the multifactor method proposed by Xi and Bazant (1999). It depends on the influence of water-cement ration, composite action of the aggregates, relative humidity, temperature, and free chloride concentration. The diffusion coefficient of temperature and other species (Na^+ , Ca^{2+} , K^+ , OH^-) can be taken up from Isgor et al.(2004), Li et al.(2000), and Wang et al.(2005).

$$\begin{bmatrix} D_{T-T} & D_{T-H} & D_{T-i} \\ D_{H-T} & D_{H-H} & D_{H-i} \\ D_{i-T} & D_{i-H} & D_{i-i} \end{bmatrix} =$$

$$\begin{bmatrix} D_{T-T} & D_{T-H} & D_{T-cl} & D_{T-Na} & D_{T-K} & D_{T-OH} & D_{T-Ca} \\ D_{H-T} & D_{H-H} & D_{H-cl} & D_{H-Na} & D_{H-K} & D_{H-OH} & D_{H-Ca} \\ D_{cl-T} & D_{cl-H} & D_{cl-cl} & D_{cl-Na} & D_{cl-K} & D_{cl-OH} & D_{cl-Ca} \\ D_{Na-T} & D_{Na-H} & D_{Na-cl} & D_{Na-Na} & D_{Na-K} & D_{Na-OH} & D_{Na-Ca} \\ D_{K-T} & D_{K-H} & D_{K-cl} & D_{K-Na} & D_{K-K} & D_{K-OH} & D_{K-Ca} \\ D_{OH-T} & D_{OH-H} & D_{OH-cl} & D_{OH-Na} & D_{OH-K} & D_{OH-OH} & D_{OH-Ca} \\ D_{Ca-T} & D_{Ca-H} & D_{Ca-cl} & D_{Ca-Na} & D_{Ca-K} & D_{Ca-OH} & D_{Ca-Ca} \end{bmatrix} \quad \text{Eq.(6-10)}$$

6.3.2. Coupling parameters

The coupling parameters in diffusivity matrix have been studied by many researchers. The Soret effect (thermal diffusion) is the occurrence of a diffusion flux due to a temperature gradient. The Dufour effect is the reciprocal phenomenon, the occurrence of a heat flux due to a chemical potential gradient. The temperature effect on chloride diffusion (D_{cl-T}) was proposed by Isteita (2009). Abarr et al. (2005, 2010) studied the effect of moisture due to chloride diffusion and chloride influence due to moisture gradient was demonstrated by Ayman and Xi (2002). The more detailed information is described below.

6.3.2.1. D_{T-H} and D_{H-T}

In diffusivity matrix of Eq.(6-10), the coupling parameters of temperature effect on moisture diffusion (D_{H-T}) and moisture effect on temperature diffusion (D_{T-H}) were proposed by Bazant et al. (1978, 1981). Based on the limited test data, the flux due to the gradient of temperature (Soret flux) is rather small. That is, approximately $D_{H-T} \approx 0$. Also, the coupled heat flux (D_{T-H}) may be neglected in this numerical model.

6.3.2.2. D_{T-i} and D_{i-T}

In Eq.(6-10), the coupling parameter of temperature effect on chloride diffusion (D_{cl-T}) was proposed by Isteita (2009) as following Eq. (6-11), which was evaluated based on the experimental study of temperature effect on chloride penetration into saturated concrete. It depends on the effect of aging and temperature.

$$D_{cl-T} = f_1 \cdot C_{free_cl} \cdot f_2(t) \cdot f_3(T) \quad \text{Eq.(6-11)}$$

In Eq.(6-11), f_1 is the coefficient 5×10^{-8} , which depends on concrete composition. C_{f-cl} is the free chloride concentration (%).

$f_2(t) = 4/t$ is a factor that accounts for the effect of the aging of concrete, which is due to hydration reactions of cement.

$f_3(T) = \text{Exp}(0.1 * U/R * (\frac{1}{T_{ref}} - \frac{1}{T}))$ is the factor of temperature effect. U is the activation energy of the diffusion process, and R is the gas constant, T and Tref are current and reference temperature, respectively. Based on the Soret effect, the heat flow in concrete can carry chloride ions as well as other ions in concrete pore solution, so that we may apply this coupling parameter to all other ionic species (Na^+ , Ca^{2+} , K^+ , OH^-), it could be used as Eq.(6-12).

$$D_{Na-T} = D_{K-T} = D_{OH-T} = D_{Ca-T} = f_1 \cdot C_{free_i} \cdot f_2(t) \cdot f_3(T) \quad \text{Eq. (6-12)}$$

The material models for the coupling parameters between ion transport (D_{i-H}) and moisture diffusion (D_{H-i}) in concrete have not been sufficiently developed and researched. According to Ababneh and Xi (2002) and Abarr (2005) studies, both coupling parameters D_{cl-H} and D_{H-cl} are dependent on the free chloride concentration. For the other species and moisture coupling parameter, a proper assumption is

needed because the moisture movement can carry any other ions in the same way as it carries the chloride ions. That is, the coupling parameters are proportional to the ratio of the diffusion coefficient of the ion and the diffusion coefficient of chloride.

6.4. NUMERICAL MODEL

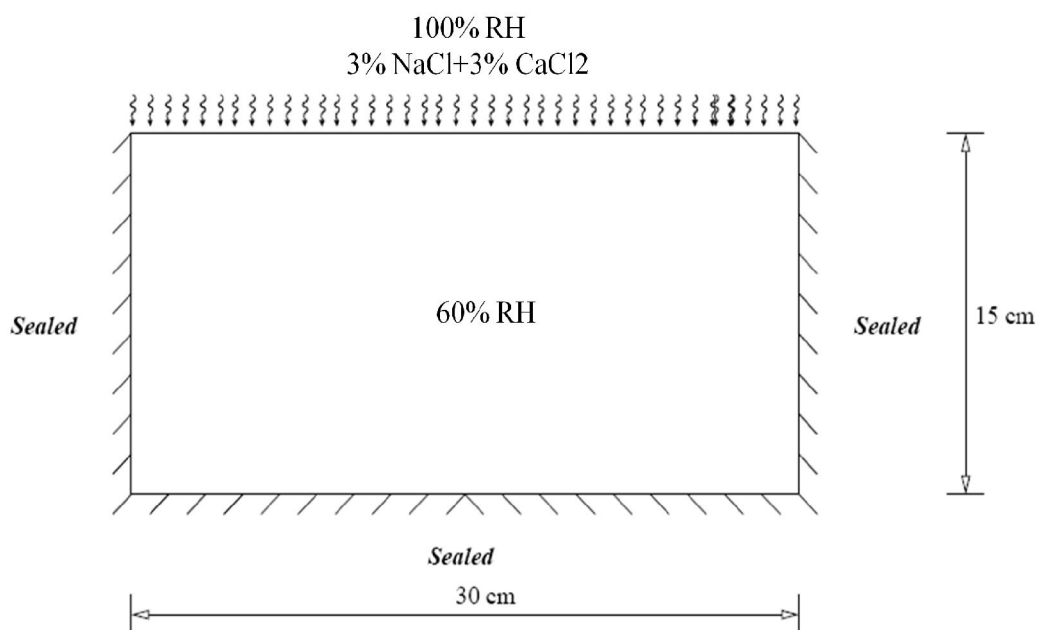
In order to employ the parallel finite element computation for coupled moisture, multi-species, and temperature diffusion problem, large sparse matrix should be derived and the continuous variables, temperature (T), relative humidity (H_m) and other 5 species (Na, Ca, OH, K and Cl), in Nernst-planck equations, were spatially discretized over the space domain, Ω . In order to solve the numerical model in time space, the semi-implicit method called Crank-Nicholson method was used in this study.

The study focuses on the chloride penetrating into concrete sample from the top surface. The ions in concrete pore solution, Na⁺, K⁺, and OH⁻, are involved in the numerical analysis. The material parameters and input data for numerical simulations related to the governing equations are shown in Table 6.1. These are diffusion coefficients, initial concentration at the top surface, and initial concentration in concrete pore solution of each ionic species, water-to-cement ratio, and volume fraction of aggregate. The concentration of alkali ions in pore solution, Na⁺ and K⁺, are obtained from cement manufacturing company which provides the chemical composition of cement used in experimental study (Damrongwiriyanupap, 2010). The numerical simulations were performed in non-saturated condition. This means relative humidity inside and outside concrete is not equal initially. The units of all ionic concentrations are in grams of chloride/gram of concrete weight (g/g).

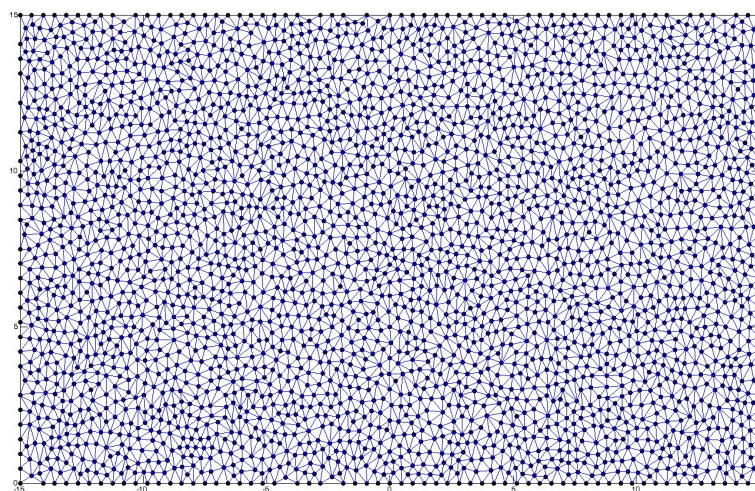
The geometry of concrete block used in numerical simulation is shown in Fig. 6.1. It is a 15 cm by 30 cm concrete specimen. The concrete block on the top surface was exposed to 3% of NaCl and CaCl₂ solution. The other boundaries are assumed to be insulated. The moisture condition inside the concrete block was assumed to be partially saturated, 60% RH. The numerical domain was divided into about 6,000 triangle elements and 3,000 nodes for finite element analysis.

Table.6.1 Material parameters and input data for Numerical analysis

Species	K	Na	Cl	OH	Ca
Charge number	+1	+1	-1	-1	+2
Diffusion coefficient (m ² /s)	4.00E-11	2.80E-11	Refer to Eq.(3-16)	5.30E-10	1.60E-11
Initial condition at top surface (mol/liter)	0	0.531	1.053	0	0.27
Initial condition in pore solution (mol/liter)	0.0995	0.0389	0	0.1384	0
Heat capacity (J/kg.°C)	1,000				
Thermal diffusivity (W/m.°C)	2				
Coupling parameter	Eq.(6-11) and Eq.(6-12)				
Cement type	I/II				
Water-cement ratio (w/c)	0.55				
Volume fraction of aggregate (g)	0.65				
Outside RH (%) / Temp. (°C)	100 % / 20°C, 35°C, 50°C				
Inside RH (%)	60 % / 20°C				



(c) Geometry information for numerical analysis



(d) Meshes for numerical analysis

Fig.6.1 Numerical simulation model

6.5. NUMERICAL RESULTS AND DISCUSSION

6.5.1. *Validation of numerical model in saturated concrete*

In order to verify the result of the chloride concentration predicted from the numerical model, the available test data obtained by Isteita (2009) was used in this chapter. The tests were conducted on chloride ponding test at different initial temperature conditions. The comparisons between numerical and experimental results exposed to 3% NaCl at $T = 35\text{ }^{\circ}\text{C}$ and $50\text{ }^{\circ}\text{C}$ for 3, 6, 12, and 24 days of exposure. Table 6.2 shows total chloride profile associated with two different water-cement ratio, temperature, and time period on depth.

Table.6.2 Total chloride profile associated with two different water-cement ratio, temperature, and time period on depth.

w/c	Temp.	Time	0-6	6-12	12-18	18-24	24-30	30-36	36-42
0.55	35°C	3	0.416	0.169	0.091	0.060	0.037	0.036	0.031
		6	0.785	0.329	0.094	0.066	0.054	0.049	0.045
		12	0.986	0.389	0.117	0.092	0.065	0.055	0.053
		24	1.452	0.590	0.483	0.136	0.155	0.080	0.072
	50°C	3	0.650	0.225	0.136	0.088	0.048	0.045	0.038
		6	1.159	0.390	0.173	0.131	0.095	0.081	0.067
		12	1.357	0.622	0.241	0.168	0.110	0.099	0.092
		24	2.594	1.452	0.899	0.446	0.265	0.209	0.153
0.65	35°C	3	0.312	0.166	0.049	0.040	0.035	0.032	0.021
		6	0.471	0.180	0.099	0.055	0.079	0.070	0.059
		12	0.541	0.238	0.115	0.113	0.090	0.079	0.070
		24	0.785	0.483	0.205	0.158	0.139	0.117	0.102
	50°C	3	0.377	0.221	0.054	0.044	0.037	0.034	0.023
		6	0.717	0.356	0.162	0.127	0.089	0.076	0.066
		12	1.122	0.405	0.216	0.157	0.097	0.092	0.068
		24	2.000	1.076	0.529	0.433	0.228	0.134	0.125

Fig.6.2 through Fig.6.9 show the total chloride profiles obtained from the experiment compared with the numerical results. One can observe two effects from these results; effect of water-cement ratio and effect of temperature gradient in saturated concrete.

In the effect of water-cement, numerical result with 0.55 water-cement ratio is better fit for the experimental result than one with 0.65 water-cement ratio, regardless of exposure time. This means that the material model used in numerical model is more proper and effective to predict the penetration of chloride into concrete made by 0.55 water-cement ratio.

In the effect of temperature gradient, it can be seen both at $T = 50\text{ }^{\circ}\text{C}$ and $35\text{ }^{\circ}\text{C}$, that the results obtained from the present model have a good agreement with test data. Therefore, the present comprehensive model taking into account the diffusion mechanism, ionic interaction, and the coupled temperature effect can be used to predict the chloride penetration into concrete structures not only in isothermal condition but also in non-isothermal condition.

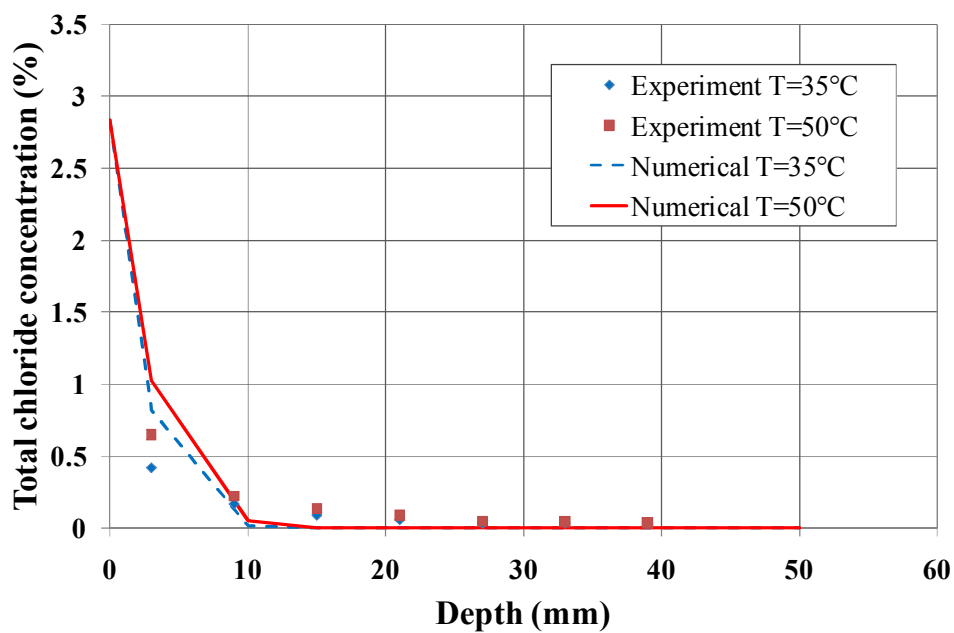


Fig.6.2 Chloride profile in concrete sample (0.55 w/c, 3 days)

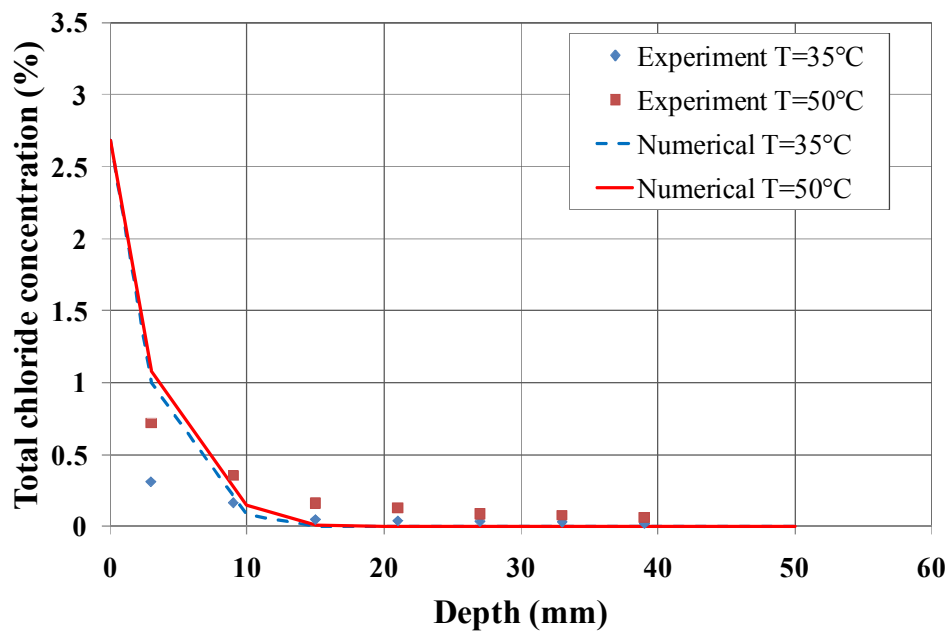


Fig.6.3 Chloride profile in concrete sample (0.65 w/c, 3 days)

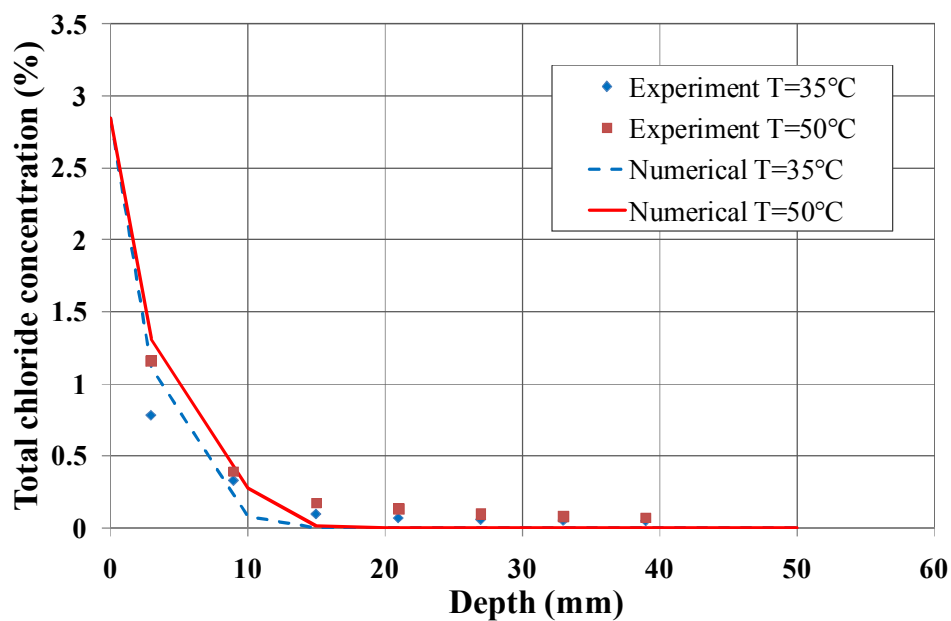


Fig.6.4 Chloride profile in concrete sample (0.55 w/c, 6 days)

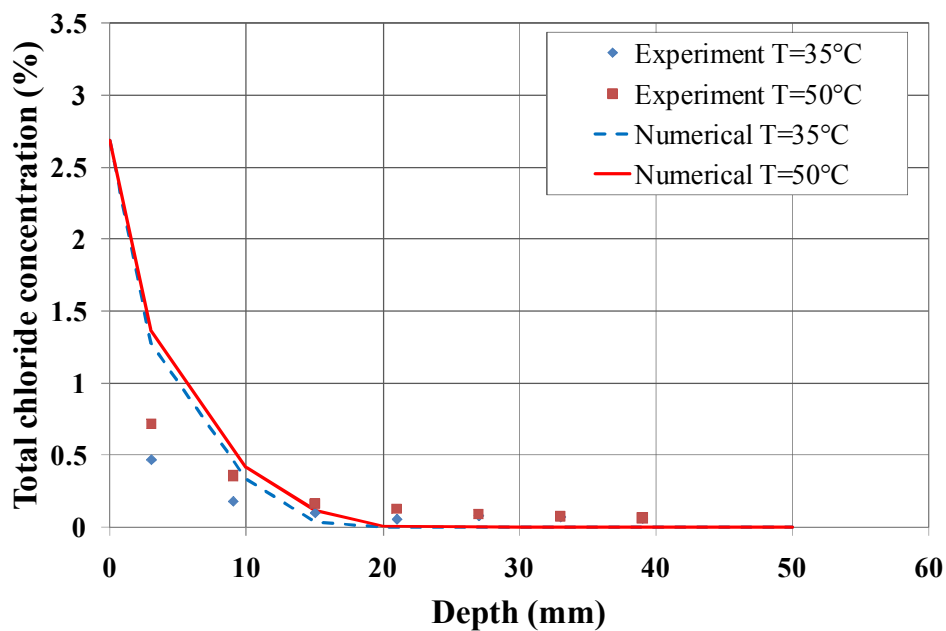


Fig.6.5 Chloride profile in concrete sample (0.65 w/c, 6 days)

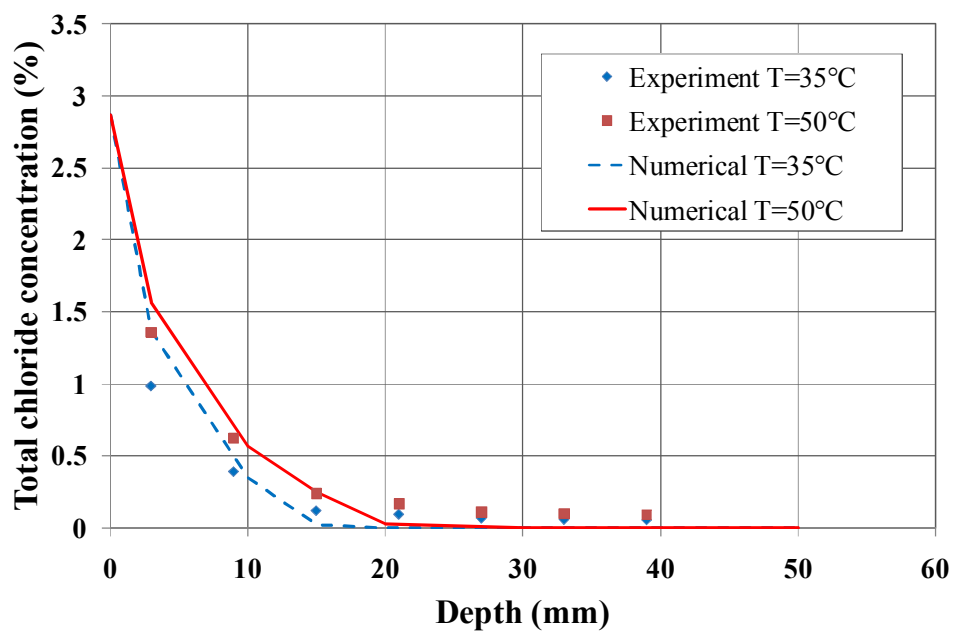


Fig.6.6 Chloride profile in concrete sample (0.55 w/c, 12 days)

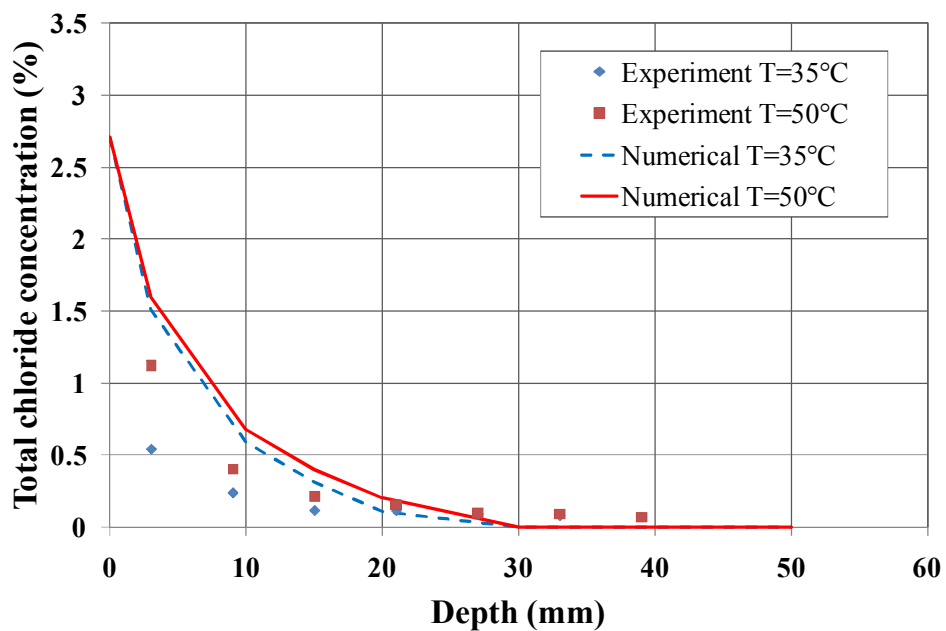


Fig.6.7 Chloride profile in concrete sample (0.65 w/c, 12 days)

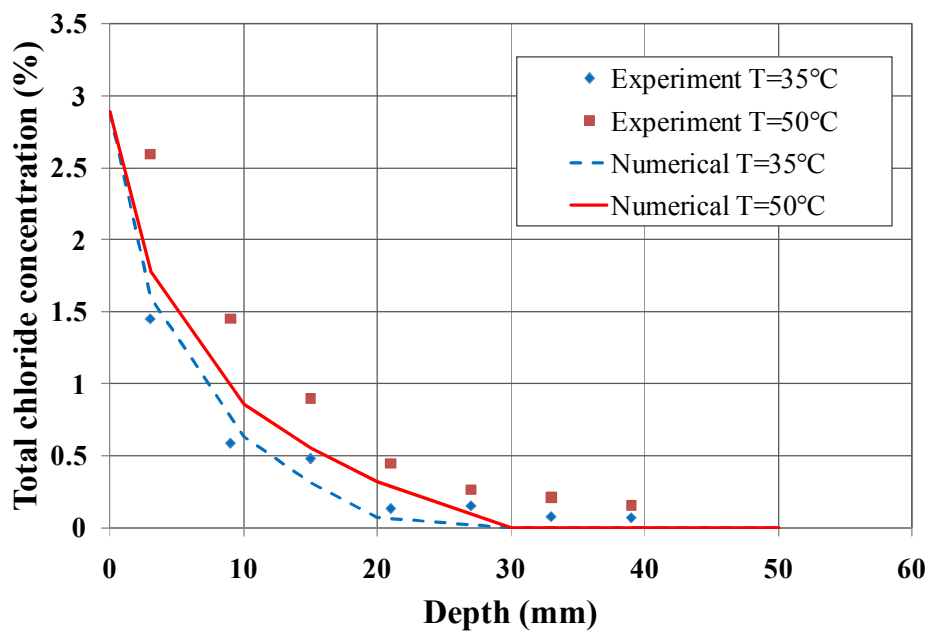


Fig.6.8 Chloride profile in concrete sample (0.55 w/c, 24 days)

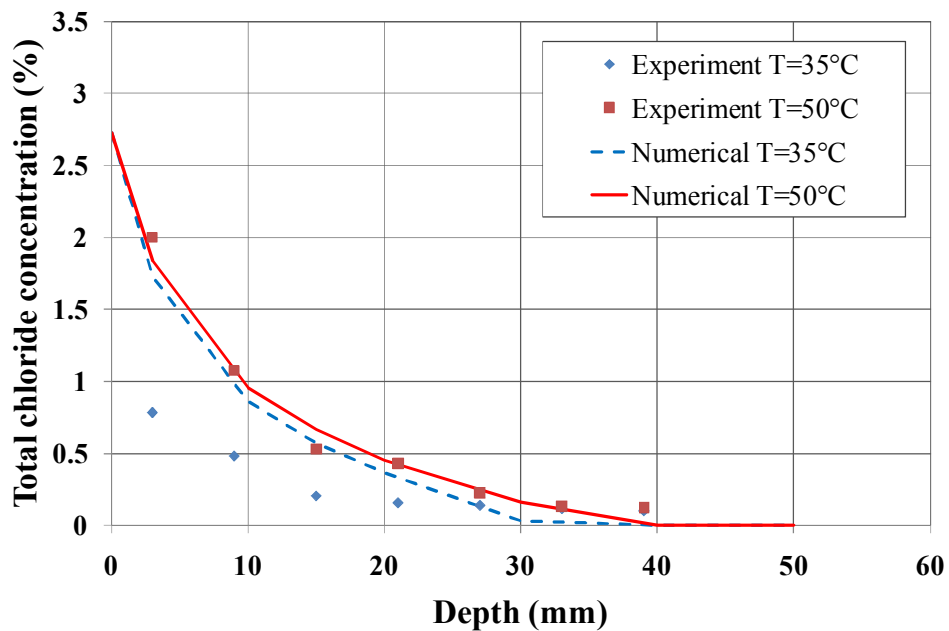


Fig.6.9 Chloride profile in concrete sample (0.65 w/c, 24 days)

6.5.2. Multi-species diffusion in non-saturated concrete considering temperature effect

For prediction of ions in non-saturated concrete, numerical model and material data were used as shown in table 6.1 and Fig.6.1. In order to observe the chloride penetration under the effect of coupled temperature and humidity gradient, parameter study was conducted. The temperature on the top surface of concrete model is $T=50^{\circ}\text{C}$ and inside 20°C . The moisture condition is partially saturated condition, which is changed from 100% outside to 60% inside. At 24days, the total chloride concentration was measured.

6.5.2.1. Effect of water-cement ratio

In order to investigate the effect of water-cement ratio under temperature and moisture diffusion, 0.55 and 0.65 of the water-cement ratio as material input data were used. The moisture condition is partially saturated and temperature gradient is 30°C . As the result in Fig.6.10, the effect of water-cement ratio is clear. That is, the chloride concentration of concrete with 0.65 water-cement ratio is much higher than one of 0.55 water-cement ratio. That is because chloride diffusivity obviously depends on water-cement ratio as shown in Eq.(2-16).

6.5.2.2. Effect of temperature gradient

In order to observe the chloride penetration under the effect of temperature gradient, the temperature on top surface of concrete model is changed from $T=20^{\circ}\text{C}$ to 50°C . The moisture condition is partially saturated and water-cement ratio is 0.55. As the result in Fig.6.11, the effect of low temperature gradient was obviously observed because the chloride diffusivity relies on temperature associated with Arrhenius law. As the temperature rises up, the moisture gradient increases. The increment of moisture gradient accelerates the movement of chloride ions.

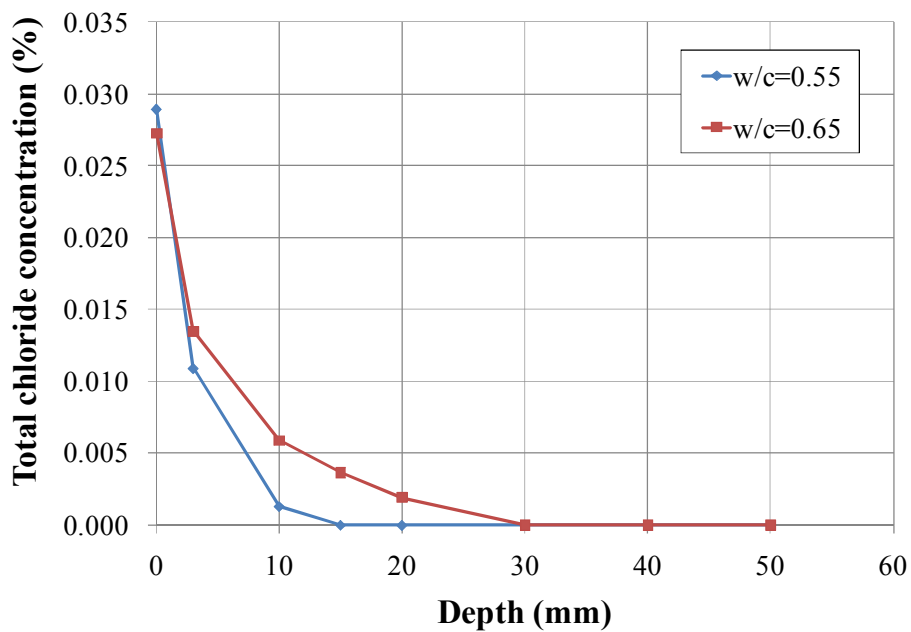


Fig.6.10 Chloride profile according to different water-cement ratio

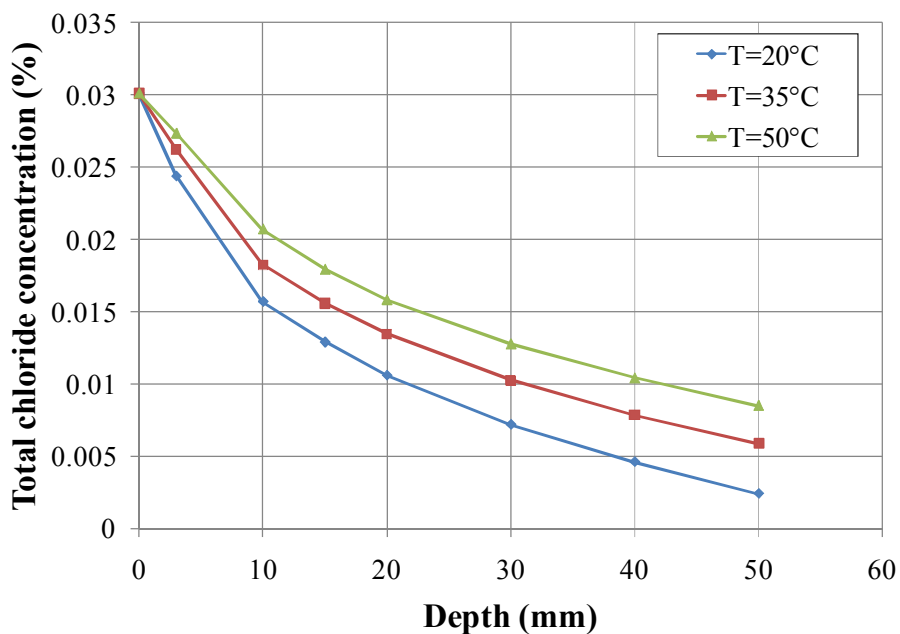


Fig.6.11 Chloride profile according to different initial temperature gradient

6.6. CONCLUSIONS

1. A mathematical model was developed to predict the chloride penetration into non saturated concrete structures under non-isothermal condition. The model takes into account diffusion mechanism and ionic interaction which is formulated based on Nernst-Planck equation. The ionic fluxes are modified by incorporating the coupling term of temperature effect. The ions in the pore solution (Na^+ , K^+ , and OH^-) are considered and the numerical simulations are performed by assuming a concrete sample exposed to chloride solution at different initial temperature conditions.

2. In this study, the coupling parameters of temperature effect on moisture diffusion (D_{H-T}) and moisture effect on temperature diffusion (D_{T-H}) were neglected. The other coupling parameters of temperature effect on ions diffusion were used as proposed by experimental data. The coupling parameters of ions effect on temperature diffusion were neglected.

3. In order to verify the mathematical model, the numerical simulation was performed by using finite element method, where the results were compared with an available chloride ponding test data, conducted under the different temperature gradient. It was found that the numerical results correspond well with the experimental results. Specially, the numerical result with 0.55 water-cement ratio is better fit on experimental result than one with 0.65 water-cement ratio. That is because the material model used in numerical model is more proper and effective to predict the penetration of chloride into concrete made by 0.55 water-cement ratio.

4. In order to observe the chloride penetration under the effect of coupled temperature and humidity gradient, parameter study was conducted for capturing the water-cement ratio and the temperature effect. The chloride concentration of concrete with 0.65 water-cement ratio is much higher than one of 0.55 water-cement ratio. However, the temperature effect was unclear.

5. The present comprehensive model can be used to predict the chloride ingress into non saturated concrete structures not only isothermal but also non-isothermal conditions. It can also be used to estimate the service life and time for rehabilitation of concrete structures in temperature change condition.

CHAPTER 7

DURABILITY OF INSULATION MORTAR WITH FINE RUBBER POWDER

7.1. INTRODUCTION

According to the report of Rubber Manufacturers Association (RMA) in 2006, the United States generates approximately 299 million scrap tires per year. That is, the ratio of total scraped tires to total U.S. population is approximately 1.01. The waste tires represent a significant environmental, human health, and aesthetic problem. Innovative solutions have to be developed to solve this problem by many researchers (Eldin et al., 1993; Epps, 1994; Amirkhanian 1997; Everett et al., 1998; Goulias et al., 1998; Jang et al. 1998; Khatib and Bayomy 1999; Brown et al. 2001). Therefore, in 2005, nearly 87% of the scrap tires were consumed through the variety of markets for reusing scraped tires such as TDF (Tire-Derived Fuel), Civil engineering, and ground rubber application (RMA, 2006).

For civil engineering application, recently, many researchers lead to study the rerutilization of waste rubber to the building and infrastructures as a cement-based material. A. Turatsinze et al (2005) investigated the mechanical characteristics of mortar composed of the rubber aggregate, instead of natural sand. In this experimental result, the strength and deformation modulus of rubber mortar is decreased. Also, rubber particles give the high strain capacity to the mortar before microcracking. N.Segre et al(2000) conducted the experiments about increasing the adhesion of cement paste using the surface treated rubber particles. The surface treatment of rubber powders did with NaOH aqueous solution for 20min. As a result, flexural strength and fracture energy are increased with the use of NaOH treated rubber particles,

compared with cement paste. Also, the modulus of Elasticity is not different with cement paste. Adhesion of rubber-matrix interface is significantly improved, the rubber particles are not separate from cement matrix after contact with liquid nitrogen (195 °C). In order to investigate the composite effect of rubber mortar, N.Segre et al (2004) was used the NaOH treated rubber particles as addition, instead of cement or aggregate. In this study, the rubber particles as soft material act on the reduction of modulus of rupture (MOR). However, the weibull modulus of specimen with rubber is higher than control (cement paste) specimen. Also, the rubber particles improved the water absorption since the porosity of rubber mortar is increased. In order to enhance the crack resistance and strain capacity of cement based structures, A.Turatsinze et al (2007) used the rubber particles and fulfilled Shrinkage test. For evaluating the strain capacity, the tensile tests were carried out. In this result, the elongation corresponding to the peak load was increased. That is, the rubber aggregate significantly improved the strain capacity of cement-based mortar. In free shrinkage test, the rubber aggregate reduced the internal restraint and increase shrinkage. Also, the ring-tests well demonstrated the benefit of rubber aggregate substitution, considering the detected time of shrinkage crack. Also, Topco (2007) suggested the economical and effective way of recycling the discarded tires with performing the durability test of mortar and concrete with crumbed tire chips in various environments such as high temperature, seawater, and freeze-thaw.

The purpose of this test is to investigate the mechanical characteristics of rubberized insulation mortar. The important experimental parameters are the rubber replacement as fine aggregate filler, the content of RPP, and the size of rubber powders. The experimental properties of insulation mortar with fine rubber powder are reported with aid of compression test, rapid chloride permeability test, the dry shrinkage test, and pull-out debonding test.

7.2. EXPERIMENTAL DETAILS

7.2.1. *Materials and mixture portion*

The Portland cement used for this test is ASTM Type I/II Portland cement (ASTM C150). The average size of sand as fine aggregate is about 0.15mm (diameter, #100), not longer than about 0.6mm

(diameter, #30). Rubber particles made by the used tire have the average size of about 0.075mm (diameter, #200). There are three additives; cellulose ether (MH10007 P4) slows down the water evaporation and improves the workability. wood fibers (Technocel 1004-7N) manufactured by Elotex will be used. It can improve workability, enhance the crack resistance of the mortar under plastic stage, and increase the sliding resistance. RPP (Redispersible Polymer Powder- MP2050) manufactured by Elotex will be used. It can enhance adhesion to the substrate, and increase cohesion of the mortar.

Table.7.1 Mix design for insulation mortar

(unit : /g)

No.	cement	sand	rubber (replacement)	cellulose ether MH10007 P4	wood fiber 1004-7N	RPP MP2050	water
1A	500	1250	0 (0%)	5	6	40	400
1B	500	625	230 (50%)	5	6	40	400
1C	500	375	324 (70%)	5	6	40	400
1D	500	125	417 (90%)	5	6	40	400
No.	cement	sand	rubber (replacement)	cellulose ether MH10007 P4 (% of cement)	wood fiber 1004-7N (% of cement)	RPP MP2050 (% of cement)	water
2A	500	625	230 (50%)	5 (1%)	6 (1.2%)	30 (6%)	400
2B	500	625	230 (50%)	5 (1%)	6 (1.2%)	40 (8%)	400
2C	500	625	230 (50%)	5 (1%)	6 (1.2%)	50 (10%)	400
2D	500	625	230 (50%)	5 (1%)	6 (1.2%)	60 (12%)	400
3A	500	625	230 (50%, #100)	5	6	50	400
3B	500	625	230 (50%, #200)	5	6	50	400

The mix design for the mortar specimens is shown in table 7.1. There are 3 groups of rubber mortar; Group 1 is for the effect of content that is represented by the rubber replacement rate of fine aggregate, Group 2 for the effect of RPP as an admixture, and Group 3 for the effect of size of rubber powder. Figure 7.1 shows the size distribution of two types of rubber powder.

It should be noted that the rubber replacement rates were calculated based on the equivalent volume not on the weight. For example, 50% replacement rate means that 50% of total weight of sand, 625g, was taken out of the mixture and replaced by the same volume (not same weight) of rubber particles. The bulk specific gravities of the sand and rubber are 2.7 and 1.0, respectively. So, the weight of rubber $W_r = W_s/2.717$ where W_r and W_s are the weights of rubber and sand, respectively. For 50% replacement rate, the weight of rubber is $W_r = 625/2.717 = 230\text{g}$, which is shown in the table for specimen mix designs.

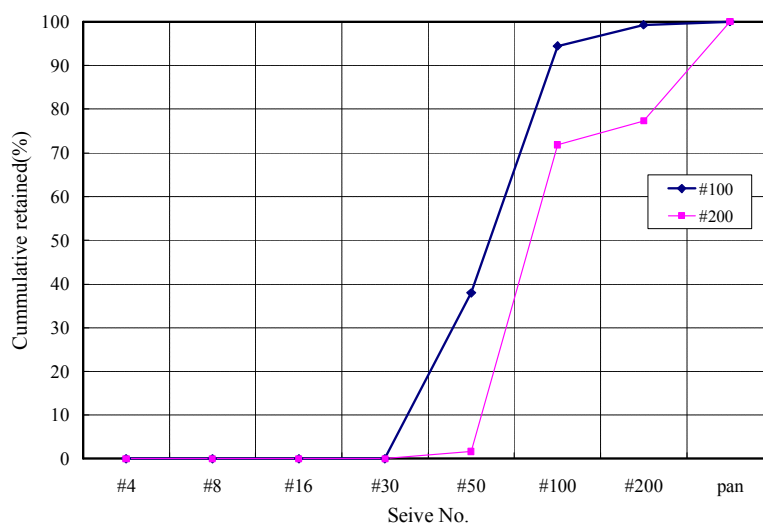
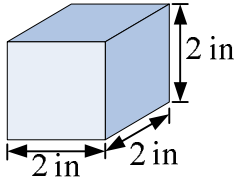
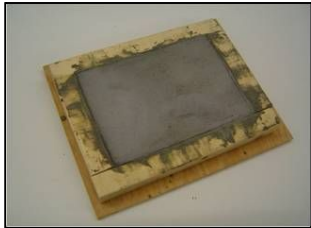



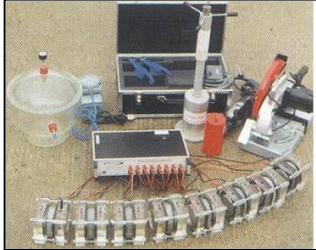



Fig.7.1 Size distribution of two types of rubber particles

7.2.2. Specimen preparation

For the cast of rubberized insulation mortar, the preparation and mix of mortar follows ASTM C305 (“Standard Practice for Mechanical Mixing of Hydraulic Cement Pastes and Mortars of Plastic Consistency”) and C1439 (“Standard test methods for polymer- modified mortar and concrete”). The rubber mortar specimens were placed in a curing room of 68°F, 100% relative humidity for curing time (7 days). Table 7.2 shows the specimen specifics and testing method used in this study.

Table.7.2 Preparation of specimen

	Compressive test		
Number of specimens	4 group×3=12 specimens		
Size of specimens	2” cube		
Facility	MTS		
ASTM	C109		
			
	Pull-off debonding test	Permeability test	Dry shrinkage test
Number of specimens	4 specimens	2 specimens	2 specimens
Size of specimens	10”× 8”×1” 	4”×2” 	1”×1”×11” prism 
Facility	Portable Pull-off tester 	PROOVE’it tester 	SPI digital indicator 
ASTM	D 4541	C 1202	C 157

7.2.3. *Test methods*

To evaluate the mechanical properties of mortar with rubber powder, several mechanical tests can be performed. When the rubber mortar specimens reached the specific ages (7 days), the following tests will be performed.

7.2.3.1. *Compression test and flexural test*

The compression tests were performed according to ASTM C 109. Three 2” cube specimens were used. The interior faces of specimen molds are applied a thin coating of release agent such as oils and greases using an impregnated cloth. And also the surface of the halves of the mold is sealed with coating agent. The amount should be sufficient to extrude slightly when the two halves are tightened together. After placing the mold on its base plate carefully remove with a dry cloth any excess agent. The mixing procedure follows the ASTM C305. The consolidation of mortar in mold is completed by hand tamping and a vibration table. The cube specimens were molded within 2min and 30s after completing the original mixing of the mortar batch. Tamping the mortar in each cube compartment is 32 times in about 10 sec in 4 rounds. Immediately after completion of molding, the test specimens are placed in moist room for 24 hr. Molds were removed and then the specimens were continued to cure in the same moist room. After seven days of curing, the compressive strength test was conducted with a MTS loading machine shown in the left figure of Figure 7.2. Flexural tests were performed in accordance with ASTM 293-08. An Instron 5869 Universal Testing Machine was used as shown in the right figure of Figure 7.2. Loading speeds and data acquisition rates for the tests were 0.003 sec./lb. and 0.1 sec./point, respectively.

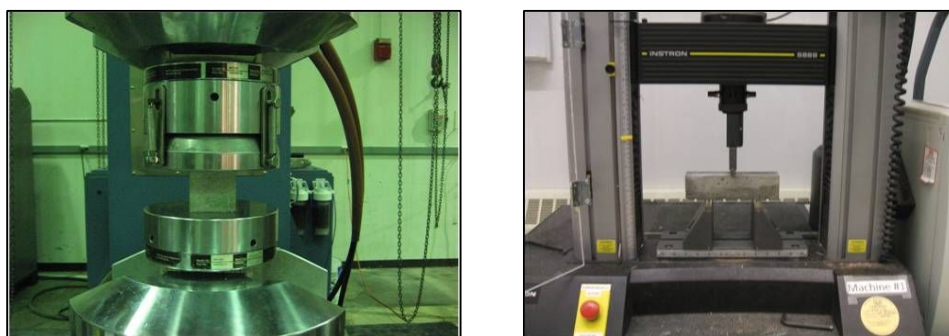


Fig.7.2 Experimental set-ups for compression and flexural tests

7.2.3.2. Pull-out debonding test

According to ASTM D 4541, the pull-off tests were performed after 7 days of curing in the standard curing condition. The plate mold of 10" by 8" by 1" was used for preparing the specimens of the pull-off strength test (see Figure 7.3). The pull-off test was performed with a portable adhesion tester, loading fixtures, and adhesive. The first step is to prepare the loading fixtures. A loading fixture commonly called a dolly or stud is glued to the surface. The bonding surface must be cleaned and smoothed with sandpaper (400 grit or finer). A portable adhesion tester is then used to apply an increasing force until the coating debond or the glue fails. The pull is applied perpendicular to the surface, so tensile strength of bond between the mortar and the wood plate is measured. Figure 3.3 shows the procedure of pull-off debonding testing with Dyna Z16 (Proceq USA, INC., www.proceq-usa.com).

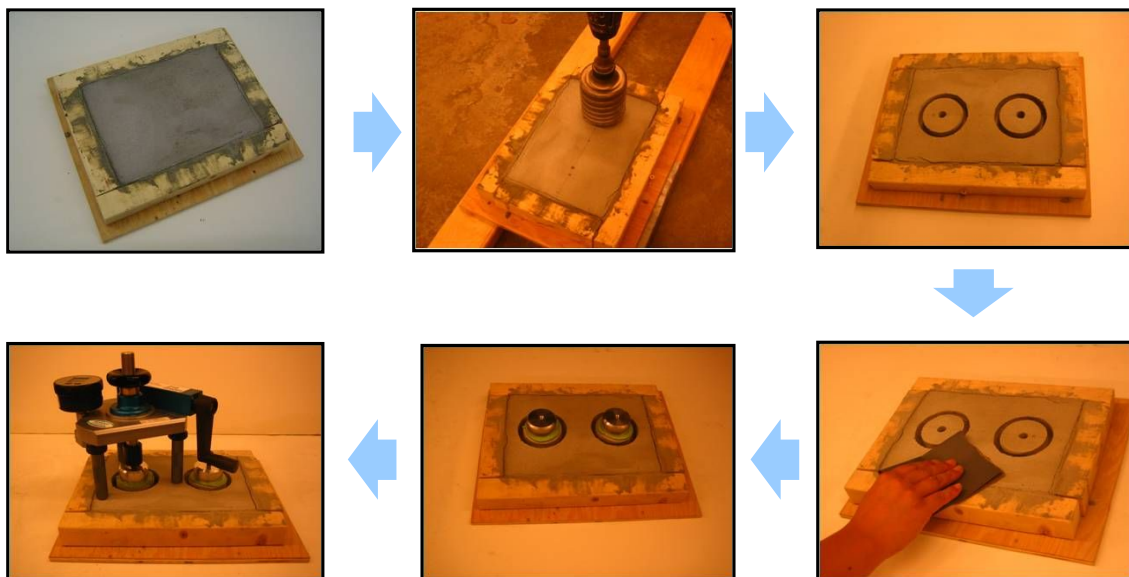


Fig.7.3 Procedure of Pull-off debonding test

7.2.3.3. Rapid chloride ion penetration test (RCPT)

The insulation mortar should have proper resistance to the penetration of moisture and aggressive chemicals from the environment, which requires a low permeability. The permeability test for PRIM was performed according to ASMT 1202 with seven days of curing. Two cylindrical specimens of 4" in diameter by 2" in height were used for the permeability test. The experimental apparatus used for this test, PROOVE-It tester, is shown in Figure 7.4. The cylindrical specimens were prepared by sealing the cylinder walls with silicone and allowing it to dry for 1 hour. This coating is to prevent the leaking of the fluid from the sidewalls of the specimen and to create a linear flow of the electrical current through the specimen. The specimens were vacuumed for three hours and saturated according to the ASTM standard for 18 hours. Each specimen was then immediately loaded into the device called Proove-It. Once loaded, solutions were added to the two chambers; one with a 3% solution of NaCl, and the other with 0.3N NaOH. The testing device applies a 60 Volt potential across the faces of the specimen for six hours. The apparatus measures the impedance in Coulombs over the total duration of the test.

This test method actually measures the electrical conductivity of the specimen, which can be considered as an indicator of the permeability of cementitious materials. The permeability depends on total porosity of the material and the connectivity of the pores. Apparently, to have high resistance to penetration of moisture and aggressive chemicals, the permeability should be as low as possible.

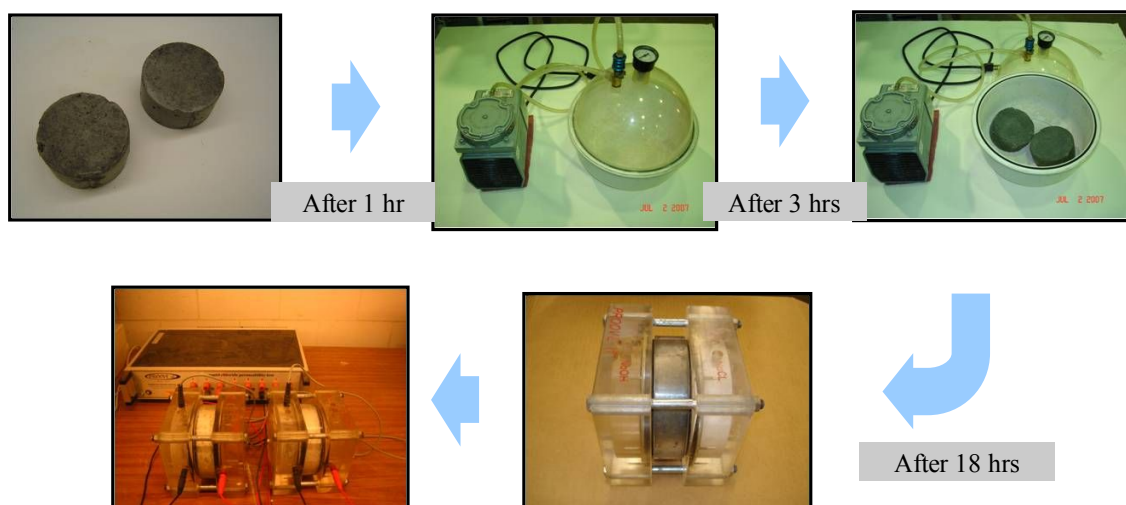


Fig.7.4 Procedure of chloride ion permeability test

7.2.3.4. *Dry shrinkage test (ASTM C-157)*

According to ASTM C 157, concrete prisms of 1” by 1” by 11” were made for the drying shrinkage test. After seven days of curing in the curing room (68°F and 100% Relative Humidity), the prisms were removed from the curing room and placed in the lab (temperature 72°F and relative humidity 35%). Due to the loss of moisture in the mortar specimen, there will be drying shrinkage in the specimen. Shortening of the prisms due to drying shrinkage is then measured. The drying shrinkage is a very important parameter for the mortar especially when the mortar is applied on a large flat surface. Large drying shrinkage of the mortar will lead to considerable surface cracks and may cause debonding between the mortar and substrate. Therefore, different mix designs were examined to obtain the mortar with smaller drying shrinkage.

7.3. TEST RESULTS AND DISCUSSIONS

7.3.1. *Compressive and flexural strengths*

The aim of this test is to investigate the mechanical properties of rubberized mortar and to observe the effect of different size of fine rubber powders.

7.3.1.1. *Effect of rubber replacement rate*

Compression test of rubber mortar were tested after 7 days of standard curing. There were three specimens for each group. The following figure 7.5 and 7.6 are rubber mortar cube specimens of each group and experimental set-up. Table 3 and figure 7.7 shows the average values of the compressive strengths on rubber dosage. As the result of compressive test, the increase of rubber particles in mortar significantly had an effect on the strength of rubber mortar. That is, as using rubber powder to replace equal volume of fine aggregate by 50%, the strength of rubber mortar was reduced up to 30%.

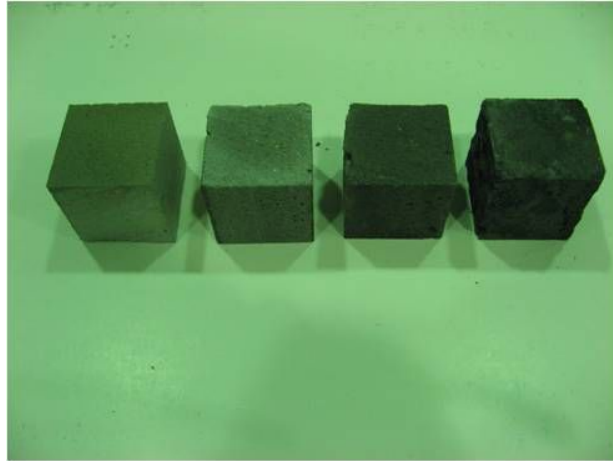


Fig.7.5 Rubber mortar cube specimen

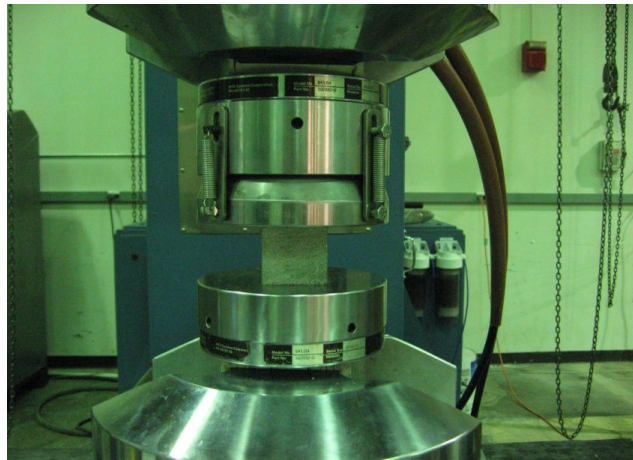


Fig.7.6 compressive test set-up

Table.7.3 Compressive strength according to different rubber dosage

No.	rubber (replacement)	# 1	# 2	# 3	Ave. max. strength
A	0%	1,803	2,272	2,049	2,041
B	50%	485	682	682	616
C	70%	375	386	227	329
D	90%	163	152	102	139

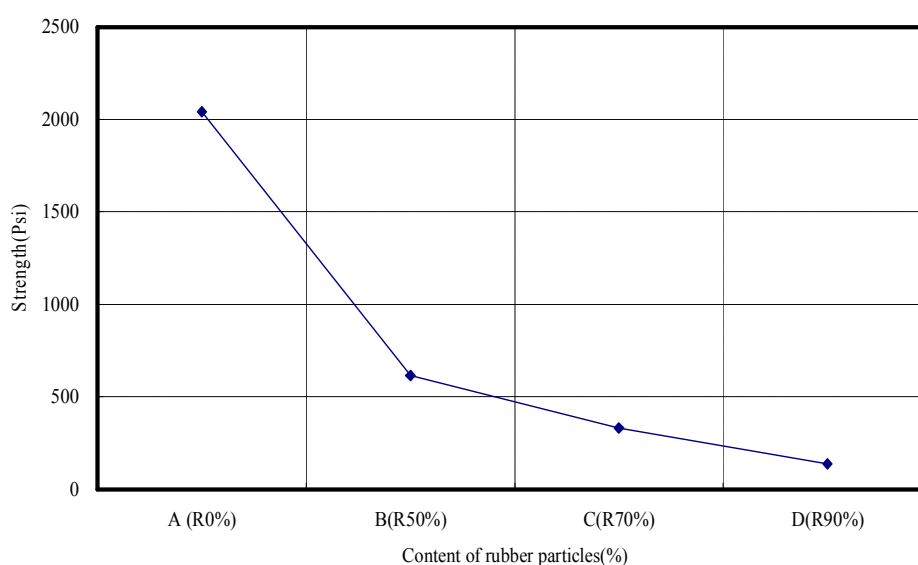


Fig.7.7 Strength of rubber mortar according to different rubber dosage

7.3.1.2. Effect of Redispersible Polymer Powder (RPP)

Table 7.4 and Figure 7.8 show the compressive strengths on different RPP contents. In this group of specimens, the rubber replacement rate was fixed at 50%, and only RPP content was varied. From the figure and the table, it is very clear that an increase of RPP in the mortar increases the strength of the mortar (2A, 2B, and 2C).

However, the improvement on the compressive strength is not significant when the RPP content is larger than 10% of the cement (2D). In fact, there was a slight decrease of the strength. This means that the enhancement to compressive strength reaches an optimum point at 10% of RPP.

Table.7.4 Compression strength of each specimen according to contents of RPP

No.	RPP MP2050 (% of cement)	# 1	# 2	# 3	Ave. max. strength
2A	30 (6%)	625	621	488	578
2B	40 (8%)	485	682	682	618
2C	50 (10%)	780	818	731	776
2D	60 (12%)	737	720	813	757

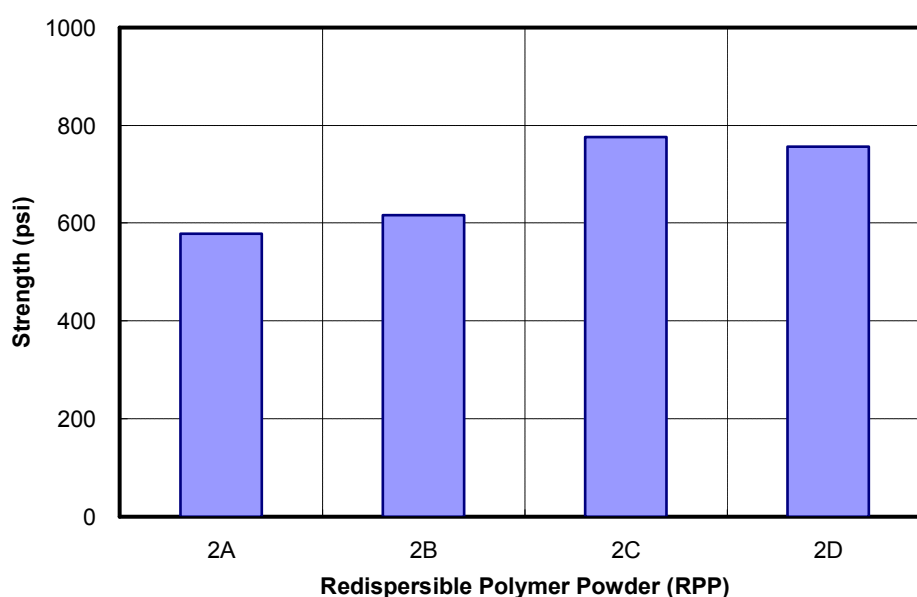


Fig.7.8 Strength of rubber mortar according to different RPP content

7.3.1.3. Effect of different size of fine rubber powder

In order to evaluate the effect of rubber particle size on the strength of PRIM, two different sizes of rubber powders were used to replace the fine sand. The two different sizes were #100 mesh (150 μ m) and #200 mesh (75 μ m). The compressive strength of mortar was tested after seven days of standard curing.

Table 7.5 lists the test data of compressive strengths and figure 7.9 shows the average compressive strength of cubic specimens with different sizes of rubber powder. As the results show, the compressive strength of the cubic specimens with #200 mesh rubber powder is higher than that with #100

mesh rubber powder up to about 30%, which means that the rubber size has a significant effect on the mechanical property of rubber mortar. As mentioned earlier, the smaller size of rubber particles allows them to better fit into the pores of cement paste and thus reduces the effect of incompatibility in mechanical properties of the rubber and cement paste.

Table.7.5 Results of compression test with different size of rubber powders

<i>Specimen No.</i>	<i>#100</i>	<i>#200</i>
#1 specimen	780	1180
#2 specimen	818	1250
#3 specimen	731	1134
Average	776	1188

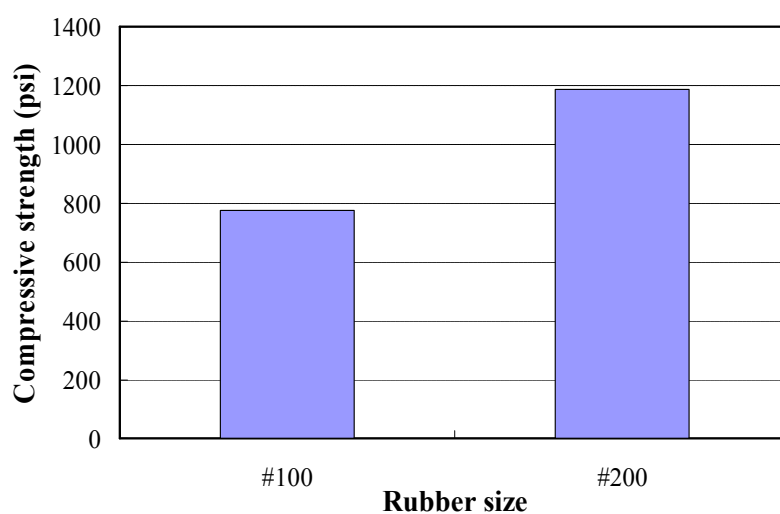


Fig.7.9 Average compressive strength of different size of rubber powders

7.3.1.4. Modulus of rupture

In order to evaluate the flexural strength of the rubber mortar, 3-point bending test was conducted. The modulus of rupture of ordinary cement mortar is about 940 psi (Serge et al, 2004). As shown in Table 7.6, the average flexural strength of the rubber mortar is about 550 psi, which is about 41% lower in

comparison with ordinary cement mortar. The reduced flexural strength is apparently due to the added rubber particles.

Table.7.6 Modulus of rupture

<i>Specimen No.</i>	<i>7 days</i>
#1 specimen	528.5 psi
#2 specimen	545.3 psi
#3 specimen	578.3 psi
Average	550.7 psi

7.3.2. **Bonding strength**

Pull-out test was carried out on the mortar slab to measure the bonding strength of the interface between wood and the rubber mortar. The specimens were tested after 7 days and 28 days. The results of the debond test are shown in Table 7.7. Figure 7.10 shows the specimens after the debond test. One can see that the failure took place right on the interface between the mortar and the wood panel. The minimum bond strength recommended by ASTM 1329-29 is 70 psi at 28days for type N mortar. Based on the result, the bond strength does not satisfy the minimum required strength. The reason is that the rubber particles do not bond well to the wood plate. When the rubber particles were added into the mixture, the effective bond surface area of the specimens is reduced.

It is worthwhile to mention that in the actual application of insulation mortar on wood panels for exterior walls of timer structure, a layer of metal mesh is nailed on the panel prior to the installation of the mortar layer. After the mortar is applied on the panel, the metal mesh is embedded in the mortar layer providing a significant adhesive force to keep the mortar layer on the wall. Thus, the low bond strength of the rubber mortar does not become a problem for its application.

Table.7.7 Bond strength of rubber mortar

<i>Specimen No.</i>	Bond strength (psi)
#1 specimen	63
#2 specimen	38
Average	50.5

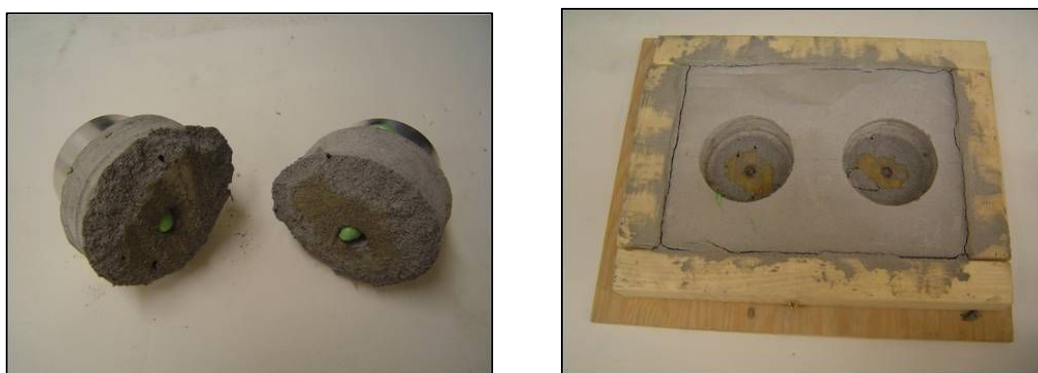


Fig.7.10 Pull-out debonding test specimen

7.3.3. *Dry shrinkage*

After a curing period of seven days in the curing room, readings were taken for the initial length of mortar bars. The specimens were then placed in the lab environment with 23 °C ambient temperature and 40% relative humidity for 90 days. In the first 4 weeks, drying shrinkage was measured every 2 days, and after 4 weeks, once a week. Figure 7.11 shows the shrinkage strains of the specimens up to 90 days. Drying shrinkages of the two rubber mortar specimens are between 1,400 and 1,600 microstrains. Heath et al. (1999) conducted various tests on drying shrinkage and thermal expansion of ordinary cement mortars and concretes. Their results showed that long-term drying shrinkage of the mortar is typically between 800 and 2,000 microstrains, depending on mix design of mortar and curing time. With a long curing time such as 28 days or 56 days, the drying shrinkage tends to reach the low end of about 800 microstrains, and with a short curing time such as seven days used in this study, the drying shrinkage tends to reach the high end of about 2,000 microstrains. Therefore, the drying shrinkage of PRIM is comparable to the dry shrinkage of ordinary cement mortar.

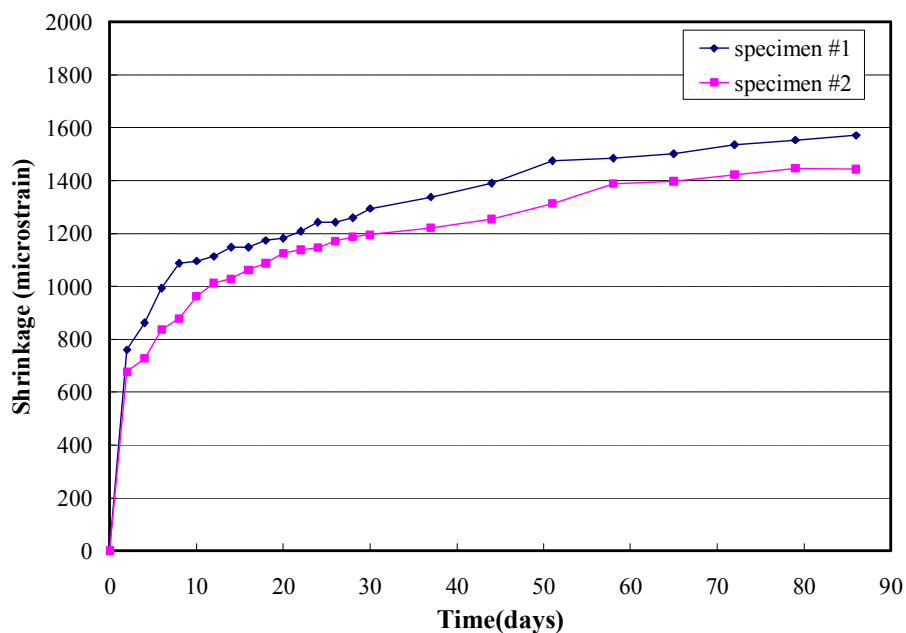


Fig.7.11 Dry shrinkage of insulation mortar with rubber powder for 90days

It is important to point out that there are other types of time-dependent deformations in addition to drying shrinkage. One of them is called autogeneous shrinkage which is induced by the chemical reactions in the mortar such as the hydration reactions between Portland cement and water, and another is called basic creep that is caused by sustained mechanical loading applied on the specimen. There are also time-dependent coupling effect between the moisture loss and applied loading, the corresponding long-term deformation is called drying creep. These time-dependent deformations are shown in figure 7.12, and these deformations are important for the long-term performance of the mortar. With limited funding and project period, these long-term deformations were not studied for the rubber mortar.

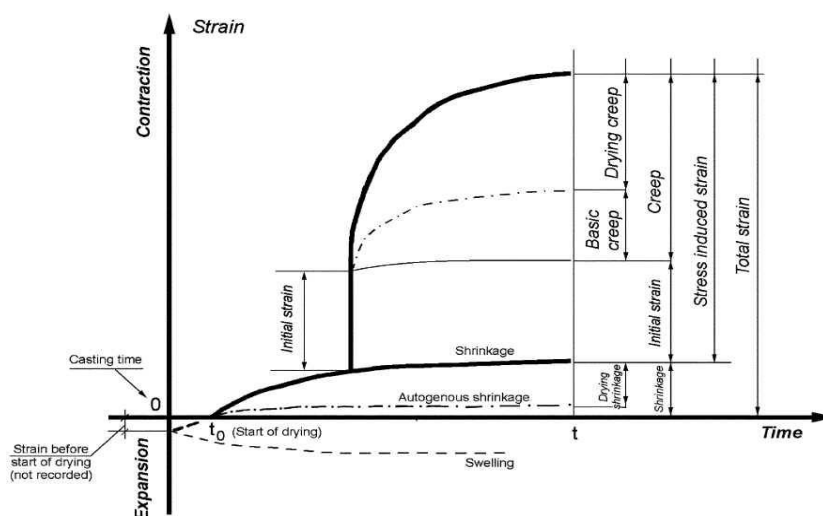


Fig.7.12 Relationship between various measured and derived strain values (ACI, 2005)

7.3.4. Permeability

The purpose of this test is to evaluate the resistance of the mortar to chloride ion penetration. The test measures the electrical current passing through a specimen (4 by 2 inch) for a period of 6 hours at 60 voltages, according to ASTM 1202. The testing result in coulomb provides an indication of the penetration resistance of the mortar. As shown in Table 7.8, when the applied voltages were lower than the required 60 voltages, reasonable readings were obtained; while at the 60 voltages, the readings were more than 500mA, which is considered as overflow. The overflow indicates that there is too much current passing through the specimen, implying a very low penetration resistance to the ions.

Table.7.8 Results of chloride ion permeability test

<i>Voltage</i>	Coulombs
10 V	232
20 V	463
30 ~ 60 V	Over flow

Low permeability is a basic requirement for any mortar to be used on exterior walls. Therefore, it is important to identify the reasons for such a low penetration resistance of the mortar. There are two possible reasons. One is that the mortar might be extremely porous, which leads to low penetration resistance. Another is that the mortar is not porous but one or more than one additive used in the mortar is conductive.

In order to identify the reason(s) for the low penetration resistance of the mortar, additional tests were conducted. Table 7.9 shows the mix designs of the additional test. Specimen 4A is made of cement, sand, and water without any additives. 4A was designed to examine the penetration resistance of the pure mortar, to see whether the mortar has very high porosity (and low resistance). In Specimens 4B, 4C, and 4D, each additive was added separately in the specimens. These three specimens were designed to examine the effect of each additive, to see if any one of them is conductive or not. Specimen 4E was for the rubber mortar. It was designed to compare with 4A to see the improvement in the permeability. The amount of water in 4A was reduced due to the workability of the specimen.

Table.7.9 Mix designs for additional tests

No.	cement	sand	rubber	cellulose ether	wood fiber	RPP	water
4A	500g	625g	0	0	0	0	250g
4B	500g	625g	0	0	0	50g	400g
4C	500g	625g	0	0	6g	0	400g
4D	500g	625g	0	5g	0	0	400g
4E	500g	625g	230g	0	0	0	400g

Table 7.10 shows testing results of the additional specimens using the required 60 voltages. 4A (pure mortar) had 2060 Coulombs, which is a proper value according to the ASTM standard. 4B with RPP as additive had 5352 Coulombs, which is considered as a high current flow and thus low resistance to chloride ions. The low resistance is actually due to the increased water-cement ratio (comparing with 4A). The specimen 4C with wood fibers as additive exhibited a similar result as that of 4B. 4B and 4C

did not result in any overflow, which means RPP and wood fibers are not conductive. In the case of 4D, cellulose ether was used as additive, and there was an overflow. So, the additional testing results provided solid evidence that the cellulose ether is a conductive material in the rubberized mortar. Specimen 4E exhibited a very low value which means its resistance to the current is very high.

Table.7.10 Test data of additional rapid chloride permeability tests

<i>Specimen No.</i>	<i>Coulombs</i>	<i>Chloride ion penetrability</i>
4A	2060	Moderate
4B (+RPP)	5352	High
4C (+wood fiber)	4644	High
4D (+cellulose ether)	Over flow	-
4E (+Rubber)	184	Very low

As discussed earlier, the rapid chloride ion penetration test (ASTM 1202) is for electric conductivity of the material, which is an indirect testing method for the permeability (chloride permeability and moisture permeability). Cellulose ether is conductive to the electric current might not mean it has low resistance to chloride ions and moisture. Therefore, caution should be taken when cellulose ether is to be used in the mix design for the mortar when low permeability is required for the construction project. Since the test result of specimen 4E is very low, we can conclude that the permeability of the rubber mortar is very low.

7.3.5. *Microstructure observed by Scanning Electron Microscope (SEM)*

In order to investigate the porosity and the distribution of admixtures, Low Vacuum Scanning Electron Microscope (LVSEM) in Nanomaterials Characterization Facility (NCF) was used for this study. As shown in **Error! Reference source not found.**, the images of (a) and (c) captured the distribution of additives such as wood fiber and rubber powder, and the images of (b) and (d) showed the distribution of composite matrix and porosity.

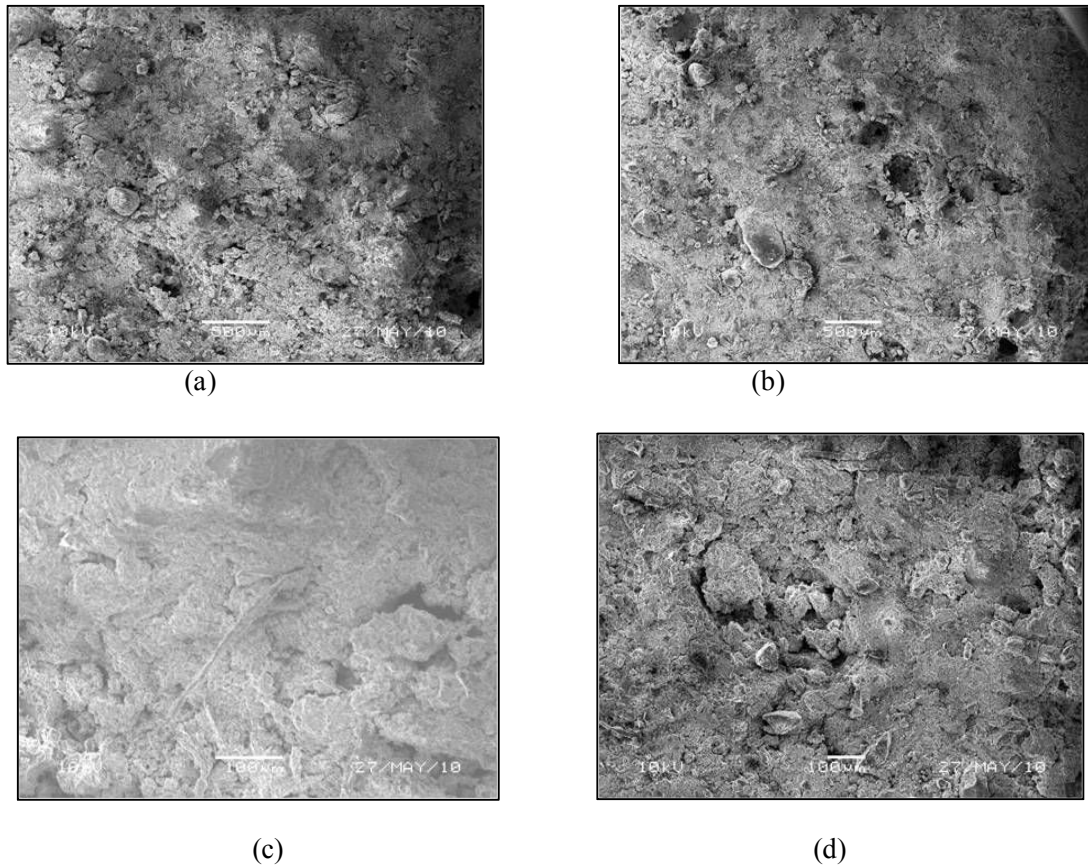


Fig.7.13 Images of SEM on the mortar specimens.

7.4. CONCLUSIONS

1. Rubber powders (very fine rubber particles) were used to make PRIM. Two different sizes of rubber powder were used: #100 mesh (0.15 mm) and #200 mesh (0.075 mm). The compressive strength of the rubber mortar with #200 mesh was higher than that of #100 mesh, which means smaller rubber particles result in higher strength. Therefore, smaller rubber particles should be used in order to obtain high strength rubber mortar.

2. The average flexural strength of the PRIM was about 550 psi at 50% rubber replacement rate, which is comparable to the flexural strength of ordinary cement mortar.

3. Different amounts of rubber powder were used to replace fine sand. With increasing content of rubber powder, the compressive strength of the rubber mortar decreased. RPP is an effective

additive which can improve the compressive strength of the rubber mortar. However, the improvement on the compressive strength is not significant when the RPP content is larger than 10% of the cement.

4. In order to measure the bond strength between wood panel and rubber mortar, a pull-out debond test apparatus was used. The bond strength did not satisfy the minimum requirement. This is because the rubber powder in mortar does not have bond strength with the wood panel, and therefore, the effective bonding surface area is reduced.

5. When the rubber mortar was exposed to the ambient environment after seven days of curing, the drying shrinkage of the rubber mortar is about the same as the dry shrinkage of ordinary cement mortar.

The chloride permeability of the rubber mortar is very low. Caution must be taken when using ASTM 1202 (the rapid chloride permeability test) to evaluate the permeability of rubber mortars with various additives. This is because certain types of additives may be electrically conductive. For instance, cellulose ether as an additive used in the present study is conductive.

6. The rubber mortar made of fine rubber powders can be used as an insulation mortar. Either #100 or #200 sieve rubber powder can be used in the mortar. #200 rubber powder gives higher compressive strength of the mortar. The rubber replacement rate and the RPP dosage can be adjusted to satisfy strength requirements. Drying shrinkage and permeability are comparable to those of ordinary cement mortar. Bond strength is low and thus a metal mesh should be used together with the mortar to ensure the bond between the mortar layer and the wood panel.

CHAPTER 8

DURABILITY OF SULFUR RUBBER CONCRETE

8.1. INTRODUCTION

For decades, many researchers have attention to use the scrap tires in portland cement concrete mixtures (Eldin et al, 1993; Biel et al ,1994; Schimizzate et al., 1994; Segre et al, 2000; Topcu, 1995 and 1997). Because the use of rubber particles from waste tires helps to recycle the waste tires, and provides a viable solution to alleviate the disposal problem of waste tires. However, there have been enough efforts to investigate the potential use of recycled rubber tires in sulfur concrete so far.

Sulfur concrete is characterized by its high strength, high abrasion resistance and high chemical corrosion resistance. It does not support combustion, sulfur presented in the surface can slowly burn when exposed to direct flame but it self-extinguishes when the flame is removed. On the other hand, the sulfur cement that bonds the aggregates in the concrete has thermoplastic properties. Consequently, the concrete can be crushed, re-melted and reformed without loss of strength or other properties. In another words, it can be completely recycled. Though its cost of one-time application is higher, the cost for recycling will be much lower (Vroom, 1998).

At present, sulfur concrete is mainly applied in some structures suffering chemical corrosion, for some chemical plants, offshore structures, food plants, etc. The uses of sulfur concrete are expanding progressively, for example, using sulfur concrete in such applications as highway pavement and airfield runway, etc. Iran has carried out a successful test on the applications of sulfur concrete, and Canada has

already made railway crossties using sulfur concrete (Vroom, 1998).

Rubber particles used in Portland cement concrete suffer from the weak interface between the particles and the Portland cement matrix. This is because rubber is an elastic material and cement paste is a brittle material, and the inconsistency of the two components results in the weak interface. Several methods have been examined to enhance the interface strength, and sulfur rubber concrete is one of the methods. Although sulfur cement matrix is brittle, we expect that there will be a thermoplastic reaction between the matrix and rubber particles under high processing temperature, which may be able to improve the bond between the two components and thus enhance mechanical properties of sulfur rubber concrete. However, we still need to study for durability performances because the optimized mix design for the mechanical property does not mean the optimized durability performance of SRC.

The purpose of this test is to investigate an additional mechanical property and durability performance of SRC according to rubber contents on the basis of the optimized strength mix design. The durability performance is reported with aid of chloride permeability and, freeze-thaw test in this study.

8.2. EXPERIMENTAL DETAILS

8.2.1. *Optimum mix design*

The optimum content value of sulfur-rubber concrete through the compressive strength test is investigated. In order to find the optimal mix design of the sulfur-rubber concrete, the mix design of sulfur and rubber by total volume is firstly fixed at about 33.6% and 19.9% respectively. From several compressive strength tests, the mix design with the highest compressive strength was obtained. In the mix design, the optimal content of sand and fly ash (class F) was about 46.5%. It was also found that the compressive strength is decreased as the content of rubber is increased from 0% to 50%.

8.2.2. *Materials and mixture portion*

Sulfur, sand, fly ash (Class F) and rubber particles were used as constituents for the sulfur-rubber concrete in the present study. Fly ash with specific gravity 143.58 pcf. [2.3 g/cm³] was used as the

mineral filler. The general purpose sand produced commercially was used. The crumb rubber was from JaiTire Industries Inc. The average size of the rubber particles was 0.16 in. [4.12 mm]. The bulk density and specific density of the rubber particles were 31.21 pcf. [0.5 g/cm^3] and 62.43 pcf. [1.0 g/cm^3], respectively. The sulfur was from Test Mark Industries, Pennsylvania, the specific density of which was 116 pcf. [1.87 g/cm^3].

Referencing to ASTM C 1312-97 (Making and Conditioning Chemical-Resistant Sulfur Polymer Cement Concrete Test Specimens in the Laboratory), all materials should be weighed accurately. Then, for the wet process, the sulfur and rubber particles are put together into the pot and heated, but for the dry process, the sulfur in the hot-pot is firstly heated for 45min and rubber and other contents, which are preheated, are put into the sulfur. At this time, fly ash (class F) is used as the mineral filler.

To inspect the ductility and durability performance in this study, the optimized wet process in the previous study is used in both wet and dry process. The mix design is shown in Table 8.1.

Table.8.1. Mix design

No.	Sulfur (%)	Fly ash (%)	Rubber (%)	Sand (%)	Fly ash: Rubber : Sand (%)
R0	33.6	6.6	0	59.8	10 : 0 : 90
R1	33.6	6.6	6.6	53.2	10 : 10 : 80
R2	33.6	6.6	13.3	46.5	10 : 20 : 70
R3	33.6	6.6	19.9	39.9	10 : 30 : 60
R4	33.6	6.6	26.6	33.2	10 : 40 : 50
R5	33.6	6.6	33.2	26.6	10 : 50 : 40

8.2.3. *Specimen preparation*

The gauge length of the axial extensometer is 4.5 inch. To measure axial deformation with the extensometer, 3 by 6 inch specimens are used in the compressive strength test. If the size of the specimen is bigger than 3 by 6 inch, the preparation of specimen is no easy because the sulfur is hardened very fast. The size and preparation of specimen according to the test is as shown in Table 8.2.

Table.8.2 Preparation and size of specimens

% of rubber		R0	R1	R2	R3	R4	R5	Total
Compressive test (3(D)×6(H) in cylinders)	Dry	3	3	3	3	3	3	33
	Wet		3	3	3	3	3	
Total		3	6	6	6	6	6	33

8.2.4. *Mixing process*

There are two mixing processes for sulfur-rubber concrete; dry and wet process. For the dry process, the sulfur is placed into a hotpot and heated first under the heating temperature of 294.8 °F [146 °C]. At the same time, the other materials (the rubber particles, sand and Portland cement) are preheated to about 203°F [95 °C] in an oven. In order to mix them up well, blender should be used for 1 min. The heating time for the dry process is about 30min until the sulfur had completely melted to a slurry. The other materials (the rubber particles, sand and Portland cement) are added into the melted sulfur and mixed uniformly with a hand paddle.

For the wet process, the sulfur and rubber particles are put together into the hotpot and heated under the recommended heating temperature for 45min. Simultaneously, the other materials (other than sulfur and rubber particles) are preheated to about 215.6 °F [102 °C] in an oven for 30 min. before added to the pot.

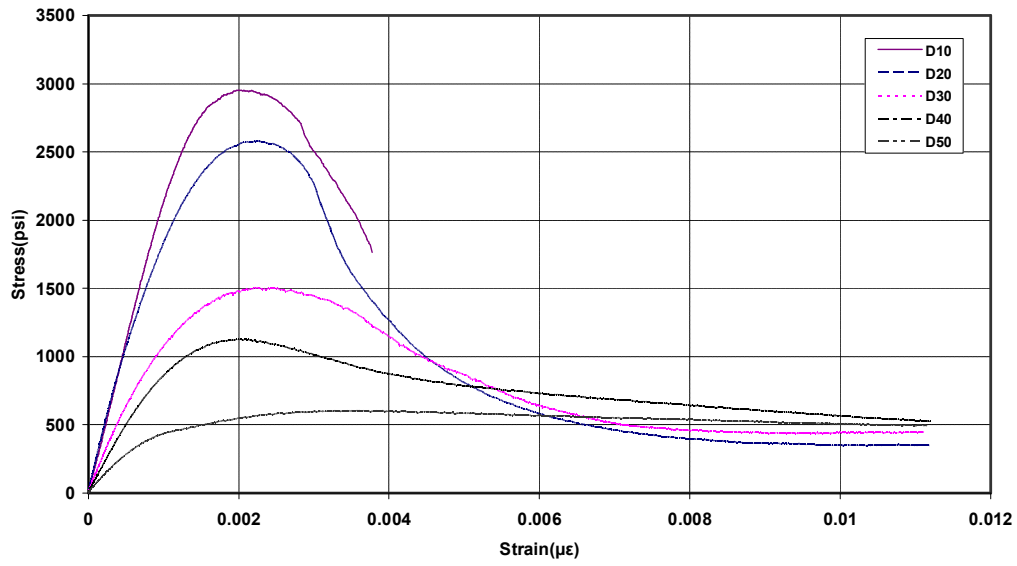
8.3. TEST RESULTS AND DISCUSSION

8.3.1. *Compression test*

To investigate the mechanical properties of SRC from stress-strain curve, the compressive test was conducted with 3 by 6 inch specimens. The facilities used for this test were MTS machine and axial extensometer. Figure 8.1 shows the set-up and procedure of compressive test. Figure 8.2 shows variation of compressive stress-strain curve according to the various rubber dosages in the dry and wet process. In these results, as the rubber dosage is increasing from 10% to 50%, the maximum strength is decreasing up to about 80%, but the ductility of SRC is increasing in both processes. The area under the stress-strain curve represents the fracture energy of the material which is a measure of toughness. And the strain corresponding to the maximum stress reflects the failure mode of the material (brittle or ductile). Figure 8.3 shows the peak stress in various rubber contents in different mixing process. In this figure, one can recognize the strength of SRC in dry process is higher than that in wet process. Figure 8.4 shows normalized stress-strain curve at 30% of rubber dosage in dry and wet process. Stress-strain curve in both processes is almost same. This result indicates that the ductility of SRC is same, regardless of mixing process.

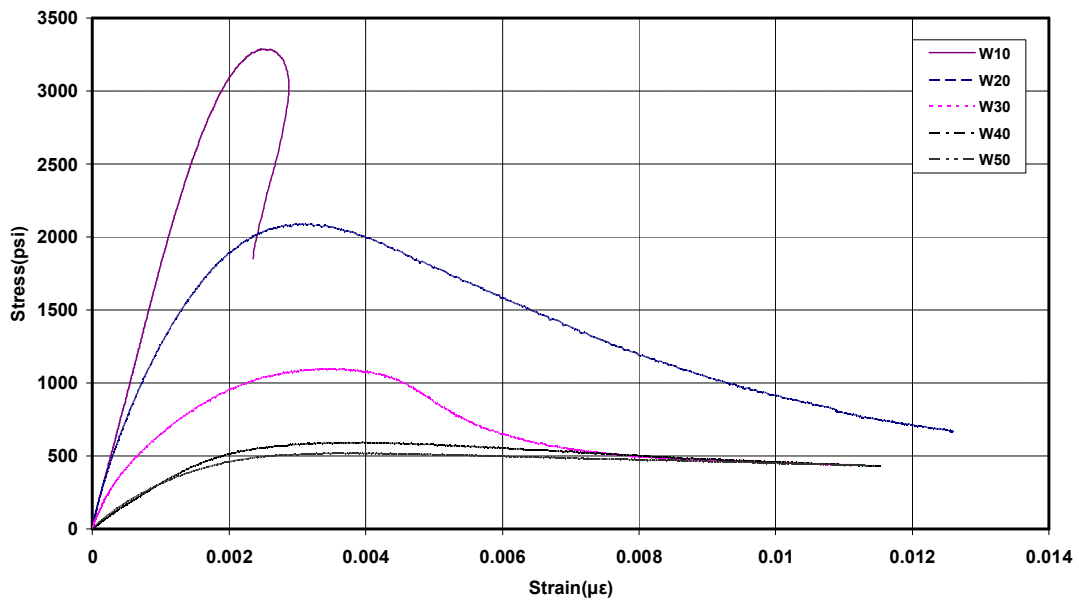


Fig.8.1 Set-up and procedure of compression test



(a) Stress-strain curve of SRC in Dry process

Stress-Strain curve (Wet process)



(a) Stress-strain curve of SRC in Wet process

Fig.8.2 Stress-strain curve in dry and wet process

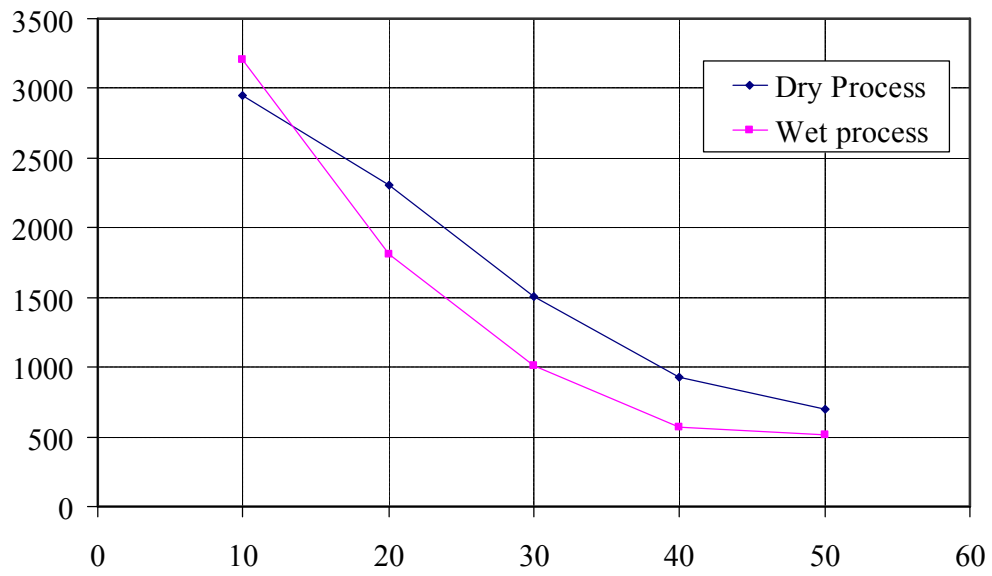


Fig.8.3 Strength in dry and wet process according to rubber dosage

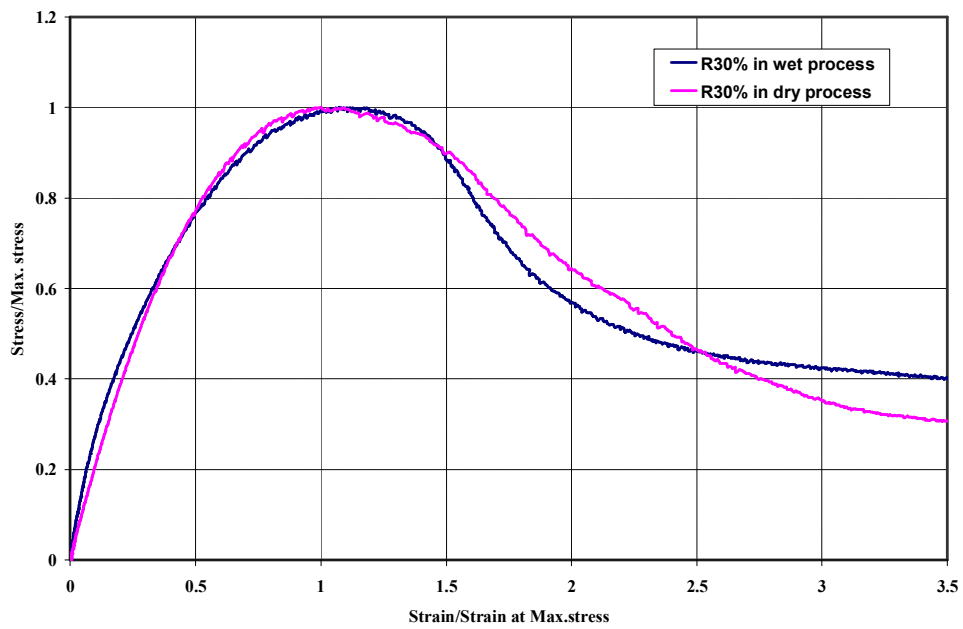


Fig.8.4 Normalized stress-strain curve at 30% of rubber dosage

8.3.2. *Suggestion of mix process*

The noticeable difference between the wet and the dry process is that only the sulfur is preheated in the dry process, while the sulfur and the rubber particles are preheated together in the wet process. That is, the main distinction is the time when the rubber particles are mixed with sulfur. However, when the SRC is made by the wet process, rubber particles can be burned before sulfur is completely melted for 45min. To solve this problem, improved wet process is suggested as figure 8.5.

Figure 8.6 shows the comparison of strength of SRC specimen made by three different mixing processes. The strength of SRC with suggested mixing process is improved up to almost the same as the strength of dry process.

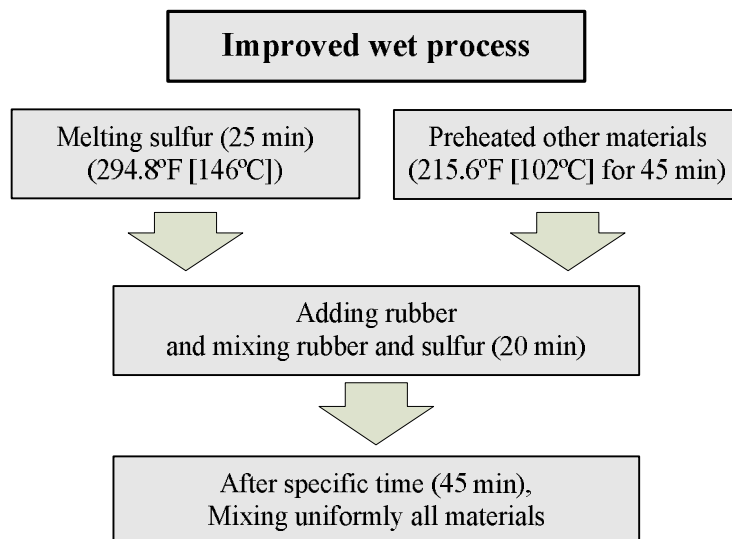


Fig.8.5 Combined mixing process

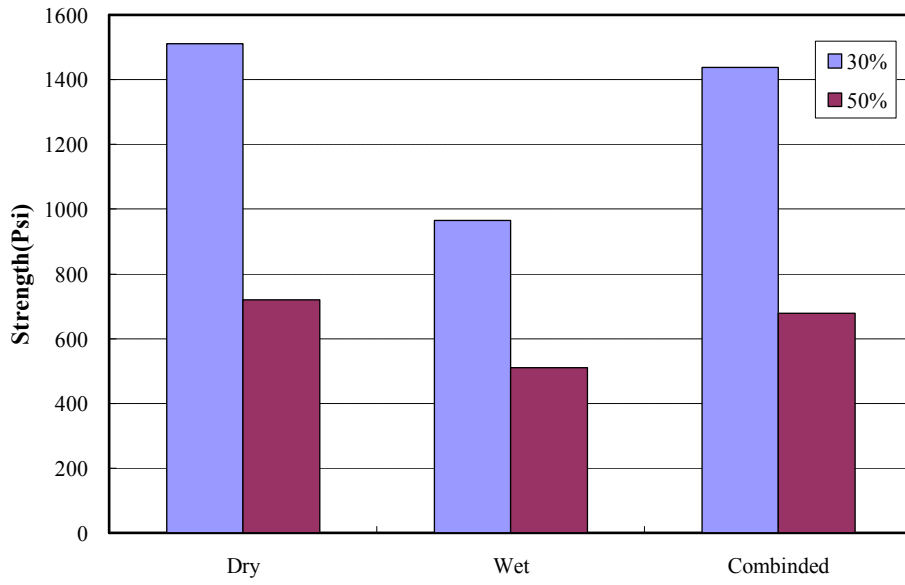
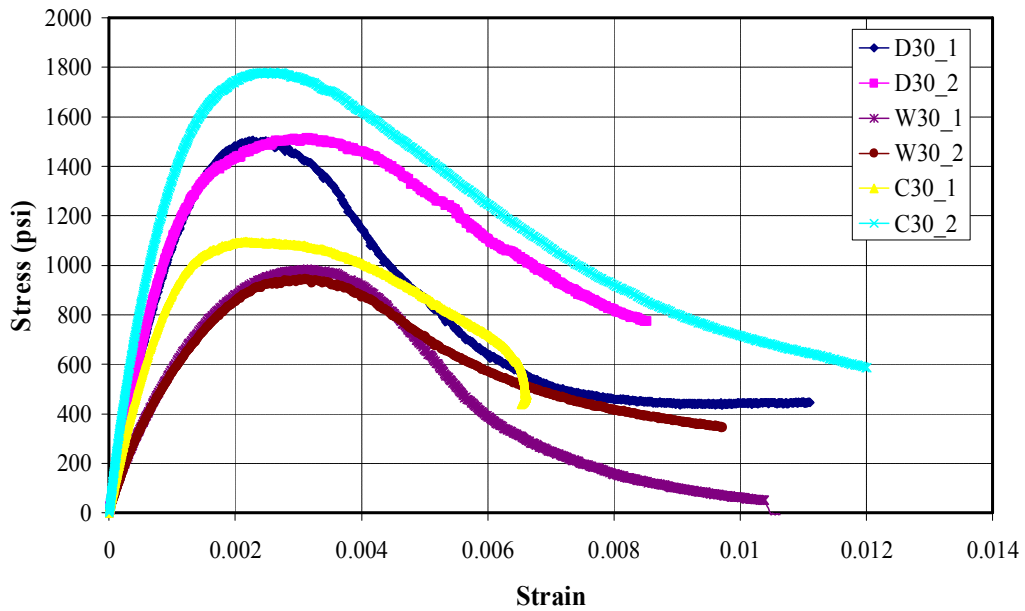


Fig.8.6 Strength comparison with various process



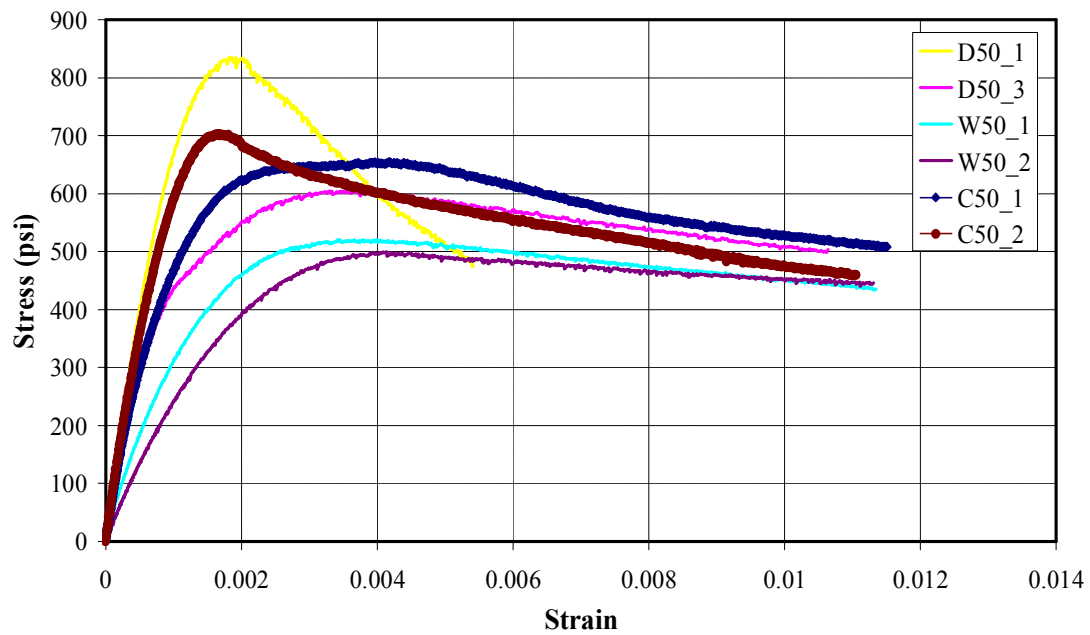


Fig.8.7 Strain-stress curve of SRC specimen made by combined processor

8.3.3. Permeability

This following figure shows the chloride ion penetration according to the rubber dosage. As the rubber content in SRC is increasing, the penetration of chloride ion through SRC disc specimen (4 by 2 inch) is decreasing. That is, when there is no rubber particle in SRC specimen, the value of ion penetrability is about 3400 coulomb and that is moderate according to the indication table of ASTM C 1202. But as increasing of the rubber content, the internal organization of SRC is more sophisticated. So the penetration of chloride ion is getting lower.

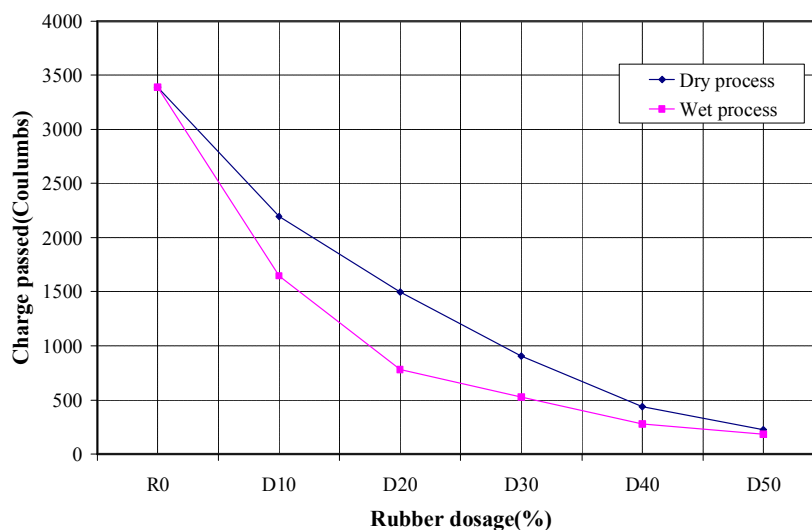
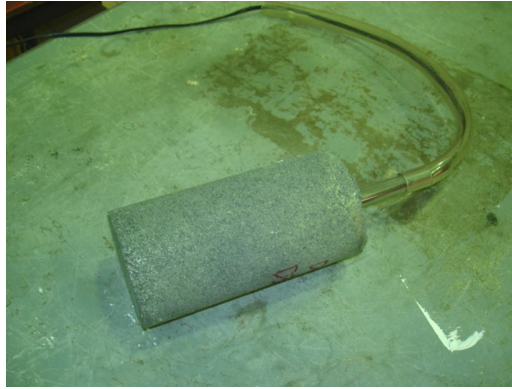


Fig.8.8 Charge according to rubber dosage

8.3.4. Freezing –thaw resistance

The purpose of this test is to investigate the resistance of concrete to rapidly repeat cycles of freezing and thawing in the water standardized by ASTM C666. The freezing-and-thawing machine consists of a suitable chambers in which the specimens can be subjected to the specified freezing-and-thawing cycle, together with the necessary refrigerating and heating equipment and controls to produce continuously, and automatically, reproducible cycles within the specified temperature requirements.

For this experiment, 3 by 6 cylindrical SRC specimens made by dry process are used. In order to monitor the temperature in chamber and the center of specimen, temperature sensor is installed as shown in Figure 8.9 (a) and (b). Figure 8.10 is the temperature cycles in the center of SRC specimen and chamber and figure 8.11 shows the test set-up of SRC specimens in the freeze-thaw chamber. The temperature range in the center of specimen is from 0°C to -13°C and ambient temperature range is about 20°C to -12°C.



(a) Set-up the sensor in the center of specimen



(b) Sensor for measuring the ambient temperature in the chamber

Fig.8.9 Temperature sensors in the center of specimen and chamber

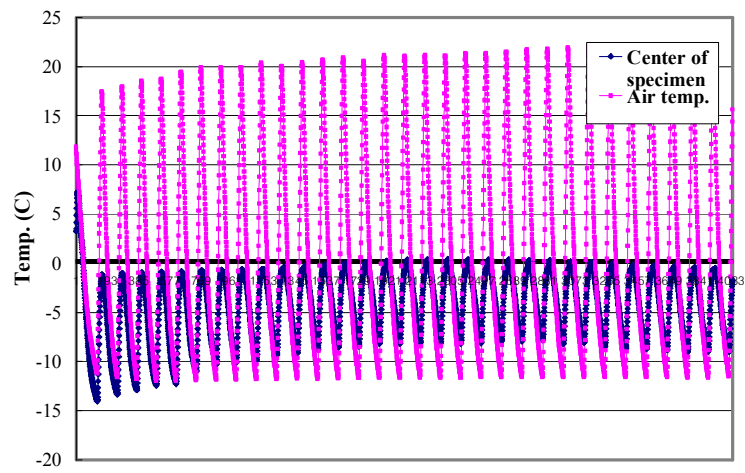
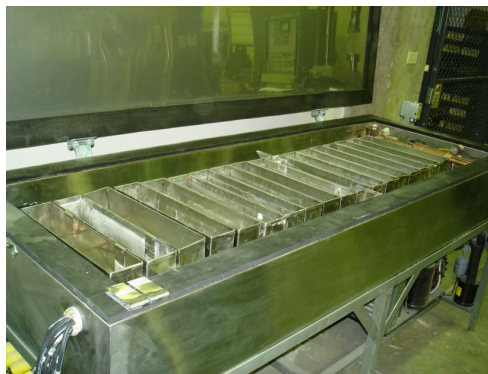


Fig.8.10 Temperature cycles in chamber and center of specimen



(a) Freeze- thaw chamber and containers



(b) Frozen specimen after 30cycles

Fig.8.11 Specimens set-up in freeze-thaw chamber

This freeze-thaw test is performed until 300 cycles and each cycle is to take 3 hrs. After 30 cycles, the transmission time is measured with ultrasonic pulse velocity (UPV) as shown in Figure 8.12. As the result of Figure 8.13, the transmission time for measuring the travel velocity through the specimen gradually increases due to the effect of freezing-thawing cycles. Accumulation of freezing-thawing cycles occur the damage in the specimen, especially in lower rubber dosage. That is, rubber particles are the main factor to increase the durability of SRC.

In order to investigate the effect of mechanical property, compression test is performed after 300 freezing-thawing cycles. In Figure 8.14 and 8.15, the reduction of compression strength in D10 is 40%, but the other specimens have about 25% reduction of strength. That means the amount of rubber particles has an important effect on the contraction and expansion of SRC for freezing and thawing. Furthermore, the stiffness of SRC in Figure 8.16 is decreased up to about 40% and 90%, respectively. In SRC of 50% rubber content, the difference of stiffness is less than about 10%. That is, the rubber particles have main effect on the durability of SRC.



Fig.8.12 Equipment of ultrasonic pulse velocity (UPV)

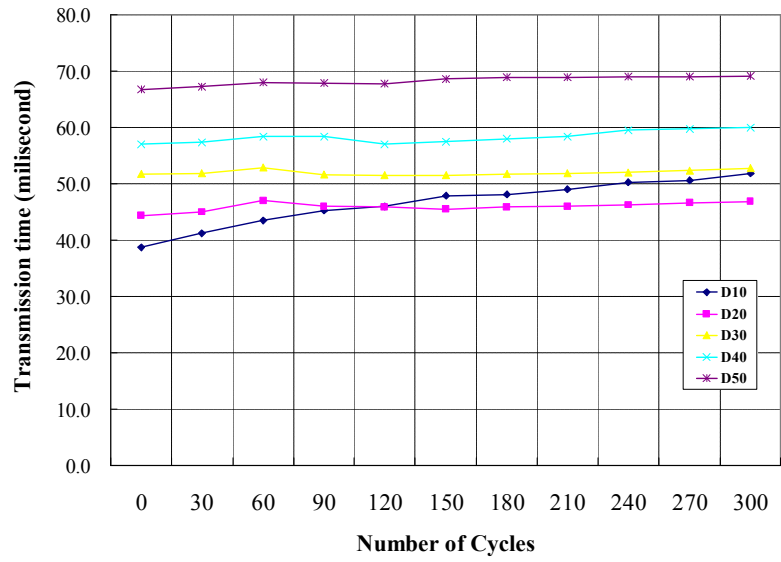


Fig.8.13 Transmission time after 300 cycles

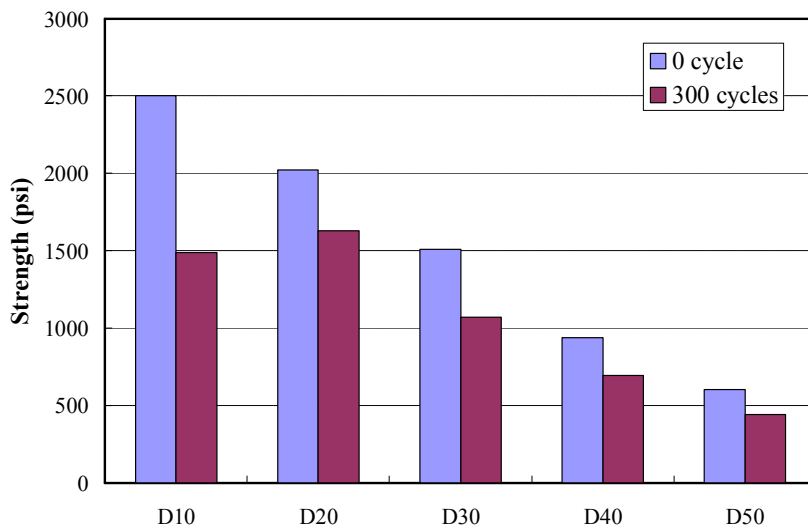


Fig.8.14 Equipment of ultrasonic pulse velocity (UPV)

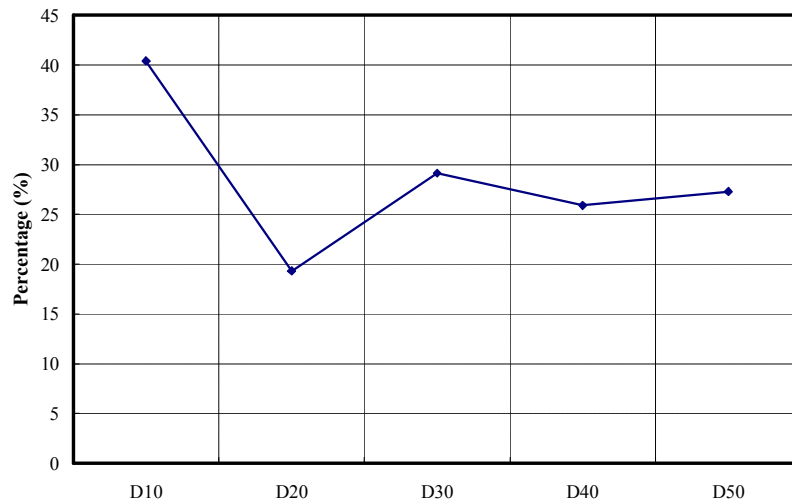


Fig.8.15 Difference of strength after 300 freeze-thaw cycles

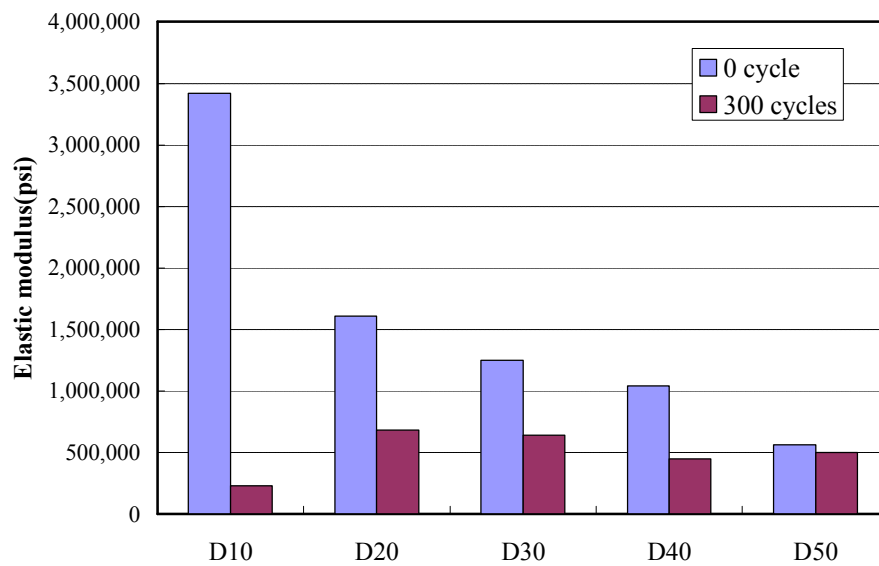


Fig.8.16 Comparison of stiffness of SRC after 300 freeze-thaw cycles

8.4. CONCLUSIONS

1. In order to investigate the mechanical properties of sulfur-rubber concrete, the compression test was performed, according to the different amount usage of rubber particles instead of aggregates. As the rubber dosage was increased from 10% to 50%, the compression strength was reduced up to about 80%. Also, the strength of SRC in dry process is higher than that in wet process. The rubber particles can improve the ductility of SRC, but the strength of SRC is reduced.

2. In wet process, the sulfur is not completely mixed with rubber particles during the optimized heating time. The rubber tends to be burned before the sulfur is melted. Therefore, the improved wet process is suggested. After melting sulfur for 20min, rubber is put into the hat pot to mix with the melted sulfur. After well stirring them for 10min, the preheated other materials can be uniformly mixed with sulfur-rubber.

3. For long term durability of sulfur rubber concrete, freeze-thaw resistant was performed. The increasing of freezing-thawing cycles results in the damage in the specimen, especially in lower rubber dosage. That is, rubber particles are one of the main factors to increase the durability of SRC.

CHAPTER 9

CONCLUSIONS AND FUTURE RESEARCH RECOMMENDATIONS

9.1. CONCLUSIONS

This thesis can be largely classified as two numerical model, two theoretical model, and two experimental studies. Numerical model using parallel finite element method was developed based on the fick's law to predict the chloride induced corrosion in concrete. Then, theoretical model was extended for multi species aggressive chemical and temperature effect in non saturated concrete. Furthermore, experimental studies were conducted to investigate the durability performance of sustainable material related to waste rubber.

1. In **Chapter 3**, in order to develop the parallel finite element program with overlapping domain decomposition method and predict the chloride and humidity diffusion for long term durability in non-saturated concrete, theoretical and numerical model were studied as below;

The parallel finite element program was developed based on the robust mathematical material model. The program is used to simulate the coupled moisture and chloride penetration into non-saturated concrete structures. As de-icing salts are the sources of chloride ions that can cause the steel corrosion in reinforced concrete structures. The material parameters related to chloride and moisture diffusion in concrete are taken into account. These parameters are chloride and moisture diffusion coefficients, moisture capacity, and chloride binding capacity.

For the implementation of parallel FE analysis, Triangle for mesh generation, ParMetis, PETSc,

and MPI are employed. Also, this program used the overlapping domain decomposition method with additive schwarz preconditioner. As the result of simulation, the computation time is decreased when the number of processors is increased. But, with more processors, the communication between the processors increases.

The present model can be used to simulate the non saturated concrete structures subjected to other aggressive chemicals from de-icing salt. The framework of present model can be extended to simulate the multi-species de-icing salts ingress into non-saturated concrete structures in future work. The parallel finite element method is an effective tool and widely used for solving the partial differential equations of mass diffusion.

2. In **Chapter 4**, in order to simulate more realistically structural performance of concrete bridges, the parallel finite element program was developed based on the handling of large scale meshes and number of processor. Also, material model and mathematical model was developed. The results were as follows;

In order to measure the performance of the parallel implementation of finite element program, Speed-up was investigated to solve the optimum number of processors with about 1.5 million nodes. When using up to 8 processors, the program was not operated due to memory capacity. As increasing the number of processors, however, speed up is improved up to 512 processors. After more processors are used in the analysis, speed up gradually increased, which means that the communication time between the processors increases. The optimum number was 256 processors.

In order to actualize the numerical model and observe the effect of boundary condition, the constant and periodic boundary conditions were used to comparing the diffusion of chloride and humidity within concrete. Temperature effect was assumed as constant in this study. The concentration of chloride and humidity is continuously accumulated and increased inside concrete. Due to the seasonally change of the humidity distribution, relative humidity inside concrete might not be continuously increased in reality, so that periodic humidity model should be applied to the boundary condition.

Environmental humidity model associated with random process was used as boundary condition. At the 50mm from the top surface of concrete, the maximum value of humidity is decreased up to 20% comparing with using constant boundary condition. Also, the result about 500 days indicates that the humidity trend is reversed between 10mm and 50mm and humidity easily is exchanged near concrete surface. Therefore, this prediction model is reasonable and effective to observe the diffusion of chloride and humidity and to predict the chloride initial time on reinforcement. The parallel finite element method is an effective tool and widely used for solving the partial differential equations of mass diffusion in large scale concrete structure.

3. In **Chapter 5**, mathematical models of the transport theory of multi-species due to deicing salts was presented with Nernst-Planck equation incorporated in the coupled effect of moisture and multi-ions diffusion. The numerical results were solved by parallel finite element method with extending the mathematical model. The results were as follows;

A mathematical model was developed based on the Nernst-Planck equation and null current condition to solve for the ionic-induced electrostatic potential. The model can be used to simulate the multi-species deicing salts penetration into non-saturated concrete structures by taking into account the moisture effect and simulated based on the material models of diffusion mechanisms in cement paste and aggregate.

Moisture diffusion has significant effect on penetration of deicing salts into concrete by accelerating the penetration rate of chloride, sodium, and calcium ions. The coupling parameter was assumed because of no experimental data or material models of coupling parameters for other species. The parameter considering the effect of moisture on ionic diffusion can be assumed by the same as used for chloride due to carrying any other ions as it carries the chloride ions. The coupling parameter of each species can be estimated by the ratio between a specific ionic species and the chloride ion.

In order to verify the mathematical model, the numerical simulation was performed using finite element method and the results are compared with an available chloride ponding test data. It was found that the numerical results agree well with the experimental results.

The numerical simulation was conducted in non-saturated condition to investigate the diffusion of ionic species such as chloride, sodium, calcium, hydroxyl and potassium. The penetration of chloride, sodium, and calcium increase when time goes by, because the initial concentration outside concrete is much higher and moisture gradient have an effect on accelerating the diffusion rate of ions. However, the concentration of hydroxyl and potassium is decreased due to opposite reason. This model can be used to predict satisfactorily the penetration of aggressive chemicals such as deicing salts into non-saturated condition.

4. In **Chapter 6**, the mathematical model was developed to predict the influence of coupled temperature and moisture on multi species penetration into partially saturated concrete structures.

A mathematical model was developed to predict the chloride penetration into non saturated concrete structures under non-isothermal condition. The model takes into account diffusion mechanism and ionic interaction which is formulated based on Nernst-Planck equation. The ionic fluxes are modified by incorporating the coupling term of temperature effect. The ions in the pore solution (Na^+ , K^+ , and OH^-) are considered and the numerical simulations are performed by assuming a concrete sample exposed to chloride solution at different initial temperature conditions.

In this study, the coupling parameters of temperature effect on moisture diffusion (D_{H-T}) and moisture effect on temperature diffusion (D_{T-H}) were neglected. The other coupling parameters of temperature effect on ions diffusion were used as proposed by experimental data. The coupling parameters of ions effect on temperature diffusion were neglected.

In order to verify the mathematical model, the numerical simulation was performed using finite element method and the results are compared with an available chloride ponding test data conducted under the different temperature gradient. It was found that the numerical results agree well with the experimental results. Specially, the numerical result with 0.55 water-cement ratio is better fit on experimental result than one with 0.65 water-cement ratio. That is because the material model used in numerical model is more proper and effective to predict the penetration of chloride into concrete made by 0.55 water-cement ratio.

In order to observe the chloride penetration under the effect of coupled temperature and humidity gradient, parameter study was conducted for capturing the water-cement ratio and temperature effect. The chloride concentration of concrete with 0.65 water-cement ratio is much higher than one of 0.55 water-cement ratio. However, the temperature effect was not observed.

The present comprehensive model can be used to predict the chloride ingress into non saturated concrete structures not only isothermal but also non-isothermal conditions. It can also be used to estimate the service life and time for rehabilitation of concrete structures in temperature change condition.

5. In **Chapter 7**, the mechanical and durability properties of mortar with fine rubber powder were studied based on experimental methods: compression test, rapid chloride permeability test, the dry shrinkage test, and pull-out debonding test.

Rubber powders (very fine rubber particles) were used to make PRIM. Two different sizes of rubber powder were used: #100 mesh (0.15 mm) and #200 mesh (0.075 mm). The compressive strength of the rubber mortar with #200 mesh was higher than that of #100 mesh, which means smaller rubber particles result in higher strength. Therefore, smaller rubber particles should be used in order to obtain high strength rubber mortar.

The average flexural strength of the PRIM was about 550 psi at 50% rubber replacement rate, which is comparable to the flexural strength of ordinary cement mortar. Different amounts of rubber powder were used to replace fine sand. With increasing content of rubber powder, the compressive strength of the rubber mortar decreased. RPP is an effective additive which can improve the compressive strength of the rubber mortar. However, the improvement on the compressive strength is not significant when the RPP content is larger than 10% of the cement.

In order to measure the bond strength between wood panel and rubber mortar, a pull-out debond test apparatus was used. The bond strength did not satisfy the minimum requirement. This is because the rubber powder in mortar does not have bond strength with the wood panel, and therefore, the effective bonding surface area is reduced.

When the rubber mortar was exposed to the ambient environment after seven days of curing, the

drying shrinkage of the rubber mortar is about the same as the dry shrinkage of ordinary cement mortar.

The chloride permeability of the rubber mortar is very low. Caution must be taken when using ASTM 1202 (the rapid chloride permeability test) to evaluate the permeability of rubber mortars with various additives. This is because certain types of additives may be electrically conductive. For instance, cellulose ether as an additive used in the present study is conductive.

The rubber mortar made of fine rubber powders can be used as an insulation mortar. Either #100 or #200 sieve rubber powder can be used in the mortar. #200 rubber powder gives higher compressive strength of the mortar. The rubber replacement rate and the RPP dosage can be adjusted to satisfy strength requirements. Drying shrinkage and permeability are comparable to those of ordinary cement mortar. Bond strength is low and thus a metal mesh should be used together with the mortar to ensure the bond between the mortar layer and the wood panel.

6. In **Chapter 8**, the mechanical and durability properties of sulfur rubber concrete with waste tire were studied based on experimental methods: compression test, rapid chloride permeability test, freeze-thaw test.

In order to investigate the mechanical property of sulfur-rubber concrete, the compression test is performed, according to the different amount of rubber particles instead of sand. As the rubber dosage is increased from 10% to 50%, the compression strength is shorten up to about 80%. Also, the strength of SRC in dry process is higher than that in wet process. The rubber particles can improve the ductility of SRC, but the strength of SRC is reduced.

In wet process, the sulfur is not completely mixed with rubber particles during the optimized heating time. The rubber tends to be burned before the sulfur is melted. Therefore, the improved wet process is suggested. After melting sulfur for 20min, rubber is put into the hat pot to mix with the melted sulfur. After well stirring them for 10min, the preheated other materials can be uniformly mixed with sulfur-rubber.

For long term durability of sulfur rubber concrete, freeze-thaw test is performed. The increasing of freezing-thawing cycles results in the damage in the specimen, especially in lower rubber dosage. That

is, rubber particles are the main factor to increase the durability of SRC.

9.2. FUTURE RESEARCH RECOMMENDATIONS

1. For prediction of the realistic diffusion effect, the incorporation of environmental humidity and temperature model need to be considered in the numerical study of hygro-chemo-thermal diffusion in non saturated concrete.

2. The theoretical and numerical diffusion model of multi-species and carbonation in non-saturated concrete need to be further developed based on ambient as well as high temperature. Furthermore, the Chemical reactions consume various types of ions, which should be considered in the transport models. That is, the carbonation reaction consumes CH crystals.

3. The theoretical and numerical model of multi-species and carbonation transport in non-saturated concrete need to be incorporated in the mechanical model such as damage due to mechanical loading affects transport properties of concrete.

4. The further development of material model through experimental and numerical studies are needed on the effect of mineral additives such as fly ash and silica fume on chloride penetration and ion transport in concrete.

5. Material models for some of the coupling parameters need to be developed and verified with experimental data. For example, the effect of hydroxyl due to moisture diffusion, $D(H-OH)$.

BIBLIOGRAPHY

- Ababneh, A. (2002). "The Coupled Effect of Moisture Diffusion Chloride Penetration and Freezing-Thawing on Concrete Durability." Ph.D. Dissertation of the University of Colorado at Boulder.
- Ababneh, A. and Xi, Y. (2002). "An Experimental Study on the Effect of Chloride Penetration on Moisture Diffusion in Concrete." *Materials and Structures*, 35, 659-664.
- Ababneh, A., Benboudjema, F., and Xi, Y. (2003). "Chloride penetration in Nonsaturated concrete", *J. of Materials in Civil Engineering*, 15(2), pp 183-191.
- Abarr, L. (2005). "The Effect of Moisture Diffusion on Chloride Penetration." M.S. Thesis of the University of Colorado at Boulder.
- A. Turatsinze, S.Bonnet, J.-L.Granju(2005), "Mechanical characterization of cement-based mortar incorporating rubber aggregate from recycled worn tyres", *Building and Environment*, 40, pp.221-226
- ACI Committee 209, (2005). "Report on Factors Affecting Shrinkage and Creep of Hardened Concrete" ACI 209 1R-05.
- Adamidis, P.A., Resch, M.M., (2003) "Parallel coupled thermomechanical simulation using hybrid domain decomposition", *ICCSA*, 2667, pp.472-482.
- Amirkhanian, S. (1997). "Utilization of waste materials in highway industry—A literature survey", *J. Solid Waste Technol. Manage.*, 24(2), pp.94–103.
- Ali, H.A., (2010) "Numerical simulation of chloride diffusion in RC structures and the implications of chloride binding capacities and concrete mix", *IJCEE*, 10, pp.22-35.
- Balay,S., Buschelman, K., Eijkhout, V., Gropp, W. D., Kaushik, D., Knepley, M. G., McInnes, L. C., Smith, B. F., and Zhang, H. (2008). "PETSc: Portable, extensible toolkit for scientific computation", [http:// www.mcs.anl.gov/petsc](http://www.mcs.anl.gov/petsc).

- Balay, S., Buschelman, K., Eijkhout, V., Gropp, W. D., Kaushik, D., Knepley, M. G., McInnes, L. C., Smith, B. F., and Zhang, H. (2008). "PETSc-users manual", Technical Report ANL-95/11 - Revision 2.1.5, Argonne National Laboratory.
- Basheer, P.A.M., Chidiac, S.E., and Long, A.E. (1996). "Predictive models for deterioration of concrete structures", *Construction and Building Materials*, V. 10(1), pp 27-37.
- Basu, R., Breshears, J. S., and Clausen, E. C. (1999). "Calcium Magnesium Acetate at Lower Production Cost: Production of CMA Deicer from Biomass", FHWA-RD-98-055, Federal Highway Administration, Virginia.
- Bazant, Z.P., and Najjar, L. J. (1972). "Nonlinear water diffusion of nonsaturated concrete", *Materiaux et Constructions*, V.5(25).
- Bazant, Z.P., Thonguthai, W., (1978) "Pore Pressure and Drying of concrete at high temperature", *J. of the eng. Mech. division*, 5, pp.1059-1079
- Bazant, Z.P., Chern, J., Thonguthai, W., (1981) "Finite element program for moisture and heat transfer in heated concrete", *Nuclear Engineering and Design*, 68, pp.61-70.
- Bazant, Z.P., Xi, Y., (1993) "Stochastic Drying and Creep Effects in concrete structures", *J. Struct. Engrg.* 119, pp.301-322.
- Benazzouk, A., Douzane, O., Mezreb, K., Laidoudi, B., Queneudec, M. (2008). "Thermal conductivity of cement composites containing rubber waste particles: Experimental study and modelling", *Construction and building materials* 22, pp.573-579.
- Benazzouk, A., Marmoret, L., Mezreb, K., Khenfer, M.M., Bali, A. (2007). "Effect of the addition of wood shavings on thermal conductivity of sand concretes: Experimental study and modelling", *Construction and building materials* 21, pp.662-668.
- Biel, T.D., and Lee, H. (1994). "Use of recycled tire rubbers in concrete", *Proc., ASCE 3rd Mat. Engineering. Conf., Infrastructure: New Mat. and Methods of Repair*, pp. 351–358.
- Brown, K. M., Cummings, R., Mrozek, J. R., and Terrebonne, P. (2001). "Scrap tire disposal: Three principles for policy choice." *Nat. Resour.J.*, 41(1), pp.9–22.
- Bulent Yesilata, Paki Turgut (2007). "A simple dynamic measurement technique for comparing thermal insulation performances of anisotropic building materials", *Energy and building*, 39, pp.1027-1034.
- Cai, X.-C., Saad, Y. (1996). "Overlapping Domain Decomposition Algorithms for general Sparse Matrices", *Numer. Lin. Alg. Applic.*, 3, pp.221-237.

- Cai, X.-C, Sarkis, M. (1999). "A Restricted Addictive Schwarz Preconditioner for general Sparse linear systems", *SIAM J. Sci. Comput.*, 21(2), pp.1-5.
- Chatterji, S. (1994). "Transportation of ions through cement based materials. Part1 Fundamental equation and basic measurement techniques", *Cement and Concrete Research*, 24(5), pp.907-912.
- Christensen, R. M. (1979). "Mechanics of composite materials", Wiley, New York.
- Conciatori, D., Denarie, E., Sadouki, H., Bruhwiler, E., (2004) "Chloride Penetration Model Considering Microclimate", *IABMAS*, pp.68-74.
- Conciatori, D., Sadouki, H., Bruhwiler, E., (2008) "Capillary suction and diffusion model for chloride ingress into concrete", *Cement and Concrete Research*, 38, pp.1401-1408.
- Conciatori, D., Laferriere, F., H., Bruhwiler, E., (2010) "Comprehensive modeling of chloride ion and water ingress into concrete considering thermal and carbonation state for real climate", *Cement and Concrete Research*, 40, pp.109-118.
- Damrongwiriyanupap, N. (2010). "Modeling the Penetration of Multi-Species Aggressive chemicals into Concrete Structures.", Ph.D. Dissertation of the University of Colorado at Boulder.
- Dalcín, L. D., Paz, R. R., Anca, A. A., Storti, M. A. and D'Elia, J. (2005). "Parallel FEM application development in Python", *Mecanica Computational*, 24, pp 1823-1838.
- Eldin, N. N., and Senouci, A. B. (1993). "Rubber-tire particles as concrete aggregate" *J. Mater. Civ. Eng.*, 5(4), pp.478-496.
- Epps, J. A. (1994). "Uses of recycled rubber tires in highways", *Synthesis of Highway Practice 198*, Transportation Research Board, National Research Council, Washington, D.C.
- Everett, J. W., and Douglah, S. (1998). "Scrap tire disposal (II): Case study and recommendations" *J. Solid Waste Technol. Manage.*, 25(1), pp.51-60.
- Fafach, D., Shing, B., Chang, S., Xi, Y., (2005) "Evaluation of the FRP-Retrofitted Arches in the Castlwood Canyon Bridge", CDOT.
- FHWA, (1998). "Corrosion costs and preventive strategies in the United States", FHWA-RD-01-156, Federal Highway Administration.
- Goulias, D. G., and Ali, A. H. (1998). "Evaluation of rubber-filled concrete and correlation between destructive and nondestructive testing results", *Cem. Concr. Aggregates*, 20(1), pp.140-144.

- Güneyisi, E., Gesoğlu, M., and Özturan, T. (2004). "Properties of rubberized concretes containing silica fume", *Cement and Concrete Research*, 34, pp.2390-2317.
- Han, S. H. (2007). "Influence of diffusion coefficient on chloride ion penetration of concrete structure", *Construction and Building Materials*, 21(2), pp.370-378.
- Heath, A. C., Roesler, J. R. (1999). "Shrinkage and hermal Cracking of Fast Setting Hydraulic Cement Concrete Pavements in Palmdale, California", Report for CALTRAN.
- Isteita, M.H., (2009) "The Effect of Thermal Conduction on Chloride Penetration in Concrete", Ph.D. Dissertation of the University of Colorado at Boulder.
- Jang, J. W., Woo, T. S., Oh, J. H., Iwasaki, I. (1998). "Discarded tire recycling practices in the United States, Japan, and Korea", *Resour. Conserv. Recycl.*, 22(1-2), pp.1-14.
- Karypis, G. (1996–2005). "ParMETIS: Parallel graph partitioning and sparse matrix ordering", <http://www-users.cs.umn.edu/~karypis/metis/parmetis/>.
- Khatib, Z. K., and Bayomy, F. M. (1999). "Rubberized Portland cement concrete", *J. Mater. Civ. Eng.*, 11(3), pp.206-213.
- Kulasiri, D., Woodhead, I., (2005) "On modeling the drying of porous materials: Analytical solutions to coupled partial differential equations governing heat and moisture transfer", *Mathematical Problems in Engineering*, 3, pp.275-291.
- Li, L.Y., Tenchev, R.T., Purkiss, J.A., (2001) "An Engineering model for coupled heat and mass transfer analysis in heated concrete", *J. Mechanical Engng. Science*, 216, pp.213-224.
- Li, G., Stubblefield, M.A., Garrick, G. et al. (2004). "Development of waste tire modified concrete", *Cement and Concrete Research*, 34, pp.2283-2289.
- Li, L.Y. and Page, C.L. (1998). "Modelling of electrochemical chloride extraction from concrete: Influence of ionic activity coefficients", *Computational Material Science*, 9, pp. 303-308.
- Li, L.Y. and Page, C.L.(2000), " Finite element modeling of chloride removal from concrete by an electrochemical method.", *Corrosion Science*, 42, pp2145-2165.
- Lien, H.P., Wittmann, F.H., (1998) "Mass transfer in inhomogeneous porous media under thermal gradients", *Nuclear Engineering and Design*, 179, pp.179-189.
- Martin-Perez, B., Pantazopoulou, S.J., and Thomas, M.D.A. (2001). "Numerical solution of mass transport equations in concrete structures", *Computers and Structures*, 79, pp.1251-1264.

- MPI Forum. (1994). "MPI: A message passing interface standard", *International Journal of Supercomputer Applications*, 8(3/4),pp.159-416.
- MPI Forum. (1998). "MPI2: A message passing interface standard", *High Performance Computing Applications*, 12(1-2), pp.1-299.
- MPICH Team. (2004). "MPICH: A portable implementation of MPI", <http://www-unix.mcs.anl.gov/mpi/mpich/>.
- Nielsen, E.P., and Geiker, M.R. (2003). "Chloride diffusion in partially saturated cementitious material", *Cement and Concrete Research*, V. 33, pp 133-138.
- Nguyen, T.Q., Baroghel-Bouny, V. and Dangla, P.,(2006), "Prediction of chloride ingress into saturated concrete on the basis of multi-species model by numerical calculations.", *Computers and Concrete*, 3(6), pp401-422.
- Oh, B.H., and Jang, S.Y. (2007). "Effect of material and environmental parameters on chloride penetration profiles in concrete structures", *Cement and Concrete Research*, 37, pp.47-53.
- Rubber manufacturers association (2006). "Scrap tire markets in the United States".
- Saetta, A.V., Schrefler, B.A., Vitaliani, R., (1993) "The carbonation of concrete and the mechanism of moisture, heat and carbonation dioxide flow through porous materials", *Cement and Concrete Research*, 23, pp.761-772.
- Samson, E., Lemaire, G., Marchand, J., and Beaudoin, J.J. (1999). "Modeling chemical activity effects in strong ionic solutions", *Computational Materials Science*, 15, pp. 285-294.
- Samson, E. Marchand, J. (1999). "Numerical Solution of the Extended Nernst-Planck Model", *Journal of Colloid and Interface Science*, 215, pp. 1-8.
- Samson, E. and Marchand, J. (2007). "Modeling the transport of ions in unsaturated cement-based materials", *Computers and Structures*, 85, pp.1740-1756.
- Saouma, V. E., Chang, S. (2004). " Numerical simulation of reinforced concrete deterioration due to steel corrosion, freezing-thawing and mechanical load effects", *IABMAS*, pp.165-174.
- Schimizze, R., Nelson, J., Amirkhanian, S. et al. (1994). "Use of waste rubber in light-duty concrete pavements", *Proc., ASCE 3rd Mat. Engineering Conf., Infrastructure: New Mat. and Methods of Repair*, pp.367-374.

- Segre, N., Joekes, I. (2000). "Use of tire rubber particles as addition to cement paste", *Cement and Concrete Research*, 39, pp.3319-3327.
- Segre, N., Joekes, I. (2004). "Rubber-mortar composites: Effect of composition on properties", *J. of Material Science*, 39, pp.3319-3327.
- Sih, G.C., Shih, M.T., (1980) "Transient hygrothermal stresses in composites: Coupling of moisture and heat with temperature varying diffusivity", *Int. J. Engng. Sci.*, 18, pp.19-42.
- Song, H.W., Lee, C.H., and Ann, K.Y. (2008). "Factors influencing chloride transport in concrete structures exposed to marine environments", *Cement and Concrete Composite*, 30, pp.113-121.
- Suwito, Cai, X.C., and Xi, Y. (2006). "Parallel finite element method for coupled chloride moisture diffusion in concrete", *International J. of Numerical Analysis and Modeling*, 3(4), pp.481-503.
- Tamimi, A.K., Abdalla, J.A., and Sakka, Z.I. (2007). "Prediction of long term chloride diffusion of concrete in harsh environment", *Construction and Building Materials*, 22(5), pp.829-836.
- Tang, L., and Nilson, L. O. (1993). "Chloride binding capacity and binding isotherms of OPC pastes and mortars", *Cement and Concrete Research*, 23, pp.247-253.
- Tenchev, R.T., Li, L.Y., Purkiss, J.A., (2001) "Finite element analysis of coupled heat and moisture transfer in concrete subjected to fire", *Numerical Heat Transfer, Part A* (39), pp.685-710.
- Topcu, I.B. (1995). "The properties of rubberized concretes", *Cement and Concrete Research*, 25, pp.304-310.
- Topcu, I.B. (1997). "Assessment of the brittleness index of rubberized concretes", *Cement and Concrete Research*, 27(2), pp.177-183.
- Topcu, I.B., and Demir, A. (2007). "Durability of rubberized mortar and concrete", *ASCE, J. of Materials in Civil Eng.*, 19(2), pp.173-178.
- Shewchuk, J. R. (2005). "Triangle; A Two-Dimension Quality Mesh Generator and Delaunay Triangulator", Carnegie Mellon University.
- Truc, O., Olliver, J.P., Nilsson, L.O. (2000). "Numerical simulation of multi-species diffusion", *Material*

- and Structures, 33, pp566-573.
- Turatsinze, A., Bonnet, S., Granju, J. L. (2005). "Mechanical characterization of cement-based mortar incorporating rubber aggregate from recycled worn tyres", Building and environment, 40, pp.221-226.
- Turatsinze, A., Bonnet, S., Granju, J.L. (2007). "Potential of rubber aggregates to modify properties of cement based-mortars: Improvement in cracking shrinkage resistance", Construction and Building Materials, 21, pp.176-181.
- Vroom, A.H. (1998). "Sulfur Concrete Goes Global", Concrete International, ACI, 20, pp.68-71.
- Wang, Y., Li, L.Y. and Page, C.L. (2001) A two-dimensional model of electrochemical chloride removal from concrete, 20, pp.196-212.
- Wang, Y., Li, L.Y. and Page, C.L. (2005) Modeling of chloride ingress into concrete from a saline environment. Building and Environment, 40, pp1573-1582.
- Xi, Y., Bazant, Z. P., Molina, L., Jennings, H. M. (1994a). "Moisture diffusion in cementitious materials: Adsorption isotherm", Adv. Cem.Based Mater., 1, pp.248–257.
- Xi, Y., Bazant, Z. P., Molina, L., and Jennings, H. M. (1994b). "Moisture diffusion in cementitious materials: Moisture capacity and diffusivity", Adv. Cem. Based Mater., 1, pp.258–266.
- Xi, Y. (1995a). "A model for moisture capacities of composite materials. I: Formulation", Comput. Mater. Sci., 4, pp.65–77.
- Xi, Y. (1995b). "A model for moisture capacities of composite materials. II: Application to concrete", Comput. Mater. Sci., 4, pp.78–92.
- Xi, Y., Bazant, Z. P. (1999). "Modeling chloride penetration in saturated concrete", J. of Materials in Civil Engineering, 11(1), pp.58-64.
- Xi, Y., Willam, K., Frangopol, D. M. (2000). "Multiscale modeling of interactive diffusion processes in concrete", J. of Eng. Mech., 126(3), pp.258-265.

Zhang, J. Z., McLoughlin, I.M., Buenfeld, N.R. (1998). "Modelling of chloride diffusion into surface-treated concrete", *Cement and Concrete Composite*, 20, pp.253-261.

APPENDIX A

DERIVATION OF DIFFUSIVITY MATRIX

The physical problems such as heat transfer, fluid flow, and mass diffusion can be explained in terms of Partial Differential Equations (PDE). These PDE can be approximately solved by numerical method such as finite element method, or finite difference method. Finite element method is an effective tool to solve the governing equation for the diffusion problem and it is widely used to predict the chloride transport and the moisture movement in concrete. The diffusion phenomena of multi species in concrete is described with the Nernst-Planck equation. Not only diffusion mechanism due to concentration gradient but also the electrical coupling between the different ions due to the deicing salt and pore solution in the concrete is accounted for the Nernst-Planck equation.

In order to develop the finite element program, first of all, the space domain, Ω , is discretized into a large number of finite elements as mentioned in chapter 3. If the problem is time dependent, it is considered as ordinary differential equation and time need to be discretized.

For the flux of each species in the pore solution of saturated concrete, the Nernst-Planck equation is employed.

$$J_i = - \left[D_i \nabla C_{f-i} + z_i D_i \left(\frac{F}{RT} \nabla \phi \right) C_{f-i} \right] \quad \text{Eq.(A-1)}$$

where J_i is the flux of ions, D_i is the diffusion coefficient, C_{f-i} is the concentration of multi-species (Na⁺, Ca²⁺, K⁺, OH⁻, Cl⁻), z_i is the charge number, F is the Faraday's constant, R is the gas constant, T is the temperature, Φ is the electrostatic potential, and index i represents for i -th species.

In order to solve the system of equations, a supplemental relation is needed to consider the electrical potential due to inherently caused by the movement of all species. In this study, null current condition is used.

$$\sum z_i J_i = 0 \quad \text{Eq.(A-2)}$$

From the null current condition, we have

$$\sum_{i=1}^n z_i \left(-D_i \nabla C_i - z_i D_i \left(\frac{F}{RT} \nabla \phi \right) C_i \right) = 0 \quad \text{Eq.(A-3)}$$

And then,

$$\frac{F}{RT} \nabla \phi = - \frac{\sum_{i=1}^n z_i D_i \nabla C_i}{\sum_{i=1}^n z_i^2 D_i C_i} \quad \text{Eq.(A-4)}$$

The governing equation is

$$\frac{\partial C_i}{\partial t} = \nabla \left(D_i \nabla C_i + z_i D_i \left(\frac{F}{RT} \nabla \phi \right) C_i \right) = \nabla \left(D_i \nabla C_i + z_i D_i \left(- \frac{\sum_{j=1}^n z_j D_j \nabla C_j}{\sum_{j=1}^n z_j^2 D_j C_j} \right) C_i \right) \quad \text{Eq.(A-5)}$$

Let us consider three different ions in concrete,

In the case of $i=1$,

$$\begin{aligned}
\frac{\partial C_1}{\partial t} &= \frac{\partial}{\partial x} \left\{ D_1 \cdot \frac{\partial C_1}{\partial x} + z_1 \cdot D_1 \cdot C_1 \cdot \left(-\frac{\sum_{i=1}^3 z_i \cdot D_i \cdot \frac{\partial C_i}{\partial x}}{\sum_{i=1}^3 z_i^2 \cdot D_i \cdot C_i} \right) \right\} \\
&= \frac{\partial}{\partial x} \left\{ D_1 \cdot \frac{\partial C_1}{\partial x} - z_1 \cdot D_1 \cdot C_1 \cdot \frac{\left(z_1 \cdot D_1 \cdot \frac{\partial C_1}{\partial x} + z_2 \cdot D_2 \cdot \frac{\partial C_2}{\partial x} + z_3 \cdot D_3 \cdot \frac{\partial C_3}{\partial x} \right)}{\sum_{i=1}^3 z_i^2 \cdot D_i \cdot C_i} \right\} \\
&= \frac{\partial}{\partial x} \left\{ \begin{aligned} &D_1 \cdot \frac{\partial C_1}{\partial x} - z_1 \cdot D_1 \cdot C_1 \cdot \frac{z_1 \cdot D_1}{\sum_{i=1}^3 z_i^2 \cdot D_i \cdot C_i} \cdot \frac{\partial C_1}{\partial x} \\ &- z_1 \cdot D_1 \cdot C_1 \cdot \frac{z_2 \cdot D_2}{\sum_{i=1}^3 z_i^2 \cdot D_i \cdot C_i} \cdot \frac{\partial C_2}{\partial x} - z_1 \cdot D_1 \cdot C_1 \cdot \frac{z_3 \cdot D_3}{\sum_{i=1}^3 z_i^2 \cdot D_i \cdot C_i} \cdot \frac{\partial C_3}{\partial x} \end{aligned} \right\} \quad \text{Eq.(A-6)}
\end{aligned}$$

In the case of $i=2$,

$$\begin{aligned}
\frac{\partial C_2}{\partial t} &= \frac{\partial}{\partial x} \left\{ D_2 \cdot \frac{\partial C_2}{\partial x} + z_2 \cdot D_2 \cdot C_2 \cdot \left(-\frac{\sum_{i=1}^3 z_i \cdot D_i \cdot \frac{\partial C_i}{\partial x}}{\sum_{i=1}^3 z_i^2 \cdot D_i \cdot C_i} \right) \right\} \\
&= \frac{\partial}{\partial x} \left\{ \begin{aligned} &D_2 \cdot \frac{\partial C_2}{\partial x} - z_2 \cdot D_2 \cdot C_2 \cdot \frac{z_1 \cdot D_1}{\sum_{i=1}^3 z_i^2 \cdot D_i \cdot C_i} \cdot \frac{\partial C_1}{\partial x} \\ &- z_2 \cdot D_2 \cdot C_2 \cdot \frac{z_2 \cdot D_2}{\sum_{i=1}^3 z_i^2 \cdot D_i \cdot C_i} \cdot \frac{\partial C_2}{\partial x} - z_2 \cdot D_2 \cdot C_2 \cdot \frac{z_3 \cdot D_3}{\sum_{i=1}^3 z_i^2 \cdot D_i \cdot C_i} \cdot \frac{\partial C_3}{\partial x} \end{aligned} \right\} \quad \text{Eq.(A-7)}
\end{aligned}$$

In the case of $i=3$,

$$\begin{aligned} \frac{\partial C_3}{\partial t} &= \frac{\partial}{\partial x} \left\{ D_3 \cdot \frac{\partial C_3}{\partial x} + z_3 \cdot D_3 \cdot C_3 \cdot \left(-\frac{\sum_{i=1}^3 z_i \cdot D_i \cdot \frac{\partial C_i}{\partial x}}{\sum_{i=1}^3 z_i^2 \cdot D_i \cdot C_i} \right) \right\} \\ &= \frac{\partial}{\partial x} \left\{ \begin{aligned} &D_3 \cdot \frac{\partial C_3}{\partial x} - z_3 \cdot D_3 \cdot C_3 \cdot \frac{z_1 \cdot D_1}{\sum_{i=1}^3 z_i^2 \cdot D_i \cdot C_i} \cdot \frac{\partial C_1}{\partial x} \\ &- z_3 \cdot D_3 \cdot C_3 \cdot \frac{z_2 \cdot D_2}{\sum_{i=1}^3 z_i^2 \cdot D_i \cdot C_i} \cdot \frac{\partial C_2}{\partial x} - z_3 \cdot D_3 \cdot C_3 \cdot \frac{z_3 \cdot D_3}{\sum_{i=1}^3 z_i^2 \cdot D_i \cdot C_i} \cdot \frac{\partial C_3}{\partial x} \end{aligned} \right\} \quad \text{Eq.(A-8)} \end{aligned}$$

We can rearrange Eq.(A-6) , Eq.(A-7), and Eq.(A-8) in matrix form,

$$\begin{aligned} \begin{Bmatrix} \frac{\partial C_1}{\partial t} \\ \frac{\partial C_2}{\partial t} \\ \frac{\partial C_3}{\partial t} \end{Bmatrix} &= \frac{\partial}{\partial x} \cdot \begin{bmatrix} D_1 - z_1 \cdot D_1 \cdot C_1 \cdot \frac{z_1 \cdot D_1}{\sum_{i=1}^3 z_i^2 \cdot D_i \cdot C_i} & -z_1 \cdot D_1 \cdot C_1 \cdot \frac{z_2 \cdot D_2}{\sum_{i=1}^3 z_i^2 \cdot D_i \cdot C_i} & -z_1 \cdot D_1 \cdot C_1 \cdot \frac{z_3 \cdot D_3}{\sum_{i=1}^3 z_i^2 \cdot D_i \cdot C_i} \\ -z_2 \cdot D_2 \cdot C_2 \cdot \frac{z_1 \cdot D_1}{\sum_{i=1}^3 z_i^2 \cdot D_i \cdot C_i} & D_2 - z_2 \cdot D_2 \cdot C_2 \cdot \frac{z_2 \cdot D_2}{\sum_{i=1}^3 z_i^2 \cdot D_i \cdot C_i} & -z_2 \cdot D_2 \cdot C_2 \cdot \frac{z_3 \cdot D_3}{\sum_{i=1}^3 z_i^2 \cdot D_i \cdot C_i} \\ -z_3 \cdot D_3 \cdot C_3 \cdot \frac{z_1 \cdot D_1}{\sum_{i=1}^3 z_i^2 \cdot D_i \cdot C_i} & -z_3 \cdot D_3 \cdot C_3 \cdot \frac{z_2 \cdot D_2}{\sum_{i=1}^3 z_i^2 \cdot D_i \cdot C_i} & D_3 - z_3 \cdot D_3 \cdot C_3 \cdot \frac{z_3 \cdot D_3}{\sum_{i=1}^3 z_i^2 \cdot D_i \cdot C_i} \end{bmatrix} \cdot \begin{Bmatrix} \frac{\partial C_1}{\partial x} \\ \frac{\partial C_2}{\partial x} \\ \frac{\partial C_3}{\partial x} \end{Bmatrix} \end{aligned} \quad \text{Eq.(A-9)}$$

As applying Galerkin's method to the residual functions in Eq.(A-9) and discretizing it in time space, we can have the chloride concentration.